

FINAL REPORT

**U.S. Department of Energy
Environmental Management Science Program**

**Project No. 60158
Contract No. DE-FG07-97ER62523**

**Development of Radon-222 as a Natural Tracer for Monitoring the Remediation of
NAPL in the Subsurface**

**Brian M. Davis, Lewis Semprini, and Jonathan Istok
Department of Civil, Construction and Environmental Engineering
Oregon State University
Corvallis, OR 97331**

CONTENTS

1. Executive Summary	3
2. Literature Review.....	4
3. Push-Pull Partitioning Tracer Tests Using Radon-222 to Quantify Nonaqueous phase Liquid Contamination.....	27
4. Static and Push-Pull Methods Using Radon-222 to Characterize Dense Nonaqueous Phase Liquid Saturations.....	46
5. Numerical Simulations of Radon as an In Situ Partitioning Tracer for Quantifying NAPL contamination Using Push-Pull Tests.....	69
6. A Method for determining Aqueous-Organic Partition Coefficients for 222-Radon.....	88
7. The Effect of Sample, Cocktail and Headspace Volume when Analyzing 222-Radon in 5 mL Samples by Liquid Scintillation Methods.....	102
8. Determining 222-Radon Partition Coefficients in TCE and PCE.....	113
9. Monitoring TCE DNAPL Remediation Using Naturally-Occurring 222-Radon as a Partitioning Tracer.....	115

1. EXECUTIVE SUMMARY

Naturally occurring ^{222}Rn in ground water can potentially be used as an in situ partitioning tracer to characterize dense nonaqueous phase liquid (DNAPL) saturations. The static method involves comparing radon concentrations in water samples from DNAPL-contaminated and non-contaminated portions of an aquifer. During a push-pull test, a known volume of test solution (radon-free water containing a conservative tracer) is first injected ("pushed") into a well; flow is then reversed and the test solution/groundwater mixture is extracted ("pulled") from the same well. In the presence of NAPL radon transport is retarded relative to the conservative tracer. Assuming linear equilibrium partitioning, retardation factors for radon can be used to estimate NAPL saturations. The utility of this methodology was evaluated in laboratory and field settings. Laboratory push-pull tests were conducted in both non-contaminated and trichloroethene NAPL (TCE)-contaminated sediment packs before- and after alcohol cosolvent flushing and pump-and-treat remediation; field push-pull tests were conducted in wells located in non-contaminated and light non-aqueous phase liquid (LNAPL)-contaminated portions of an aquifer at a former petroleum refinery. The laboratory and field push-pull tests demonstrated that radon retardation does occur in the presence of TCE and LNAPL and that radon retardation can be used to calculate TCE saturations. However, nonequilibrium radon partitioning and heterogeneous TCE distributions may affect the retardation factors and TCE saturation estimates. Numerical simulations were used to further investigate the influence of 1) initial radon concentration, which varies as a function of NAPL saturation and 2) heterogeneity in NAPL saturation distribution within the radius of influence of the push-pull test.

A method is described for determining the partition coefficient for radon in the presence of NAPL. The method uses sequential extractions of radon into equal volume aliquots of organic solvent. The radon-laden organic liquid is then counted on a liquid scintillation analyzer with alpha-beta separation. The high quench resistance and counting efficiency of alpha particles by liquid scintillation methods are ideal for counting a variety of aromatic, aliphatic, and cyclic organic solvent and scintillation cocktail mixtures. Accurate knowledge of the instrument counting efficiency, quench, and standard solution activity are not required. Replicate measurements of the aqueous-organic radon partition coefficient on benzene, toluene, o-xylene, n-hexane, cyclohexane, trichloroethene, and perchloroethene showed excellent agreement with theoretical radon partition coefficients derived from Ostwald solubility coefficients. The method was also used to determine the aqueous-organic radon partition coefficient for several commercial liquid scintillation solutions.

2. LITERATURE REVIEW

CHLORINATED ALIPHATICS AND DNAPLs

Chlorinated solvents have seen prolific use in the industrialized world throughout the twentieth century. These chemicals have been utilized for numerous purposes, including metal degreasing, electroplating, semiconductor production, dry cleaning, and as a feedstock for other the production of other chemicals. Over the past 30 years the problems associated with the use and disposal of chlorinated solvents have been brought to the forefront of environmental research. Some of these chemicals, including trichloroethene (TCE), are suspected human carcinogens (California EPA, 2000). Although the health risks of chlorinated solvents are widely understood, some (e.g., TCE and perchloroethene, PCE) are still classified as a High Production Volume Chemicals by the U.S. Environmental Protection Agency (EPA), with an annual production and/or importation of over 1 million pounds (EPA HPV list, 2002). The improper use and disposal of chlorinated solvents “has given rise to many of the most serious problems of contamination encountered in hydrogeologic practice.” (Domenico and Schwartz, 1998). Sources such as leaking above ground and underground storage tanks, faulty piping systems, industrial and transportation accidents, and improper burial in landfills have led chlorinated solvents to become the most common organic chemicals detected at contaminated sites (Broholm et al., 1999).

Chlorinated solvents are ethanes or ethenes that have one or more hydrogen atoms replaced by one or more chlorine atoms at various positions on the structure of the compound. For example, TCE is an ethene with three of the four hydrogen atoms replaced by chlorine atoms. A majority of chlorinated solvents have a density greater than water as well as a relatively low solubility in water. For instance, TCE has a solubility of 1100 mg/L at 20°C and 1 atm pressure, and a specific gravity of 1.46 (Domenico and Schwartz, 1998). Increasing the degree of chlorination of these compounds generally results in an increase in their density, viscosity, and nonflammability, while decreasing their solubility in water. These chemicals form a dense nonaqueous phase liquid, or DNAPL, and are subsequently often referred to as DNAPLs. When released to the subsurface, DNAPLs will volatilize in the unsaturated zone, while in the saturated zone both volatilization and dissolution will occur. These phenomena can produce large plumes of DNAPL-contaminated groundwater as the DNAPL slowly dissolves to form an aqueous phase. Selected physical characteristics of TCE, PCE, trichloromethane, and carbon tetrachloride are shown on the following page.

Table 2.1 Selected physical characteristics of chlorinated aliphatics (Domenico and Schwartz, 1998)

Compound	Formula	Specific Gravity	Solubility (mg/L)	Vapor Pressure (mm Hg)
Trichloroethene	C ₂ HCl ₃	1.46	1100	60
Perchloroethene	C ₂ Cl ₄	1.63	150	14
Trichloromethane	CHCl ₃	1.49	8200	160
Carbon Tetrachloride	CCl ₄	1.59	757	90

The mechanisms controlling the migration and fate of DNAPLs in the subsurface are complex and have been the subject of extensive research (e.g., Schwille, 1988). The migration of DNAPLs in the subsurface is affected by numerous factors, including 1) the volume released, 2) the infiltration area, 3) the release duration, 4) DNAPL properties, and 5) the physical characteristics of the subsurface (Mercer and Cohen, 1990). A number of physical properties influence DNAPL behavior in the environment and are therefore critical in optimizing site characterization and remediation. These properties are briefly summarized below.

Density

The density of the DNAPL is critical in establishing the hydrostatic pressure that drives gravity flow. A greater density results in a greater hydrostatic driving force. Density is often described in terms of specific gravity, which is the ratio of the mass of a volume of substance to the mass of an equivalent volume of water at a specific temperature.

Interfacial Tension and Wettability

Interfacial tension is defined as the free surface energy at the interface between two immiscible substances (Mercer and Cohen, 1990). This energy results from the difference between the mutual attraction of like molecules in a substance and the attraction of unlike molecules across the interface between the two substances. Figure 2.1 shows a three-phase system composed of a Liquid 1 (*L1*), Liquid 2 (*L2*), and Solid (*S*).

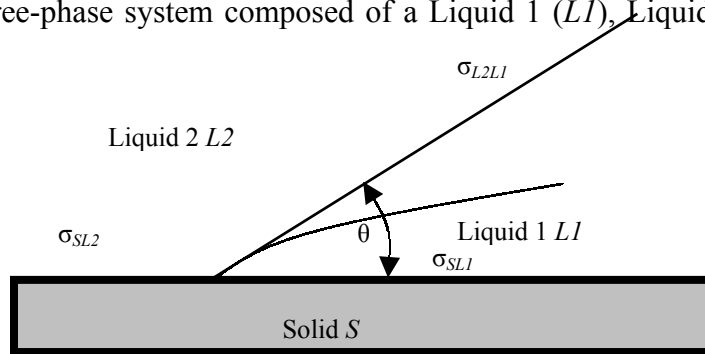


Figure 2.1 Interfacial tensions between a solid and two liquid phases.

In Figure 2.1 the relationship between the contact angle θ (measured through the denser fluid) and the interfacial tensions (σ) is given by

$$\cos\theta = \frac{\sigma_{SL2} - \sigma_{SL1}}{\sigma_{L2L1}} \tag{2.1}$$

When θ is less than 90° , Liquid *L2* will wet the solid surface, while when θ is greater than 90° , Liquid *L1* will wet the solid surface. Since water has a lower interfacial tension with solid surfaces than many DNAPLs, water tends to wet the solid surfaces in the saturated and unsaturated zones. The interfacial tension directly influences the wettability; that is, the preferential spreading of one liquid over a solid surface in a two-liquid system (Mercer and Cohen, 1990). The wetting fluid tends to occupy smaller pores and coat the

solid surfaces, while the nonwetting fluid tends to occupy larger pores and the center of those pores. Most solids are preferentially water-wet, and thus usually DNAPL forms a non-wetting fluid in the saturated and unsaturated zones.

Viscosity

Viscosity is defined as a liquid's resistance to shear. As viscosity increases a DNAPL's resistance to shear increases, potentially decreasing its rate of penetration in the saturated zone.

Capillary Pressure

Capillary pressure (P_c) defines the pore pressure of two liquids at the curved interface between those two liquids, as described by (Fetter, 1999)

$$P_c = \left(\frac{2\sigma}{r} \right) \cos\theta \quad (2.2)$$

where r is the radius of curvature of the interface between the two liquids and σ is the interfacial tension between the two liquids. This property causes the porous media to attract the wetting liquid and repel the nonwetting liquid. Thus, the pressure that must be established for DNAPL to penetrate into a pore is directly proportional to the interfacial tension and inversely proportional to the radius of curvature. Domenico and Schwartz (1998) describe capillary pressure as “the pressure required to move a particle of nonwetting fluid into a pore filled with wetting fluid.” Small pores therefore are more resistant to DNAPL penetration than large pores (since the radius of curvature is a function of pore size), with the result that DNAPLs tend to move through coarser and more permeable mediums, may bypass less permeable mediums via gravity flow or may form ‘pools’ of DNAPL above less permeable mediums.

Relative Permeability

Relative permeability (in reference to DNAPLs) refers to the reduction of the intrinsic permeability of a given medium in the presence of water and DNAPL. As DNAPL fills pores and displaces water, the relative permeability of the medium decreases for water and increases for DNAPL. The ratio of the volume of the pore filled with water to the volume of pore filled with DNAPL is referred to as the saturation ratio. As the pores fill with the water, the saturation ratio increases and the relative permeability of the medium to DNAPL decreases. Ultimately the DNAPL saturation is reduced to an irreducible, or ‘residual’ saturation where it is discontinuous and no longer mobile. Conversely, as the pores fill with DNAPL, the saturation ratio decreases as does the relative permeability of the medium to water. Ultimately the water saturation is reduced to a ‘residual’ saturation where it is discontinuous and no longer mobile.

DNAPL released at the surface will migrate downward due to hydrostatic pressure. In the presence of continuing hydrostatic pressure, DNAPL will continue to migrate downward, eventually passing through the water table. As it migrates, some DNAPL will spread laterally due to capillary forces and/or heterogeneity in the physical properties of the subsurface. Subsurface heterogeneity (e.g., layering) can cause DNAPL to migrate

due to gravity flow along pathways distinct from the groundwater flow direction. Small 'blobs' or 'ganglia' of DNAPL will occur in pores when the DNAPL (i.e., free-phase) hydrostatic pressure is reduced below a critical level (Bedient et al., 1994). The amount of mobile DNAPL from a pulse release will therefore decrease as more and more DNAPL is 'trapped' in pores during downward migration. These DNAPL ganglia form a residual saturation that slowly dissolves to the aqueous phase. The end result of a DNAPL release will often be a complex distribution of residual and mobile DNAPL.

The combination of factors affecting DNAPL flow and the inherent heterogeneity of the subsurface results in many DNAPL-contaminated sites having a complex distribution of mobile and residual DNAPL. The saturation of DNAPL in the subsurface is often found to be a function of space. Broholm et al. (1999) conducted a controlled release of 5 L of mixed solvent DNAPL (TCE, PCE and trichloromethane) in an engineered 'test cell' in a sandy, unconfined aquifer. The DNAPL saturation was found to be highly heterogeneous when the test cell was excavated at the end of the experiment. Jawitz et al. (2000) conducted soil coring at a dry cleaner site contaminated with PCE and found a heterogeneous PCE saturation distribution using soil core analysis. A typical DNAPL-contaminated site may contain numerous zones of residual DNAPL along with DNAPL 'pools' of varying size and shape. Contamination at fractured bedrock sites can result in complex DNAPL saturation distributions as the DNAPL migrates along fractures of varying size and connectivity (Fetter, 1999). These phenomena present challenges to effectively locating and quantifying the distribution of DNAPL saturations in the subsurface.

The demand for effective characterization of DNAPL contamination has led to the development of numerous techniques for locating DNAPL in the subsurface. The collection of soil samples using coring devices (e.g., hollow stem augers, direct-push samplers) and subsequent analysis of those samples for DNAPL could be classified as a traditional method of obtaining subsurface DNAPL saturation data. Numerous techniques for analyzing soil samples have been developed (Cohen and Mercer, 1993). A portable organic vapor analyzer using flame ionization detection of vapor phase organics can be used to screen samples for the potential presence of DNAPL (Griffin and Watson, 2002). Visual identification of DNAPLs in samples can sometimes be made, especially with the aid of a hydrophobic dye such as Sudan IV or Oil Red O (Kram et al., 2001). Soil/water shake tests, UV fluorescence using a field-portable light source, and laboratory-based chemical analysis of the organic phase in soil samples (incorporating phase equilibrium partitioning calculations) have been used to characterize DNAPL saturation in soil cores. Although these methods can produce direct evidence of DNAPL contamination, they typically sample small volumes of the subsurface. In order to adequately characterize a DNAPL contaminated site, a large number of samples must be obtained; this can significantly increase the costs of site characterization (Kram et al., 2001).

Groundwater samples can be obtained from monitoring wells installed at the site. The presence of DNAPL in samples obtained from monitoring wells is obviously a direct indicator of DNAPL in the subsurface, although it cannot be reliably used to estimate the

DNAPL saturation in a given volume of the subsurface. The analysis of water samples for dissolved chlorinated aliphatics can potentially locate DNAPL source zones (Broholm et al., 1999). As a rule of thumb, the presence of DNAPL is inferred if the aqueous phase concentration exceeds 1 % of the effective solubility of the DNAPL phase. However, this is not a hard and fast rule and cannot be relied on in the field to preclude the presence of DNAPL if aqueous phase concentrations are < 1 % of the effective solubility. These methods require the installation of a sufficient density of monitoring wells at a site to adequately interrogate a sufficient volume of the subsurface. Again, the costs associated with these activities increase as the number of monitoring wells increases.

Cone penetrometer (CPT) methods involve direct-push boring techniques to insert various sensors, samplers, and/or analytical devices to specified depths in the subsurface. CPT methods are best suited for relatively shallow investigations conducted in loosely compacted sedimentary deposits. More than one sensor can be mounted on a single probe to collect real-time data on sediment properties and DNAPL distributions. One of the more recent innovations in CPT technology is the membrane interface probe (MIP), which consists of a fluorocarbon polymer membrane mounted on a drive point (Griffin and Watson, 2002). The membrane is heated to 100°C to 120°C and a clean carrier gas is circulated across the internal membrane surface. Volatile organic compounds (VOCs) partition across the interface and are carried to a detector at the surface (e.g., gas chromatograph/mass spectrometer or flame ionization detector). The MIP is used as a preliminary indicator of DNAPL contamination, and positive results require obtaining confirmation samples from the area of interest. The hydrosparging technique involves the use of a CPT probe equipped with a groundwater sampling port and sparging device to sparge VOCs from the saturated zone to an above ground detection device (Kram et al., 2001). Similar to the MIP technique, the hydrosparging technique is a preliminary indicator for DNAPLs. Another CPT method incorporates Raman Spectroscopy, which enables the real time identification of specific constituents of chlorinated DNAPLs. This technique utilizes light wavelength shifts from inelastic scattering to delineate DNAPL contamination in the subsurface. Yet another CPT technique utilizes a Waterloo Profiler, which is essentially a stainless steel, multilevel groundwater sampling device that can be pushed to a specified depth. Aqueous phase samples are obtained and analyzed for chlorinated DNAPL components. This technique is similar to obtaining groundwater samples at monitoring wells, with the advantage that numerous samples can be obtained in a relatively short amount of time from essentially temporary boreholes, thus reducing the overall sampling cost. Also, CPT coupled with a Flexible Liner Underground Technologies Everting (FLUTE)[®] Membrane can be used to detect the presence of DNAPL. This method utilizes a hydrophobic absorbent ribbon that is pushed against the side of the borehole at a specified depth. DNAPLs, if present, will absorb to the ribbon. The ribbon is extracted and analyzed for DNAPL components (Kram et al., 2001). Each of the CPT techniques outlined above involves the use of a direct-push device (usually truck-mounted) to advance and retract the CPT, and requires a sufficient density of sampling locations to effectively characterize DNAPL contamination at a site. The cost of CPT methods therefore is greater at larger sites and at sites where a greater sample density is desired. Also, sampling is usually limited to shallow depths and to

unconsolidated materials. In addition, most of these techniques require further sampling to quantify DNAPL saturation, which adds additional costs to the initial CPT costs.

PARTITIONING INTERWELL TRACER TESTS

The need to interrogate larger volumes of the subsurface and quantify the DNAPL saturation in the interrogated volume has led to the development and application of the partitioning interwell tracer test. Partitioning interwell tracer tests involve the injection of non-reactive conservative and non-conservative (i.e., partitioning) tracers in an injection well. The tracers travel through the flow field to an extraction well, where samples are obtained for analysis. The conservative tracer will be transported at the pore water velocity. The partitioning tracer will partition between the DNAPL and water. If the DNAPL is immobile (i.e., at residual saturation), the velocity of the partitioning tracer will be retarded relative to the conservative tracer (Jin et al., 1995). The partitioning into immobile DNAPL results in a chromatographic separation of the conservative and partitioning tracers, with the degree of separation a function of the DNAPL saturation in the subsurface and the DNAPL:aqueous phase partition coefficient for the partitioning tracer (K), which is described by (Dwarakanath, 1999)

$$K = \frac{C_n}{C_w} \quad (2.3)$$

where C_n is the concentration of the partitioning tracer in the DNAPL phase, and C_w is the concentration of the partitioning tracer in the aqueous phase. Assuming linear, equilibrium partitioning, the retardation factor (R) is described by (Dwarakanath, 1999)

$$R = 1 + K \frac{S_n}{S_w} \quad (2.4)$$

where S_n is the DNAPL saturation, and S_w is the water saturation ($S_n + S_w = 1$). One or more partitioning tracers may be injected in an interwell partitioning tracer test, each of which may have a different DNAPL:aqueous phase partition coefficient (K). The most commonly used partitioning tracers are alcohols of varying chain length, such as 1-butanol, 1-hexanol, 1-heptanol, although SF_6 , a synthetic inert gas, has also been used (Wilson and Mackay, 1995).

The method of moments is used to determine the retardation factor for the partitioning tracer. This method involves calculating the zeroth (m_0) and first (m_1) temporal moments by integrating normalized conservative (c_{cons}) and partitioning (c_{part}) tracer concentrations (C^*) at the extraction well using

$$m_0 = \int C^*(t) dt \quad (2.5)$$

$$m_1 = \int t C^*(t) dt \quad (2.6)$$

The retardation factor (R) is computed using

$$R = \frac{\left(\frac{m_{1,part}}{m_{0,part}} \right)}{\left(\frac{m_{1,cons}}{m_{0,cons}} \right)} \quad (2.7)$$

Table 2.2 Partitioning interwell tracer test (PITT) descriptions.

Test Site	NAPL Type	Partitioning Tracers	Method of Analysis	Authors
laboratory	PCE	2,3-dimethyl-2-butanol	method of moments, numerical simulations	Jin et al. (1995)
Hill AFB, Utah	chlorinated solvents + jet fuel	1-pentanol, hexanol, 2,2-dimethyl-3-pentanol, heptanol, octanol	method of moments	Annable et al. (1998)
Portsmouth, Ohio	TCE, PCE	3-methyl-3-pentanol, hexanol, 2,4-dimethyl-3-pentanol, heptanol	method of moments, numerical simulations	Young et al. (1999)
Jacksonville, Florida	PCE	hexanol, 2,4-dimethyl-3-pentanol, 2-ethyl-1-hexanol	method of moments	Jawitz et al. (2000)
laboratory	TCE, dichloromethane o-dichlorobenzene	SF ₆	method of moments	Wilson and Mackay (1995)
Tucson, Arizona	TCE	SF ₆	method of moments	Nelson and Brusseau (1996)

The partitioning interwell tracer test (PITT) has been used in laboratory and field experiments to obtain DNAPL saturations in the volume of sediment swept by the suite of conservative and partitioning tracers. Jin et al. (1995) presented one of the first studies

of the PITT using PCE-contaminated small-scale sand columns as well as 2-D numerical simulations of the Canadian Air Forces Base Borden aquifer (Table 2.2). The residual PCE saturation calculated compared favorably with residual saturations calculated using pre- and post-contamination mass balances. Furthermore, tests conducted following surfactant remediation of the PCE showed that the PITT could be used to track remediation performance. The numerical simulations involved a complex subsurface system with a stochastic permeability field and multiple stages of PCE release, redistribution under gravity and capillary forces, and a series of PITTs conducted before and after surfactant remediation. The numerical results showed that PITTs could be used to quantify PCE saturation and track remediation. Moreover, the study highlighted the importance of selecting partitioning tracers with a K value such that adequate separation of a partitioning tracer from a conservative tracer is observed without the necessity of pumping a large volume of water from the well to obtain adequate partitioning tracer mass recovery.

Annable et al. (1998) provided results of the first PITT test applied at a field site (Table 2.2). The tests were performed in a 4.3 m (width) by 3.5 m (width) by 6.1 m (depth) test cell that was isolated from the surrounding aquifer by sheet piling and a clay aquitard. The test cell was equipped with injection wells and extraction wells located on opposite sides of the cell. A NAPL saturation of 4.6 % was estimated in the tracer swept region of the test cell. A log-linear extrapolation of the other partitioning tracer data (necessitated due to poor mass recovery) was used to estimate a NAPL saturation of 5.4 %. These results compared favorably with NAPL saturations of 3.0 and 4.6 % from soil cores. In addition, ethanol, pentanol, and hexanol showed evidence of biodegradation during the PITT, showing a potential limitation to using alcohols as partitioning tracers.

The Portsmouth Gaseous Diffusion Plant in Ohio was the site of another field application of the PITT technique (Young et al., 1999; Table 2.2). In this case the PITT results were used in conjunction with planning and analyzing the results of a remedial surfactant flood. Numerical simulations were used to optimize the PITTs in terms of test duration, mass of tracer, injection and extraction rates, and mass recovery estimates. PITTs conducted prior to surfactant flooding were used to determine the average residual DNAPL saturation in the tracer swept zone of the aquifer. Tracer concentrations from monitoring wells set at different depths between the injection and extraction wells showed spatial variability in DNAPL saturations, with an average value of 0.1 to 0.2 %. A post-remediation PITT showed a decrease estimated DNAPL saturation to 0.06 %.

Annable et al. (1998) used an adsorbing interfacial tracer in conjunction with a partitioning alcohol tracer in PITTs to estimate NAPL saturations and NAPL-water interfacial areas. Jawitz et al. (2000) used a series of PITTs to characterize and track the remediation of a PCE contaminated former dry cleaner site (Table 2.2). Wilson and Mackay (1995) conducted tests using sand-packed columns containing DNAPL to investigate SF_6 as a partitioning tracer in the laboratory. Nelson and Brusseau (1996) applied the method at a field site to investigate SF_6 as a detector of TCE saturation, as opposed to quantifying saturation. The results showed the presence of TCE in samples taken from monitoring wells along the tracer flowpath. Further evidence of the presence

of TCE was supported by constant aqueous phase TCE concentrations at the extraction well during the flushing of 71 pore volumes through the tracer swept region of the aquifer.

Although PITTs have been applied with some success, some concerns remain regarding the factors that can influence the efficacy of the tests. A study by Rao et al. (2000) discussed the potential for DNAPL saturation underestimation in PITTs due to 1) constraints on the accessibility of low hydraulic conductivity zones to partitioning tracers, and 2) the effect of nonequilibrium tracer mass transfer between the DNAPL and aqueous phases. These effects are magnified at field sites with low DNAPL saturations, highly heterogeneous physical and DNAPL saturation characteristics, or DNAPL ‘pools’. Tracer breakthrough curves (BTCs) can be highly skewed (i.e., have long ‘tails’) in such situations, which can lead to low tracer mass recoveries and greater errors in DNAPL saturation estimation. A study by Nelson et al. (1999) highlighted the effect of physical and DNAPL heterogeneity and sampling method on PITT results in laboratory flow cell experiments. The flow cell contained two zones of differing permeability and TCE saturation emplaced in a sand matrix. Experimental results showed that the PITT was less effective in characterizing TCE saturation in the zone of lower intrinsic and relative permeability, likely as a result of preferential flow around this zone and nonequilibrium partitioning (i.e., mass transfer limited partitioning). The PITT was especially poor in characterizing TCE saturation from samples taken from vertically-integrated sampling ports, since these ports intercepted a large fraction of streamlines that were not in contact with the TCE-contaminated portions of the test cell. These results gave weight to the argument that the PITT is a better ‘detector’ than ‘quantifier’ of DNAPL saturation.

The PITT is a useful test for detecting and quantifying DNAPL saturation in the subsurface. However, in addition to the issues relating to preferential flow, mass transfer limitations, and DNAPL heterogeneity outlined above, the economic feasibility of conducting multiple PITTs at contaminated sites is hampered by two factors: 1) large volumes of contaminated wastewater are produced, and must be remediated to remove aqueous phase chlorinated solvents and alcohol tracers; and 2) the tests require the installation of at least two pumping wells, plus monitoring wells if desired. Although the PITT can be used to interrogate a much larger volume of aquifer than can be sampled using coring or CPT techniques, it is still a potentially costly and time consuming endeavor. The single-well injection-withdrawal tracer test, or ‘push-pull’ test, offers the ability to conduct more numerous, smaller scale partitioning tracer tests at a lower cost.

PUSH-PULL TESTS

The push-pull test has its origins in the investigation of the mixing of injected water and groundwater for the purposes of artificial groundwater recharge (Sternau et al., 1967). Hoopes and Harleman (1967) investigated dispersion in radial flow from a recharge well. Their study included an analytical solution for a conservative tracer in a homogeneous, isotropic, confined aquifer which was tested against experimental and numerical results. Gelhar and Collins (1971) developed an approximate analytical solution to the advective-dispersive equation in radial coordinates tests whereby longitudinal dispersivity is treated as a variable for nonuniform, steady flow. In this manner conservative tracer data from

the well during the pull phase can be used to determine the longitudinal dispersivity of the aquifer. This approximate solution was later investigated by Schroth et al. (2000) and Davis et al. (2002) using empirically-derived data and numerical simulations (see below and Chapter 2). The application of the push-pull test incorporating reactive, partitioning tracers was investigated by Tomich et al. (1973) for the purposes of determining residual oil saturation in petroleum reservoirs. This application involved a novel technique of injecting a partitioning tracer (ethyl acetate) that hydrolyzed to a conservative tracer (ethanol) in the reservoir. The presence of residual oil saturation was indicated by a delay in the arrival times at the extraction well of the two tracers during the pull phase of the test (incorporating a rest period before the extraction to allow for hydrolysis of ethyl acetate).

Recently the push-pull test has been applied to a variety of environmental topics including: investigating microbial activities in a petroleum contaminated aquifer (Istok et al., 1997); determining first-order reaction rate coefficients (Haggerty et al., 1998); investigating sorption of surfactants to natural aquifer sediment (Istok et al., 1999); and characterizing the solubilization of TCE using surfactant remediation (Field et al., 1999). Additional studies have been published on topics such as: investigating TCE and TCFE transport and anaerobic biotransformation in an aqueous phase TCE contaminated aquifer (Hageman et al., 2001); assessing sulfate reduction in a petroleum-contaminated aquifer using stable sulfur isotopes (Schroth et al., 2000); and investigating the immobilization and remobilization of uranium (Senko et al., 2002).

The use of the push-pull test incorporating a partitioning tracer to quantify DNAPL saturation is a novel application of the methodology. Like the PITT, the partitioning tracer push-pull test has the ability to interrogate larger volumes of an aquifer for DNAPL location and quantification than is typically feasible using traditional coring or CPT methods. However, the push-pull test has advantages over the PITT in terms of reducing costs as a result of: 1) the need for only a single well to conduct a test; 2) the use of smaller volumes of water, with resultant decreases in test water remediation costs; 3) rapidity of test completion, with a single test often requiring less than one day from start to finish; and 4) the ease of conducting a test, since less equipment, and less costly equipment, is required. A potential disadvantage of the push-pull test is the inability to use the method of moments to estimate retardation and NAPL saturation.

Unlike the PITT, the push-pull test utilizes a single well for both the injection and extraction phases of the test. A specified volume of test solution containing known concentrations of both conservative (e.g., bromide) and partitioning tracers (e.g., alcohols) is injected into the subsurface through a well at a specified flowrate. During the injection or push phase of the test the solution is transported radially outward from the well in a nonuniform flow field to a radial distance that is a function of the volume of solution injected, aquifer thickness, effective porosity of the aquifer, and the well radius (Figure 2.2). The test solution can be injected across the entire well screen or through a selected screen interval through the use of inflatable straddle packers. The conservative tracer will be transported at the pore water velocity, while the partitioning tracer (in the presence of DNAPL) will be transported at a lesser velocity due to partitioning between

the aqueous and DNAPL phases. The injection solution interrogates an approximately cylindrical volume of aquifer; however, the exact shape of the interrogated region is a function of aquifer heterogeneities (e.g., heterogeneity in hydraulic conductivity), DNAPL saturation heterogeneities (e.g., heterogeneity in relative permeability), and the injection rate (which can affect the dispersion of the tracer front).

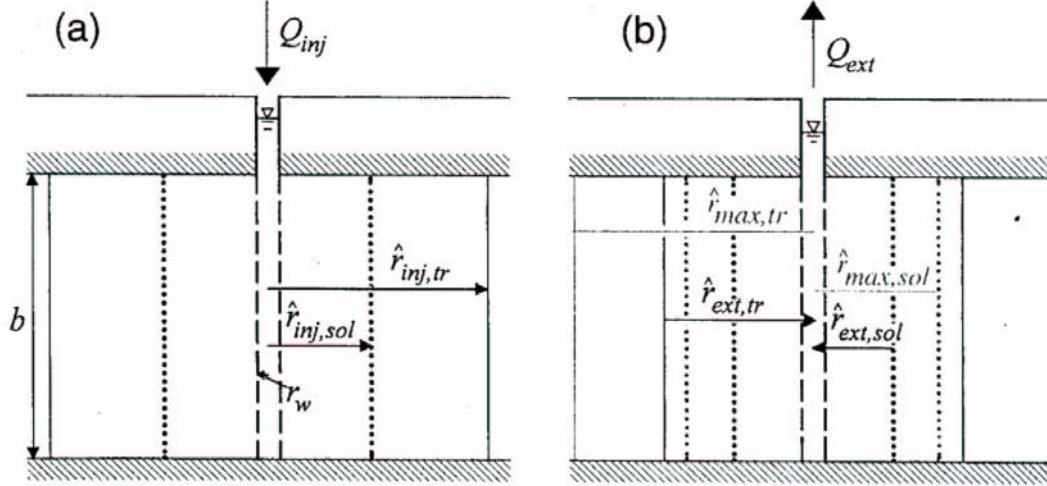


Figure 2.2 Radial positions of conservative (r_{tr}) and partitioning tracers (r_{sol}) during the injection phase (inj), at the end of the injection phase (max), and during the extraction (ext) phases. Well radius is denoted by r_w , and Q is pumping rate (Schroth et al., 2000).

The pull phase begins upon the completion of the push phase, reversing the nonuniform flow field and causing the injected tracers, which are now mixed with groundwater, to flow back toward the well (Figure 2.2). Tracer samples are taken at the extraction well during the pull phase of the test. Again, the partitioning tracer will be transported at less than the pore water velocity due to partitioning. Unlike a PITT, however, the conservative and partitioning tracers arrive simultaneously at the well; this means that partitioning tracer retardation is not manifested in a delay in arrival time of the partitioning tracer vs. the conservative tracer (Schroth et al., 2000). The manner in which retardation is manifested is a function of the dispersion coefficient (D), which is described by

$$D = \alpha_L v \quad (2.8)$$

where α_L is dispersivity (assumed to be constant) and v is pore water velocity. In nonuniform flow the pore water velocity (v) is a function of radial distance from the well (r) as described by (Schroth et al., 2000)

$$v(r) = \frac{Q}{2\pi r b n R} \quad (2.9)$$

where Q is pumping rate, b is aquifer thickness, n is porosity, and R is the retardation factor (equation 2.4). For the partitioning tracer $R > 1$, resulting in a decreased velocity.

This results in the partitioning tracer undergoing greater dispersion than the conservative tracer due to its longer residence time in the higher velocity region near the well. The effect of greater dispersion on the partitioning tracer is evident in a pull phase concentration times series, or breakthrough curve (BTC) plot of the conservative ($R = 1$) and partitioning tracers ($R > 1$) as shown in a numerical simulation of injected tracers using the Subsurface Transport Over Multiple Phases (STOMP) code (Figure 2.3). Note that C is normalized concentration and V_e/V_i is dimensionless time, where V_e is the volume extracted at the time a sample was obtained during the pull phase and V_i is the total volume injected during the push phase.

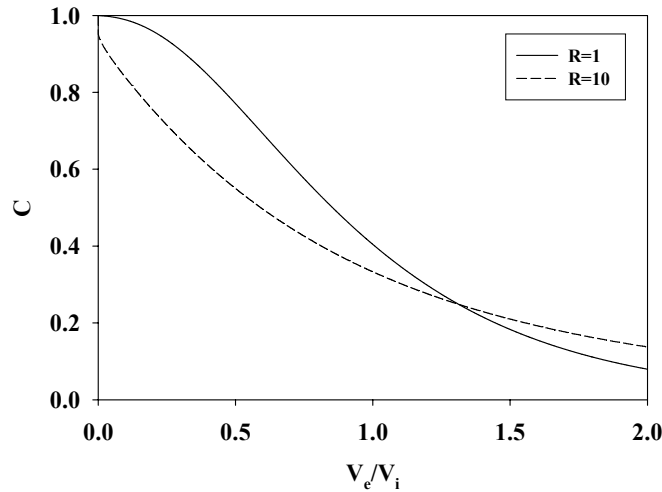


Figure 2.3 BTCs for conservative ($R = 1$) and partitioning ($R > 1$) tracers, showing greater dispersion of the partitioning tracer in the presence of DNAPL.

Assuming linear equilibrium partitioning, equation 2.10 can be used to calculate the DNAPL saturation if the partition coefficient (K) and retardation factor (R) are known:

$$S_n = \frac{R - 1}{R + K - 1} \quad (2.10)$$

However, R must be estimated from the dispersion of the partitioning tracer BTC relative to the conservative tracer BTC in order to calculate a value for DNAPL saturation (see Chapters 2, 3, and 4).

The reliable estimation of R is therefore a critical step in quantifying S_n . Schroth et al. (2000) conducted an investigation of a simplified approach to estimating retardation factors for partitioning tracers during the pull phase of push-pull tests. This approach built upon the approximate analytical solutions developed by Gelhar and Collins (1971) and was tested against numerical simulations for ideal and nonideal conditions, the latter utilizing a Langmuir isotherm for nonlinear equilibrium conditions and first-order mass transfer coefficients for linear nonequilibrium conditions. Also, linear equilibrium simulations were performed using a physically heterogeneous aquifer in 2-D. A data set of ^{131}I (conservative) and ^{85}Sr (partitioning) tracers from a radial injection dual-tracer test

conducted by Pickens et al. (1981) was used to investigate the approximate solution in a field application.

The linear equilibrium simulations revealed that the approximate solution provided a good estimate of R at low values of R , but that the estimate was less reliable as R increased. The decrease in reliability is due to the fact that the approximate solution is accurate only if (Schroth et al., 2000)

$$\left(\frac{\alpha_L}{L_o}\right)^{\frac{1}{2}} \ll 1 \quad (2.11)$$

where α_L is dispersivity and L_o is the total radial distance traveled by the partitioning tracer solute front ($L_o = 2r_{max}$). Assuming that α_L is constant, as R increases, L_o decreases and the likelihood of violating equation 2.11 becomes greater. Thus for solutes with greater values of K , or for systems with greater S_n , the radial distance L_o must be increased (i.e., a longer push phase) in order for the approximate solution to provide a reliable estimate of R . The effect of varying porosity and aquifer thickness on R was also investigated and found to be minimal since both the retarded and conservative solutes are equally affected by changes in these parameters. Overall, the approximate solution revealed errors $\leq 14\%$ between estimated and simulated R values for values ranging from 1 to 100 where equation 2.11 was not violated. The approximate solution was found to provide poor estimates of R under conditions of nonlinear equilibrium and linear nonequilibrium sorption. However, a general trend was found where the partitioning tracer BTC crossed the conservative tracer BTC at greater values of dimensionless time (V_e/V_i) as 1) concentration increased in nonlinear equilibrium conditions, and 2) the mass transfer coefficient decreased in linear nonequilibrium conditions. Thus the push-pull test may serve to qualitatively indicate the existence of nonideal transport (e.g., mass transfer limited partitioning) in aquifers. In the 2-D simulations the presence of heterogeneity in hydraulic conductivity resulted in the approximate solution seriously underpredicting R , largely as a result of the spatial variability in dispersion due to the velocity differences between layers of varying hydraulic conductivity. The field application of the method to the data set of Pickens et al. (1981) resulted in an estimated $R = 11.4$ for the retarded tracer (^{85}Sr). Using the provided values of porosity and bulk density, a solid:aqueous phase partition coefficient (K_d) = 2.33 mL/g was calculated, which closely matched the values measured by Pickens et al. (1981). This showed the ability of the approximate solution to accurately estimate R in a field application. Schroth et al. (2000) concluded that the push-pull test and approximate solution could provide reasonably accurate estimates of R under certain aquifer and test conditions.

A recent article by Istok, Field, Schroth, Davis, and Dwarakanath (2002) investigated the ability of the push-pull test method to quantify NAPL saturation in laboratory and field applications. In this study the partitioning tracer push-pull test method was combined with the use of conservative and partitioning alcohols. 1-pentanol was used as the conservative tracer, while 1-hexanol, 1-heptanol, and 2-ethyl-1-hexanol were used as the partitioning tracers. The laboratory tests were conducted in a TCE-contaminated physical

aquifer model (PAM) described in Chapter 2, with samples being obtained during the push phase (from sampling ports along the long axis of the PAM) and the pull phase (from a sampling port at the injection/extraction well). Field tests were conducted in a LNAPL contaminated aquifer at a former petroleum refinery. The experimental results were numerically simulated in order to estimate a value for R and calculate S_n (equation 2.10).

Results from a laboratory test performed in the PAM prior to TCE contamination showed slight sorption of the partitioning tracers to the sediment, while the tests performed in the contaminated PAM showed clear evidence for much greater retardation due to partitioning into TCE. The simulations provided good fits to the 1-pentanol and 1-hexanol data at the sampling ports, with the sorption-adjusted $R = 1.3$ yielding a calculated $S_n = 1.6$. This value is in agreement with the estimated $S_n = 2\%$ in the PAM. However, the simulation fits were poor for 1-heptanol and 2-ethyl-1-hexanol at the sampling ports due to BTC tailing, with calculated values of $S_n = 1.7$ for 1-heptanol and 0.7 for 2-ethyl-1-hexanol. The pull phase data were also poorly fit by the simulations, with evident tailing of the BTCs. This is possibly due to rate limited mass transfer between the aqueous and DNAPL phases. Another test was conducted at a lower flowrate to reduce the effects of mass transfer limitation. Interestingly, the simulations failed to provide better fits to the data in this test. Tailing of BTCs was evident in the push and pull phases, with calculated values of S_n increasing vs. the previous test and ranging from 1.1 to 4.7%. The increased values possibly reflect a decrease in the effects of rate limited mass transfer of the partitioning tracer as a result of the lower flowrate. The field test resulted in a calculated S_n ranging from 1.4 to 2.0%, which is in agreement with previously determined S_n values ranging from 1.7 to 2.1% from PITTs, sediment coring, and CPT tests conducted at the site.

This study showed that the push-pull test could be applied in laboratory and field settings using injected partitioning tracers (i.e., alcohols). In the field tests, costs were reduced in terms of time, equipment needs, and wastewater treatment relative to PITTs conducted at the site. Also, large volumes of the aquifer were interrogated relative to the volumes interrogated using coring and CPT methods. However, the use of an alcohol tracer is a potential hindrance to this method since regulatory approval may be required to use these tracers in the field.

RADON AS AN IN SITU PARTITIONING TRACER

The use of in situ partitioning tracers in push-pull tests provides a way to avoid the potential regulatory hurdle. Radon is well suited to serve as an in situ partitioning tracer. Radon (atomic number 86, chemical symbol: Rn) is the largest of the Group VIII noble gases, and is chemically inert due to the complete filling of its electron valence shells: $[\text{Xe}]4f^{14}5d^{10}6s^2p^6$. It is nonreactive and does not form an ionized or solid phase at earth surface temperatures and pressures. Radon is part of the uranium/thorium decay series. Like all elements with an atomic number > 82 , the radon nucleus is unstable and undergoes radioactive decay. There are three naturally occurring radon isotopes: ^{222}Rn , originating from ^{238}U ; ^{224}Rn , originating from ^{232}Th , and ^{219}Rn , originating from ^{235}U . Since ^{238}U is the most abundant of the three parents, ^{222}Rn (hereafter referred to as radon)

is the most abundant of the three isotopes. The relatively long half-life of radon (3.83 days) results in its being commonly found in the vadose and saturated zones. It is continuously produced in the subsurface via the α -decay of its parent, radium-226 (half-life of 1600 years) that is contained within the structure of aquifer minerals and/or exists as secondary mineral coatings. Radon is released (i.e., emanated) from the aquifer matrix via α -decay. The mechanism for the emanation of radon from solids is understood to involve a combination of (Rama and Moore, 1984; Semkow and Parekh, 1990; Maraziotis, 1996): 1) direct recoil of the radon atom from the solid surface to the pore fluid; 2) diffusion of the radon atom from the crystal lattice of the mineral to the grain surface; and 3) recoil of the radon atom within the crystal lattice to a dislocation plane or connected intragranular pore and diffusion to the grain surface. The emanation power is the fraction of radon produced that escapes from the solids into the pore water. Radon emanation is expressed in terms of pCi (1 pCi = 2.22 disintegrations per minute, or DPM) of radon emanated per unit mass (kg) of sediment. Radon that migrates to the pore water is available for measurement through aqueous sampling. Aqueous radon concentrations are expressed in pCi/L of water.

Radon is constantly emanating from radium-bearing aquifer solids and is also constantly decaying; thus the radon concentration in the pore water is determined by the secular equilibrium between radon emanation and decay as described by (Adloff and Guillaumont, 1993)

$$C_{Rn} = C_{Rn,\infty} (1 - e^{-kt}) + C_{Rn,0} e^{-kt} \quad (2.12)$$

where C_{Rn} is the radon concentration (pCi/L) in the pore water at time t , $C_{Rn,\infty}$ is the equilibrium radon concentration, $C_{Rn,0}$ is the radon concentration in the pore water at the time the water is removed from the pore, and k is radon's decay constant (0.181 days^{-1}). The secular equilibrium radon concentration is reached when the rate of radon emanation is equal to the rate of radon decay. Using radon's decay constant and equation 2.12, it can be shown that 25 days are required for a parcel of radon-free water to obtain a radon concentration that is 99 % of the equilibrium radon concentration. The equilibrium radon concentration is also a function of the bulk density and porosity of the aquifer. Thus the equilibrium radon concentration can be described by (Semprini et al., 2000)

$$C_{Rn} = \frac{C_{Ra} E_p \rho_b}{n} \quad (2.13)$$

where C_{Ra} is the radium concentration in the aquifer solids (pCi/kg), E_p is emanation power, ρ_b is bulk density, and n is porosity. Radon is moderately volatile, with a dimensionless Henry's coefficient of 3.9 (pCi/L_{air} / pCi/L_{water}) at 20° C (Clever, 1979).

The environmental occurrence and behavior of radon has been investigated in numerous studies across a wide range of disciplines. Radon has been used to investigate: the thermodynamic, geologic and transport properties of geothermal reservoirs (Semprini, 1986); groundwater recharge rates (Hamada and Komae, 1998); groundwater residence times (Snow and Spalding, 1997); and groundwater discharge to the ocean (Cable et al., 1996). Additional studies have been performed using radon to: quantify groundwater flow rates in fractured bedrock aquifers (Cook et al., 1999); to investigate surface water

mixing with groundwater (Bertin and Bourg, 1994); and to infer the bedrock geology underlying Quaternary aquifers (Morland et al., 1998). However, fewer studies have been performed relating to the phase partitioning behavior of radon. The ability of radon to partition from the aqueous phase into the DNAPL phase makes radon a candidate for locating and quantifying DNAPL contamination in the subsurface.

Steady-State Partitioning Theory

Semprini et al. (2000) presents the equations describing steady-state or equilibrium radon partitioning in the presence of DNAPL (these equations also apply to LNAPLs). Radon has an affinity for partitioning into DNAPL; the linear partition coefficient (K) for radon is described by

$$K = \frac{C_n}{C_{w,n}} \quad (2.14)$$

where C_n is the concentration of radon in the DNAPL phase, and $C_{w,n}$ is the concentration of radon in the aqueous phase in the presence of DNAPL. A value of $K = 50$ for radon in the presence TCE was determined using the methodology of Cantaloub (2001) as described in Appendix III.

The steady-state or ‘static’ method involves calculating DNAPL saturations from a comparison of radon concentrations in groundwater samples obtained from DNAPL-contaminated and non-contaminated portions of the same aquifer. This method assumes secular equilibrium between radon emanation and decay, equilibrium radon partitioning between the water and DNAPL phases, and a constant background radon concentration. In the presence of DNAPL, radon will be distributed between the water and DNAPL phases as described by

$$C_n S_n + C_{w,n} S_w = \frac{C_{Ra} E_p \rho_b}{n} \quad (2.15)$$

Assuming linear equilibrium radon partitioning of radon between DNAPL and water, equation 2.15 can be rearranged as

$$C_{w,n} = \frac{C_{Ra} E_p \rho_b / n}{1 + S_n (K - 1)} \quad (2.16)$$

which can be further rearranged to solve for the DNAPL saturation

$$S_n = \left(\frac{C_{w,bkg}}{C_{w,n}} - 1 \right) \left(\frac{1}{(K - 1)} \right) \quad (2.17)$$

where $C_{w,bkg}$ (the equivalent of C_{Rn} in equation 2.13) is the radon concentration in groundwater in a ‘background’ zone outside of the DNAPL contaminated zone or in the aquifer before DNAPL contamination has occurred. The sensitivity of radon to small DNAPL saturations is evident when equation 2.16 is used to plot radon concentration as a function of S_n (Figure 2.4).

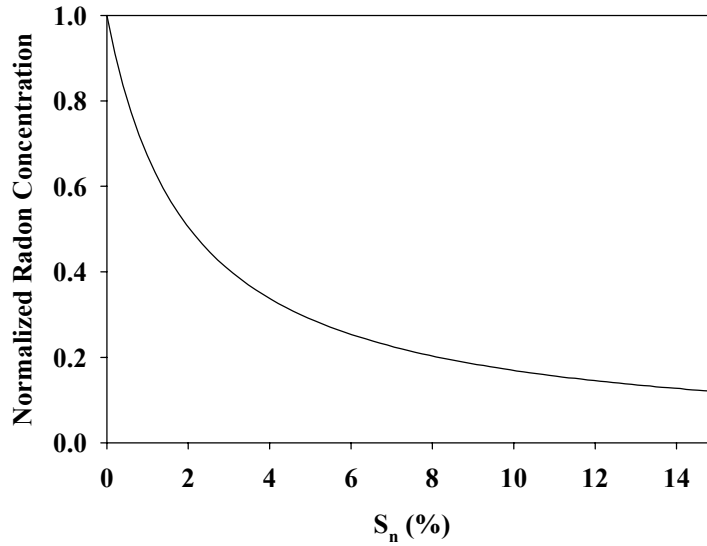


Figure 2.4 Normalized radon concentration vs. S_n using $K = 50$ for TCE.

The plot shows that radon concentrations are sensitive to changes in S_n , especially at smaller values of S_n . Thus radon has the potential to quantify DNAPL saturations and changes in saturations, with greater efficacy at smaller saturations. Also, radon's short half-life and constant emanation from aquifer solids result in rapid re-equilibration of radon concentrations in pore water following changes in DNAPL saturation.

Dynamic Partitioning Theory

Semprini et al. (2000) also developed a 1-D advective-dispersive equation to describe radon transport (i.e., dynamic partitioning) in a DNAPL-contaminated matrix. The final form of this 1-D equation, incorporating radon transport, linear equilibrium partitioning as described by equation 2.4, emanation, and decay, is

$$\frac{\partial C_{w,n}}{\partial t} = \frac{1}{S_w n R} \left[\frac{D n S_w \partial^2 C_{w,n}}{\partial x^2} - v \frac{\partial C_{w,n}}{\partial x} + E \lambda \rho_b \right] - \lambda C_{w,n} \quad (2.18)$$

where $E = E_p \times C_{Ra}$ and λ is the first-order decay rate for radon ($0.00754 \text{ hours}^{-1}$). This equation can be solved numerically using a finite difference technique to show temporal and spatial changes in radon concentration (Tasker, 1995). Equation 2.18 reduces to equation 2.16 under steady-state conditions. The steady-state and dynamic partitioning equations have been investigated in laboratory and field settings to determine the efficacy the method for locating and quantifying DNAPL contamination.

Radon as an Indicator of DNAPL Contamination

The static and dynamic methods have been investigated in the laboratory (Hopkins, 1995; Gottipati, 1996; Semprini et al., 1998, 2000) and in the field (Semprini et al., 1993, 1998, 2000; Hunkeler et al., 1997). Hopkins (1995) performed column studies using aquifer solids from the Canadian Air Forces Base Borden and Soltrol 200[®] as a NAPL. The

columns were constructed with residual NAPL saturations of 0 to 8 % and were allowed 2-4 weeks for radon concentrations to reach equilibrium. After equilibration the columns were exchanged with radon-free water and the radon concentrations measured at the column outlet. Numerical simulations were performed for each column test and the results plotted as a function of the volume exchanged in the column. The results showed an inverse relationship between the maximum NAPL saturation in the column and the maximum radon concentration measured at the outlet. In addition, as NAPL saturation increased, so did the volume of radon-free water required for the outlet concentration to reach a radon concentration = 0 pCi/L. This is due to retarded transport of radon-free water. These results are in agreement with the steady-state and dynamic equations presented above. Numerical simulations provided good fits to the experimental data.

Gottipati (1996) constructed soil columns containing sand and residual NAPL saturations ranging from 0 to 8 % using Soltrol 220[®] which were then remediated using a surfactant (Triton[®] X-100). The columns were constructed to contain 1, 5, and 8 % residual NAPL saturation and were flushed with sequential batches of surfactant to solubilize and remove the NAPL from the columns. Outlet radon concentrations were tracked to investigate the influence of NAPL solubilization and removal on the changes in the radon BTC (as defined by the “breakthrough” concentration of 0.5 when normalized to the initial radon concentration in the columns). The results showed that after surfactant remediation 1) the maximum measured radon concentrations in the columns increased, and 2) the time to the “breakthrough” concentration decreased. Thus the change in NAPL saturation in the columns was reflected in the behavior of the partitioning radon tracer, showing that radon could be used to track changes in NAPL saturation during remediation. Further evidence of the ability of radon to track changes in DNAPL saturation in PAMs using surfactant flooding was presented by Semprini et al. (1998). Using the static partitioning method, these experiments showed that radon concentrations in the contaminated portion of the PAM decreased after TCE contamination. Radon samples taken after surfactant remediation showed little change from pre-remediation samples, which was consistent with a mass balance on TCE recovered from the injection/extraction well showing that insufficient TCE had been removed to cause a change in radon concentrations.

Semprini et al. (1993; 2000) conducted two field applications of the methodologies at the Canadian Air Forces Base Borden. The first test involved the release of a mixed DNAPL (trichloromethane, trichloroethene, and tetrachloroethene) source into a shallow sand aquifer. The mixture was allowed to slowly dissolve under natural gradient conditions. Radon samples were obtained upgradient, within, and downgradient of the DNAPL source zone. The radon concentrations in the DNAPL zone decreased by a factor of 2 to 3 vs. the upgradient zone, and rebounded to upgradient zone concentrations within a few meters of the source zone. A numerical simulation of the experimental data (using equation 2.18) showed good agreement between the data sets, with a DNAPL saturation of 4.5 % predicted by the simulation (the measured DNAPL saturation was 3.8 %). A second experiment was performed in a physically isolated test cell at the site in which 5 L of DNAPL was injected. The DNAPL was allowed to distribute itself in the test cell, forming an irregular DNAPL zone. Injection and extraction wells at opposite ends of the test cell created a groundwater velocity of 10.1 cm/day within the test cell. Steady-state

radon concentrations were obtained by allowing the flow to continue for 1 month prior to radon sampling. Radon samples were then obtained at sampling wells upgradient and downgradient of the DNAPL source. The experimental data showed the presence of a DNAPL source between 0.5 and 1 m in length, with a residual DNAPL saturation of 4.5 to 7.8 %. Numerical simulations were found to be in good agreement with the experimental data. Excavation of the test cell later confirmed the presence of DNAPL in the predicted location. These studies showed that radon could be applied as a partitioning in situ tracer in the field to locate and quantify DNAPL saturation.

Hunkeler et al. (1997) performed a laboratory and field study of the method at a diesel fuel (LNAPL)-contaminated site in central Switzerland. The partition coefficient (K) for radon in diesel fuel was determined 1) using bottles containing tap water and diesel fuel, yielding a $K = 40$, and 2) in batch experiments with sand-filled separatory funnels containing varying saturations of diesel fuel and tap water, yielding $K = 45$. Two columns in series were used to model radon partitioning in an aquifer, with the first column containing clean sand and the second column containing diesel fuel. Flow rates were adjusted such that steady-state radon concentrations were achieved as the radon left the first column, thus providing a source of radon-equilibrated water for the second (contaminated) column. The calculated LNAPL saturation in the column was 1.0 %, which was in good agreement with the actual measured value of 1.4 %. The field experiment involved sampling radon concentrations under natural gradient conditions in monitoring wells upgradient and downgradient from a diesel LNAPL contamination zone in a shallow sandy aquifer. Nearly all wells containing aqueous phase hydrocarbons showed a decrease in radon concentrations relative to background concentrations. A LNAPL saturation of 1.5 % was calculated using the radon data, using $K = 45$ from the batch experiments. This value was in agreement with the value of 1.9 % measured in a core sample taken from the contaminated zone.

Semprini et al. (1998) provided further evidence for the field applicability of the method at a LNAPL and DNAPL-contaminated site at Lawrence Livermore National Laboratory. Radon samples were obtained from 17 monitoring wells at the site, with concentrations varying from 8 to > 1500 pCi/L. Since the background radon concentration was estimated to be 820 pCi/L (based on sediment emanation studies), it was likely that radon samples with concentrations well below background values were obtained from NAPL-bearing zones of the aquifer. Very low radon concentrations were measured in locations where diesel and TCE were known to have spilled. Moreover, high radon concentrations were measured in locations with high aqueous TCE concentrations, providing evidence for the transport of aqueous TCE away from a DNAPL source zone. Thus the method was able to provide evidence for both the presence of DNAPL in one location and the absence of DNAPL in a second location.

REFERENCES

Adloff, J. and R. Guillaumont, 1993. Fundamentals of Radiochemistry. CRC Press, Boca Raton, FL.

- Annable, M.D., P.S.C. Rao, K. Hatfield, W.D. Graham, A.L. Wood, and C.G. Enfield, 1998. Partitioning tracers for measuring residual NAPL: field-scale test results. *Journal of Environmental Engineering*, 124:498-503.
- Bedient, P.B., H.S. Rifai, and C.J. Newell, 1994. Ground Water Contamination. Prentice-Hall, Englewood Cliffs, NJ.
- Bernat, M. and T.M. Church, 1989. Handbook of Environmental Isotope Geochemistry. P. Fritz and J. Ch. Fontes, Eds. Elsevier Scientific Publishing, New York, NY.
- Bertin, C. and A.C.M. Bourg, 1994. Radon-222 and chloride as natural tracers of the infiltration of river water into an alluvial aquifer in which there is significant river/groundwater mixing. *Environmental Science & Technology*, 28:794-798.
- Broholm, K., S. Feenstra, and J.A. Cherry, 1999. Solvent release into a sandy aquifer. 1. Overview of source distribution and dissolution behavior. *Environmental Science & Technology*, 33:681-690.
- Cable, J.E., G.C. Bugna, W.C. Burnett, and J.P. Chanton, 1996. Application of ^{222}Rn and CH_4 for assessment of groundwater discharge to the coastal ocean. *Limnology and Oceanography*, 41:1348-1353.
- California EPA, 2002. Office of Environmental Health Hazard Assessment, Safe Drinking Water and Toxic Enforcement Act of 1986 (Proposition 65) List of Chemicals Known to the State to Cause Cancer or Reproductive Toxicity, CAS Number 79016.
- Cantaloub, M., 2001. Aqueous-organic partition coefficients for radon-222 and their application to radon analysis by liquid scintillation methods. Master's Thesis, Oregon State University.
- Clever, H.L. (Ed.), 1979. Krypton, Xenon, and Radon: Gas Solubilities, Solubility Data Series Volume 2. Pergamon Press, New York, NY.
- Cohen, R.M. and J.W. Mercer, 1993. DNAPL Site Evaluation. CRC Press, Boca Raton, FL.
- Cook, P.G., A.J. Love, and J.C. Dighton, 1999. Inferring ground water flow in fractured rock from dissolved radon. *Ground Water*, 37:606-610.
- Davis, B.M., J.D. Istok, and L. Semprini, 2002. Push-pull partitioning tracer tests using radon-222 to quantify non-aqueous phase liquid contamination. *Journal of Contaminant Hydrology*, 58:129-146.
- Domenico, P.A. and F.W. Schwartz, 1998. Physical and Chemical Hydrogeology (2nd ed.). John Wiley & Sons, New York, NY.
- Dwarakanath, V., N. Deeds, and G.A. Pope, 1999. Analysis of partitioning interwell tracer tests. *Environmental Science & Technology*, 33:3829-3836.
- EPA, 2002. Office of Pollution Prevention and Toxics, HPV Challenge Program Chemical List.
- Fetter, C.W., 1999. Contaminant Hydrogeology (2nd ed.). Prentice-Hall, Upper Saddle River, NJ.
- Field, J.A., J.D. Istok, M.H. Schroth, T.E. Sawyer, and M.D. Humphrey, 1999. Laboratory investigation of surfactant-enhanced trichloroethene solubilization using single-well, "push-pull" tests. *Ground Water*, 37:581-588.
- Gelhar, L.W. and M.A. Collins, 1971. General analysis of longitudinal dispersion in nonuniform flow. *Water Resources Research*, 7:1511-1521.

- Gottipati, S., 1996. Radon-222 as a tracer for performance assessment of NAPL remediation technologies in the saturated zone: an experimental investigation. Master's Thesis, Oregon State University.
- Griffin, T.W. and K.W. Watson, 2002. A comparison of field techniques for confirming dense nonaqueous phase liquids. *Ground Water Monitoring & Remediation*, 22:48-59.
- Hageman, K.J., J.D. Istok, J.A. Field, T.E. Buscheck, and L. Semprini, 2001. In situ anaerobic transformation of trichlorofluoroethene in trichloroethene-contaminated groundwater. *Environmental Science & Technology*, 35:1729-1735.
- Haggerty, R., M.H. Schroth, and J.D. Istok, 1998. Simplified method of "push-pull" test data analysis for determining in situ reaction rate coefficients. *Ground Water*, 36:314-324.
- Hamada, T. and T. Komae, 1998. Analysis of recharge by paddy field irrigation using ^{222}Rn concentration in groundwater as an indicator. *Journal of Hydrology*, 205:92-100.
- Hoopes, J.A. and D.R.F. Harleman, 1967. Dispersion in radial flow from a recharge well. *Journal of Geophysical Research*, 72:3595-3607.
- Hopkins, O.S., 1995. Radon-222 as an indicator for nonaqueous phase liquids in the saturated zone: developing a detection technology. Master's Thesis, Oregon State University.
- Hunkeler, D., E. Hoehn, P. Höhener, and J. Zeyer, 1997. ^{222}Rn as a partitioning tracer to detect diesel fuel contamination in aquifers: laboratory study and field observations. *Environmental Science & Technology*, 31:3180-3187.
- Istok, J.D., M.D. Humphrey, M.H. Schroth, M.R. Hyman, and K.T. O'Reilly, 1997. Single-well, "push-pull" test for in situ determination of microbial activities. *Ground Water*, 35:619-631.
- Istok, J.D., J.A. Field, M.H. Schroth, T.E. Sawyer, and M.D. Humphrey, 1999. Laboratory and field investigation of surfactant sorption using single-well, "push-pull" tests. *Ground Water*, 37:589-598.
- Istok, J.D., J.A. Field, M.H. Schroth, B.M. Davis, and V. Dwarakanath, 2002. Single-well, "push-pull" partitioning tracer test for NAPL detection in the subsurface. *Environmental Science & Technology*, 36:2708-2716.
- Jawitz, J.W., R.K. Sillan, M.D. Annable, P.S.C. Rao, and K. Warner, 2000. In-situ alcohol flushing of a DNAPL source zone at a dry cleaner site. *Environmental Science & Technology*, 34:3722-3729.
- Jin, M., M. Delshad, V. Dwarakanath, D.C. McKinney, G.A. Pope, K. Sepehrnoori, and C.E. Tilburg, 1995. Partitioning tracer test for detection, estimation, and remediation performance assessment of subsurface nonaqueous phase liquids. *Water Resources Research*, 31:1201-1211.
- Kram, M.L., A.A. Keller, J. Rossabi, and L.G. Everett, 2001. DNAPL characterization methods and approaches, part 1: performance comparisons. *Ground Water Monitoring & Remediation*, 21:109-123.
- Maraziotis, E.A., 1996. Effects of intraparticle porosity on the radon emanation coefficient. *Environmental Science & Technology*, 30:2441-2448.

- Mercer, J.W. and R.M. Cohen, 1990. A review of immiscible fluids in the subsurface: properties, models, characterization and remediation. *Journal of Contaminant Hydrology*, 6:107-163.
- Morland, G., T. Strand, L. Furuhaug, H. Skarphagen, and D. Banks, 1998. Radon in quaternary aquifers related to underlying bedrock geology. *Ground Water*, 36:143-146.
- Nelson, N.T. and M.L. Brusseau, 1996. Field study of the partitioning tracer method for detection of dense nonaqueous phase liquid in a trichloroethene-contaminated aquifer. *Environmental Science & Technology*, 30:2859-2863.
- Nelson, N.T., M. Oostrom, T.W. Wietsma, and M.L. Brusseau, 1999. Partitioning tracer method for the in situ measurement of DNAPL saturation: influence of heterogeneity and sampling method. *Environmental Science & Technology*, 33:4046-4053.
- Pickens, J.F., R.E. Jackson, K.J. Inch, and W.F. Merritt, 1981. Measurement of distribution coefficients using a radial injection dual-tracer test. *Water Resources Research*, 17:529-544.
- Rama and W.S. Moore, 1984. Mechanism of transport of U-Th series radioisotopes from solids into ground water. *Geochimica et Cosmochimica Acta*, 48:395-399.
- Rao, P.S.C., M.D. Annable, and H. Kim, 2000. NAPL source zone characterization and remediation technology performance assessment: recent developments and applications of tracer techniques. *Journal of Contaminant Hydrology*, 45:63-78.
- Schroth, M.H., J.D. Istok, and R. Haggerty, 2000. In situ evaluation of solute retardation using single-well push-pull tests. *Advances in Water Resources*, 24:105-117.
- Schwille, F., 1988. Dense Chlorinated Solvents in Porous and Fractured Media. Lewis Publishers, Chelsea, MI.
- Semkow, T.M. and P.P. Parekh, 1990. The role of radium distribution and porosity in radon emanation from solids. *Geophysical Research Letters*, 17:837-840.
- Semprini, L., 1986. Modeling and field studies of radon-222 in geothermal reservoirs. Ph.D. Dissertation, Stanford University.
- Semprini, L., K. Broholm, and M. McDonald, 1993. Radon-222 deficit for locating and quantifying NAPL contamination in the subsurface. *EOS Transactions American Geophysical Union*, 76:F276.
- Semprini, L., M. Cantaloub, S. Gottipati, O. Hopkins, and J. Istok, 1998. Radon-222 as a tracer for quantifying and monitoring NAPL remediation. In: *Nonaqueous-Phase Liquids*, G.B. Wickramanayake and R.E. Hinchey (Eds.). Battelle Press, Columbus, OH.
- Semprini, L., O.S. Hopkins, and B.R. Tasker, 2000. Laboratory, field and modeling studies of radon-222 as a natural tracer for monitoring NAPL contamination. *Transport in Porous Media*, 38:223-240.
- Senko, J.M., J.D. Istok, J.M. Suflita, and L.R. Krumholz, 2002. In-situ evidence for uranium immobilization and remobilization. *Environmental Science & Technology*, 36:1491-1496.
- Snow, D.D. and R.F. Spalding, 1997. Short-term aquifer residence times estimated from ²²²Rn disequilibrium in artificially recharged ground water. *Journal of Environmental Radioactivity*, 37:307-325.

- Sternau, R., J. Schwarz, A. Mercado, Y. Harpaz, A. Nir, and E. Halevy, 1967. Radioisotope tracers in large-scale recharge studies of groundwater. Proceedings of the symposium on isotopes in hydrology, International Atomic Energy Agency in cooperation with the International Union of Geodesy and Geophysics, Vienna, Austria, November 14-18, 1967.
- Tasker, B.R., 1995. Radon-222 as an indicator for nonaqueous phase liquids in the saturated zone: a numerical methods analysis. Master's Engineering Report, Oregon State University.
- Tomich, J.F., R.L. Dalton, H.A. Deans, and L.K. Shallenberger, 1973. Single-well tracer test method to measure residual oil saturation. *Journal of Petroleum Technology*, Feb. 1973:211-218.
- Wilson, R.D. and D.M. Mackay, 1995. Direct detection of residual nonaqueous phase liquid in the saturated zone using SF₆ as a partitioning tracer. *Environmental Science & Technology*, 29:1255-1258.
- Young, C.M., R.E. Jackson, M. Jin, J.T. Londergan, P.E. Mariner, G.A. Pope, F.J. Andrews, and T. Houk, 1999. Characterization of a TCE DNAPL zone in alluvium by partitioning tracers. *Ground Water Monitoring & Remediation*, 19:84-94.

3. PUSH-PULL PARTITIONING TRACER TESTS USING RADON-222 TO QUANTIFY NONAQUEOUS PHASE LIQUID CONTAMINATION

INTRODUCTION

Non-aqueous phase liquids (NAPLs) are common groundwater contaminants at hazardous waste sites (Mercer and Cohen, 1990; Cohen and Mercer, 1993). Due to their high toxicity and low solubility in water, NAPLs can become long-term sources for dissolved contaminants in groundwater. Thus effective remediation requires the accurate location and quantification of NAPL saturations in the subsurface. This is particularly true for dense non-aqueous phase liquids (DNAPLs) because their high density causes them to migrate below the water table and move along pathways distinct from water flow (Schwille, 1988; Nelson and Brusseau, 1996).

A number of methods have been employed to characterize NAPL distribution at contaminated sites including soil coring, cone penetrometer testing, soil gas analysis, and aqueous phase sampling. However, these methods can be costly and they typically interrogate relatively small aquifer volumes. Partitioning tracers including alcohols (e.g., 1-heptanol, 1-hexanol) and synthetic inert gases (i.e., SF₆) have been used to locate and quantify NAPL contamination in a variety of laboratory and field experiments (Jin et al., 1995; Wilson and Mackay, 1995; Nelson and Brusseau, 1996; Annable et al., 1998; Nelson et al., 1999; Young et al., 1999). In this approach, retardation factors for injected partitioning tracers are determined by measuring tracer concentrations in one or more monitoring wells. NAPL saturations are then computed from the retardation factors. Because partitioning tracer tests can be designed to sample much larger aquifer volumes (e.g., compared to sediment coring) they have the potential to accurately locate and quantify NAPL contamination.

Previous studies have suggested that naturally occurring radon-222 (hereafter referred to as radon) can be used as a partitioning tracer (Semprini et al., 1993; Hopkins, 1995; Gottipati, 1996; Hunkeler et al. 1997; Semprini et al., 1998; Semprini et al., 2000). Radon is a naturally occurring, radioactive, inert isotope that occurs in groundwater as a dissolved gas. Radon is part of the uranium-238 decay series and has a half-life of 3.83 days. It is continuously produced in the subsurface via the α -decay of its parent, radium-226 (half-life of 1600 years) that is contained within the structure of aquifer minerals and/or exists as secondary mineral coatings. The steady-state radon concentration in groundwater (C_{Rn}) is a function of the radium content (C_{Ra}) and radon emanation power (E_p) of the mineral phase and the bulk density (ρ_b) and porosity (n) of the aquifer (Semprini et al., 2000)

$$C_{Rn} = \frac{C_{Ra} E_p \rho_b}{n} \quad (3.1)$$

Values of C_{Rn} are highly variable ranging from approximately 100 to 270,000 pCi/L in groundwater (National Research Council, 1999).

Radon is moderately volatile, with a dimensionless Henry's coefficient of 3.9 at 20° C (Clever, 1979). Due to its non-polarity radon has a high affinity for partitioning into NAPLs. The linear partition coefficient (K) for radon is defined as

$$K = \frac{C_{Rn,n}}{C_{Rn,w}} \quad (3.2)$$

where $C_{Rn,n}$ is the concentration of radon in the NAPL phase, and $C_{Rn,w}$ is the concentration of radon in the aqueous phase. The K value for radon in the presence of trichloroethene DNAPL (hereafter referred to as TCE) has not been determined. An estimate of K for radon in TCE can be determined using the Ostwald coefficient, which is defined as the ratio of the concentration of gas per unit volume of liquid phase to the concentration of gas per unit volume of gas phase (Clever, 1979). A $K = 58$ for radon in trichloromethane is estimated by dividing the Ostwald coefficient for radon in trichloromethane vs. radon in air by the Ostwald coefficient for radon in water vs. radon in air. In this study we assume a $K = 58$ for radon in TCE based on the estimate for trichloromethane. For light NAPLs (LNAPLs) measured values of K for radon range from 37 (o-xylene) to 61 (cyclohexane) (Cantaloub, 2001).

Previous field applications of radon as a partitioning tracer relied on observed decreases in radon concentrations in NAPL-contaminated areas relative to radon concentrations in non-contaminated areas (Hunkeler et al., 1997; Semprini et al., 2000). In this study we evaluate the use of single-well, "push-pull" tracer tests using radon as a natural partitioning tracer to quantify TCE saturations. During a push-pull test, a known volume of test solution (radon-free water containing a conservative tracer) is first injected ("pushed") into a well; flow is then reversed and the test solution/groundwater mixture is extracted ("pulled") from the same well (Schroth et al., 2000). Laboratory push-pull tests were performed in physical aquifer models using sediment prepared with and without TCE. Field push-pull tests were performed in LNAPL-contaminated and non-contaminated portions of an aquifer at a former petroleum refinery. An approximate analytical solution to solute concentrations during the injection and extraction phases of the push-pull test was used to estimate radon retardation factors; retardation factors were then used to calculate TCE saturations in laboratory experiments. Numerical simulations were performed to investigate the validity of the approximate solution.

Our approach involves the injection of a known volume of radon-free test solution containing a conservative tracer into a single well, followed by the extraction of the test solution/groundwater mixture from the same well. TCE saturations are determined by estimating the radon retardation factor from measured conservative tracer and radon concentrations obtained during the injection and extraction phases of the test. The retardation factor (R) for radon in a NAPL-contaminated aquifer is defined as

$$R = \frac{v_w}{v_{Rn}} \quad (3.3)$$

where v_w is the groundwater velocity and v_{Rn} is the velocity of radon in groundwater. Assuming linear equilibrium partitioning the retardation factor for radon may be written as (Dwarakanath et al., 1999)

$$R = 1 + \frac{KS_n}{S_w} \quad (3.4)$$

where S_n and S_w are the NAPL and water saturations in the pore space ($S_n + S_w = 1$). Once the retardation factor is known, the NAPL saturation can then be calculated via (Dwarakanath et al., 1999)

$$S_n = \frac{R - 1}{R + K - 1} \quad (3.5)$$

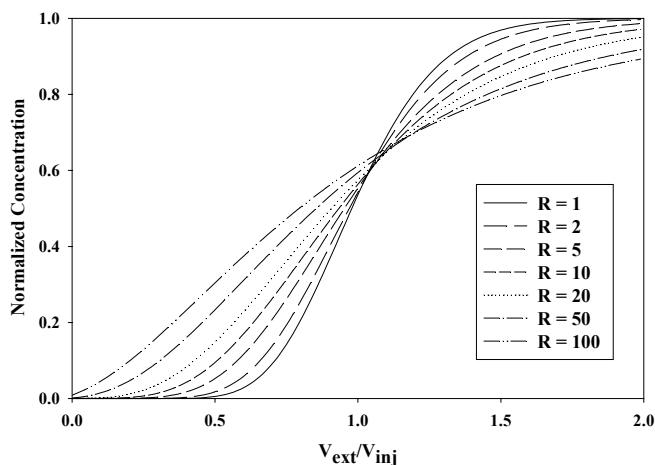


Figure 3.1 Simulated push-pull test extraction phase breakthrough curves for non-retarded and retarded in situ solutes.

Figure 3.1 shows the effect of varying retardation factor on numerically simulated extraction phase radon breakthrough curves for push-pull tests conducted by injecting radon-free water. In this figure V_{ext}/V_{inj} corresponds to the cumulative volume of extracted solution at a given time divided by the total volume of injected solution (i.e., dimensionless time). These simulations were performed by Schroth et al. (2000) using the Subsurface Transport Over Multiple Phases (STOMP) code (White and Oostrom, 2000). Note that normalized radon concentrations increase during the extraction phase since a radon-free test solution is injected. In the absence of NAPL, radon behaves like a conservative tracer ($R = 1$); in the presence of NAPL, radon transport is retarded ($R > 1$), resulting in an increased apparent dispersion during the extraction phase.

METHODS

Laboratory Push-Pull Tests

Laboratory push-pull tests were performed in physical aquifer models (PAMs) constructed in a wedge shape to simulate the radial flow field near an injection/extraction well during a push-pull test (Figure 3.2). The PAMs were constructed with polypropylene with interior dimensions of 5 cm (width at narrow end), 50 cm (width at wide end), 125 cm (length), 20 cm (height), and a total internal volume of 0.069 m³. Air-

dried sediment was packed into the PAMs to a uniform bulk density (1.9 g/cm^3) and calculated porosity (0.35).

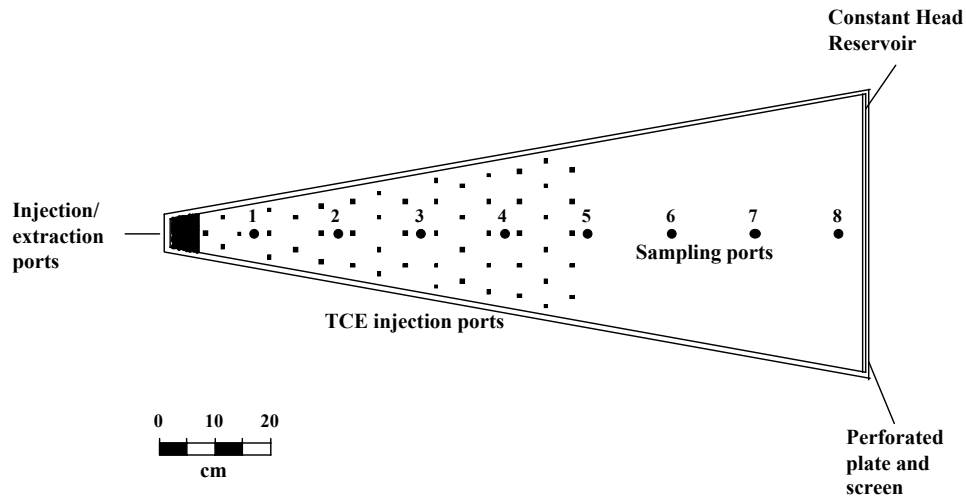


Figure 3.2 Plan view of physical aquifer model (PAM) used in laboratory push-pull tests, showing dimensions and sampling locations.

The PAMs were packed using the method of Istok and Humphrey (1995) with sediment from the Hanford Formation, an alluvial deposit of sands and gravels of mixed basaltic and granitic origin (Lindsey and Jaeger, 1993). The sediment was collected as a single batch from an outcrop at a quarry near Pasco, WA. The sediment was homogenized by manual mixing, air-dried to a water content between 2 and 3 wt %, and sieved to remove particles $> 2 \text{ cm}$ in diameter (which were $< 0.01 \%$ of the original outcrop material). The sieved sediment is a sand with approximately 30 % fine gravels and less than 5 % silt and clay. The sediment contains less than 0.001 wt % organic matter. Tap water was used as the synthetic groundwater in all laboratory experiments. The sediment packs were saturated with tap water and a lid containing eight sampling ports was installed.

For experiments involving TCE contamination, the sediment pack contained a known initial quantity of liquid (nonaqueous phase) TCE. This was achieved by first draining the sediment pack and then slowly injecting aliquots of TCE at depths between 2.5 and 17.5 cm through 52 injection ports bored through the model lid between sampling ports 1 and 5 (Figure 3.2). A total of 304 g (208 mL) of TCE was uniformly injected through the injection ports, which represents a TCE saturation equivalent to $\sim 2 \%$ of the total pore volume within the contaminated zone. After TCE injection, the sediment pack was re-saturated and then flushed for $\sim 24 \text{ h}$ with tap water to remove mobile TCE from the injection/extraction ports and to entrap TCE within the pore space. No TCE was observed in the water removed from the sediment pack during the tap water flush.

Push-pull tests were performed under confined conditions. Each push-pull test was preceded by a three-week rest period during which radon concentrations reached $> 95 \%$ of their secular equilibrium value as a result of concurrent radon emanation from sediment and decay. During the injection phase, flow was directed from the injection/extraction ports at the narrow end of the PAM toward the constant head reservoir at the PAM's wide end. During the extraction phase, flow was reversed. The

constant head reservoir was supplied with water from a second PAM containing the same sediment (without TCE) to provide a source of water with a similar and constant radon concentration. For each experiment, 8 to 16 L of test solution was injected and 16 to 32 L was extracted. Test solutions were injected and extracted using a piston pump (Fluid Metering, Oyster Bay, NY). The volumes of test solution injected were selected to ensure that no injected test solution left the PAM through the constant head reservoir. The test solution consisted of tap water containing ~ 100 mg/L bromide, prepared from sodium bromide (Fisher Scientific, Fair Lawn, NJ) to serve as a conservative tracer. Dissolved radon was removed by bubbling compressed air through the test solution prior to injection. The extraction phase began within 30 minutes after the end of the injection phase. Injection and extraction pumping rates were constant at ~ 106 mL/min. Water samples were obtained by connecting a 20 mL Luer-Lock plastic syringe (Becton-Dickinson, Franklin Lakes, NJ) to a syringe needle or a valve. During the injection phase water samples were collected from the sediment pack by inserting a stainless steel syringe needle into brass 'well' screens that fully penetrated the sediment pack beneath each sampling port. During the extraction phase water samples were collected from a valve located between the pump and the PAM injection/extraction ports.

Following these tests the sediment pack was drained and excavated in sequential 5 cm thick layers to determine the vertical distribution of TCE contamination. For each 5 cm thick layer triplicate sediment samples (~ 100 g) were collected from a single location and placed in 125 mL glass jars. Each jar was then filled with ~ 65 mL of tap water, sealed, placed on a mechanical shaker for 30 minutes, and allowed to sit overnight. A 2 mL water sample was collected by inserting a syringe needle through a septum in the jar lid and analyzed for aqueous phase TCE.

Field Push-Pull Tests

Push-pull tests were performed at a former refinery in the Ohio River Valley. The aquifer is formed in glacial outwash deposits consisting primarily of sands and gravels. Portions of the site are contaminated with LNAPL, consisting primarily of jet fuel and gasoline. Tests were conducted in wells located within non-contaminated and contaminated portions of the site. For each test, ~ 250 L of test solution was injected. The test solution consisted of tap water containing ~ 100 mg/L bromide, prepared from sodium bromide (Fisher Scientific, Fair Lawn, NJ) to serve as a conservative tracer. Dissolved radon was removed by bubbling compressed air through the test solution prior to injection. Straddle packers were used to isolate 1.5 m long depth intervals of the well screen for testing. Intervals were chosen based on the inferred presence or absence of LNAPL within the aquifer as determined by soil coring during well installation and subsequent aqueous sampling. Test solutions were injected using a peristaltic pump (Cole-Parmer, Vernon Hills, IL) and the test solution/groundwater mixture was extracted using a submersible pump (Grundfos, Bjerringbro, Denmark). Approximately 500 L of injected solution and groundwater was removed from the well. Water samples were collected for bromide and radon analyses using a sampling line and syringe.

Analytical Methods

Bromide concentrations were determined using a Dionex Model DX-120 ion chromatograph equipped with an electrical conductivity detector (Sunnyvale, CA). Aqueous radon samples were filtered through a 0.45 μm filter (Millipore, Bedford, MA) attached to a syringe and a 1.5 inch steel needle (Becton-Dickinson, Franklin Lakes, NJ). The filtered sample (15 ± 0.5 mL) was then dispensed into the bottom of a pre-weighed 20 mL borosilicate scintillation vial containing 5 mL of Ultima Gold F scintillation “cocktail” (Packard Instruments, Meriden, CT). The exact mass of filtered sample added was determined by mass difference. Counting was performed with a Packard 2500 TR/AB Liquid Scintillation Analyzer (LSA) as described by Cantaloub (2001). Aqueous TCE was quantified using a Waters HPLC using the method described by Field and Sawyer (2000).

Data Analysis

Data analysis was performed using normalized concentrations. The normalized concentration for bromide is defined as $C^* = 1 - C/C_o$ where C is the measured bromide concentration in a sample and C_o is the bromide concentration in the injected test solution (~ 100 mg/L). This calculation is performed to facilitate the comparison of bromide and radon breakthrough curves. Bromide is an injected tracer, and thus its concentrations increase with time during the injection phase and decrease with time during the extraction phase. Radon, in contrast, is an in situ tracer and thus its concentrations decrease with time during the injection phase (of radon-free water) and increase with time during the extraction phase. The normalized concentration for radon is defined as $C^* = C/C_b$, where C is the measured radon concentration and C_b is the background (equilibrium) radon concentration in the sediment pack or aquifer. Push-pull tests were performed over a time period of < 8 hours so that radon emanation from aquifer sediments during the test was negligible.

Injection phase data for the sampling ports in laboratory push-pull tests were interpreted using the method of temporal moments (Cunningham and Roberts, 1998), the approximate analytical solution of Gelhar and Collins (1971) as further described by Schroth et al. (2000), and numerical modeling. The zeroth (m_0) and first (m_1) temporal moments were computed by integrating normalized bromide and radon concentrations at the sampling ports using

$$m_0 = \int C^*(t) dt \quad (3.6)$$

$$m_1 = \int t C^*(t) dt \quad (3.7)$$

The retardation factor for radon was then computed using

$$R = \frac{\left(\frac{m_{1,Rn}}{m_{0,Rn}} \right)}{\left(\frac{m_{1,Br^-}}{m_{0,Br^-}} \right)} \quad (3.8)$$

Laboratory and field push-pull test data were interpreted using an approximate analytical solution to the advection–dispersion equation for solute transport during a push-pull test as presented by Schroth et al. (2000). The solution gives normalized concentration (C^*) as a function of time and radial distance from the injection well. For the injection phase

the solution is

$$C^* = \frac{1}{2} \operatorname{erfc} \left\{ \left(r^2 - r_{inj}^2 \right) / \left[\frac{16}{3} \alpha_L \left(r_{inj}^3 - r_{well}^3 \right) \right]^{\frac{1}{2}} \right\} \quad (3.9)$$

where r is radial distance from the injection well, α_L is the dispersivity, r_{well} is the well radius and r_{inj} (the radial distance of the $C^* = 0.5$ tracer front at time t_{inj}) is given by

$$r_{inj} = \left(\frac{Q_{inj} t_{inj}}{\pi b n R} + r_{well}^2 \right)^{\frac{1}{2}} \quad (3.10)$$

where Q_{inj} is the injection phase flowrate, t_{inj} is time, b is the saturated thickness, n is the porosity, and R is the retardation factor. For the extraction phase the solution is

$$C^* = \frac{1}{2} \operatorname{erfc} \left\{ \left(r^2 - r_{ext}^2 \right) / \left[\frac{16}{3} \alpha_L \left(2r_{max}^3 - r_{ext}^3 - r_{well}^3 \right) \right]^{\frac{1}{2}} \right\} \quad (3.11)$$

where r_{ext} (the radial distance of the $C^* = 0.5$ tracer front at time t_{ext}) is given by

$$r_{ext} = \left(r_{max} + \frac{Q_{ext} t_{ext}}{\pi b n R} \right)^{\frac{1}{2}} \quad (3.12)$$

where Q_{ext} is the extraction phase pumping rate, t_{ext} is time, and r_{max} is defined by

$$r_{max} = \left(r_{well} + \frac{V_{inj}}{\pi b n R} \right)^{\frac{1}{2}} \quad (3.13)$$

where r_{max} is the maximum radial distance traveled by the $C^* = 0.5$ tracer front at the end of the injection phase (corresponding to the radius of influence of the tracer) and V_{inj} is the total volume of test solution injected.

For the laboratory tests, sampling port data from the injection phase were analyzed by using a minimized least-squares procedure to fit equation 3.9 to the normalized bromide data to obtain an estimate for α_L . Then another minimized least-squares procedure was used to fit equation 3.9 to the normalized radon data to obtain estimates for R using the value of α_L estimated from the bromide data.

For the laboratory and field tests, extraction phase normalized bromide data were fit to equation 3.11 using a minimized least-squares procedure to obtain another estimate for α_L . Then another minimized least-squares procedure was used to fit equation 3.11 to the normalized radon data to obtain an estimate for the maximum travel radius of the radon-free water. The retardation factor was then computed using

$$R = \left(\frac{r_{\max, Br^-}}{r_{\max, Rn}} \right)^{\frac{1}{2}} \quad (3.14)$$

Field test normalized breakthrough curve results were adjusted for the bromide data by dividing V_{ext}/V_{inj} by the bromide mass fraction recovery achieved in the test. For the radon data, V_{ext}/V_{inj} was divided by 1 - the mass fraction of bromide recovered during the test. This calculation was performed because only 42 to 57 % of the bromide injected was recovered during the field tests. The calculation assumes that dilution effects are uniform for bromide and radon; that is, any loss of test solution to the aquifer is matched by an equal gain in groundwater from the aquifer. The calculation served to force the bromide $C^* = 0.5$ value through $V_{ext}/V_{inj} = 1$; this simplified the comparison of the bromide and radon breakthrough curves and best-fit approximate solutions. The extraction phase approximate solution was then fit to the normalized bromide and radon data as described above.

The validity of the approximate analytical solution was evaluated using numerical simulations performed with the STOMP code (White and Oostrom, 2000). STOMP is a fully implicit volume-integrated finite difference simulator for modeling one-, two- and three-dimensional flow and transport, which has been extensively tested and validated against published analytical solutions as well as other numerical codes (Nichols et al., 1997). The computational domain consisted of a line of 250 nodes with a uniform radial node spacing of $\Delta r = 1.0$ cm. Initial conditions were a constant hydraulic head for the aqueous phase and $C = 0$ for all solutes. Time-varying third-type flux boundary conditions were used to represent pumping at the injection/extraction ports; constant head and zero solute flux boundary conditions were used to represent aquifer conditions beyond the radius of influence of the well. Bromide and radon transport were simulated using PAM sediment pack properties, best-fit α_L values obtained from the extraction phase approximate solution, and estimated R values from the injection phase and extraction phase approximate solutions.

RESULTS

Laboratory Tests

Results for sampling ports 1 and 2 from the push phase of Test 1 conducted in the absence of TCE are shown in Figures 3.3a and 3.3b. Breakthrough curves are displayed as normalized concentration (C^*) versus dimensionless pore volume (V_{inj}/V_{pore}) for bromide and radon. In these figures V_{inj} is the cumulative volume of injected test solution at the time the sample was collected, and V_{pore} is the pore volume between the injection/extraction ports and the sampling port. At each sampling port normalized concentrations decreased smoothly as the test solution penetrated further into the sediment pack. Radon transport was somewhat retarded relative to bromide. The data were well fit by the injection phase approximate solution (equation 3.9), with best-fit α_L values of 3.8 cm for port 1 and 6.6 cm for port 2 (Table 3.1). Estimated radon retardation factors for ports 1 and 2 were 1.0 and 1.2 using the method of temporal moments and 1.1 and 1.4 using the injection phase approximate solution (Table 3.1). Numerical simulations using STOMP were also conducted for the injection phase data using $R = 1.0$ and 1.1 at port 1 and $R = 1.0$ and 1.4 at port 2. The simulated breakthrough curves

matched the injection phase approximate solution moderately well at port 1 but did not match at port 2.

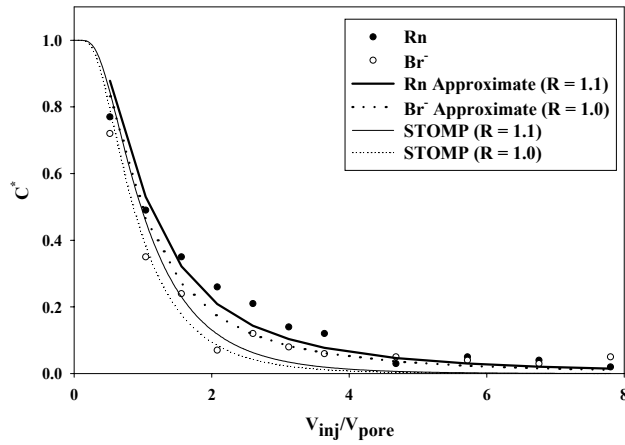


Figure 3.3a Injection phase breakthrough curves for lab Test 1, port 1 in the absence of TCE.

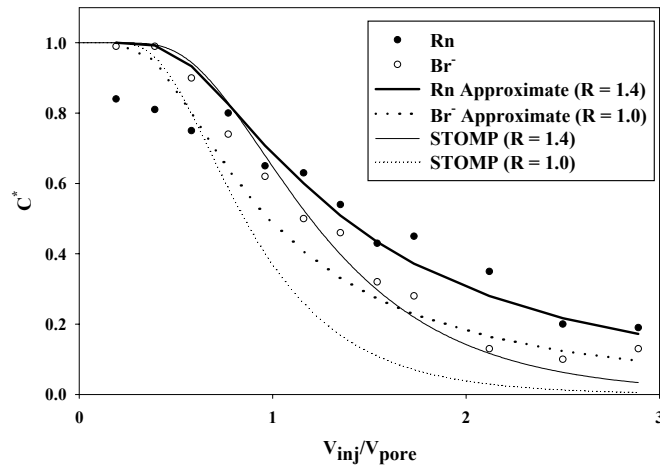


Figure 3.3b Injection phase breakthrough curves for lab Test 1, port 2 in the absence of TCE.

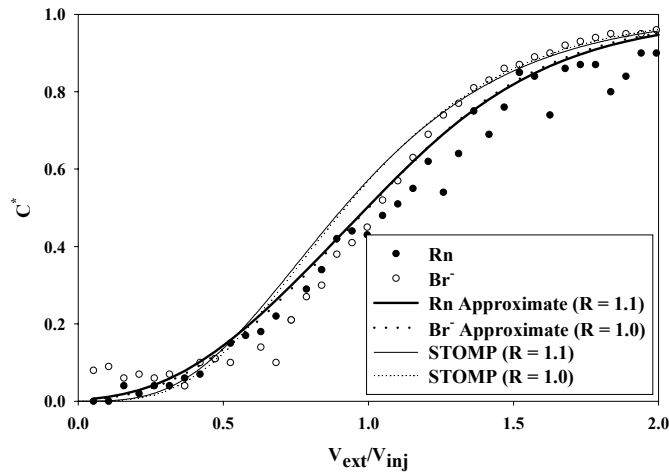


Figure 3.3c Extraction phase breakthrough curves for lab Test 1 in the absence of TCE.

Retarded radon transport was not very apparent in extraction phase breakthrough curves for Test 1 (Figure 3.3c) where normalized concentration (C^*) is plotted as a function of the ratio $V_{\text{ext}}/V_{\text{inj}}$, where V_{ext} is the cumulative volume of water extracted at the time the sample was collected and V_{inj} is the volume of injected test solution. Normalized concentrations increased smoothly as the test solution was extracted from the sediment pack. The data were well fit by the extraction phase approximate solution (equation 3.11), with a best-fit α_L of 3.2 cm (Table 3.1). A best-fit value of $R = 1.1$ was obtained for radon (Table 3.1). Numerical simulations using STOMP were also conducted for the extraction phase data using $R = 1.0$ and $R = 1.1$. The simulated breakthrough curves matched the extraction phase approximate solution moderately well.

Table 3.1 Radon retardation factors (R), adjusted retardation factors for the effect of trapped gas (*in italics*), approximate solution best-fit dispersivities (α_L), and TCE saturations (S_n) from push-pull tests.

	Method of Moments			Injection Phase Approx. Solution			Extraction Phase Approx. Solution		
	R	α_L (cm)	S_n (%)	R	α_L (cm)	S_n (%)	R	α_L (cm)	S_n (%)
Test 1 Port 1	1.0	-	-	1.1	3.8	-	-	-	-
Test 1 Port 2	1.2	-	-	1.4	6.6	-	-	-	-
Test 1 Injection/Extraction Ports	-	-	-	-	-	-	1.1	3.2	-

Test 2 Port 1	1.4/1.4 - 0.7	1.4/1.3 3.4 0.5	- - -
Test 2 Port 2	1.7/1.5 - 0.9	1.5/1.1 2.1 0.2	- - -
Test 2 Injection/Extraction Ports	- - -	- - -	5.1/5.0 4.0 6.5
Field Test No LNAPL	- - -	- - -	1.6 38.6 -
Field Test With LNAPL	- - -	- - -	7.3/6.7 20.3 -

Radon transport was retarded during the push phase of Test 2 conducted in the presence of 2 % TCE (Figures 3.4a and 3.4b). The data were well fit by the injection phase approximate solution, with best-fit α_L values of 3.4 cm at port 1 and 2.1 cm at port 2 (Table 3.1). Estimated radon retardation factors for ports 1 and 2 were 1.4 and 1.7 using the method of temporal moments and 1.4 and 1.5 using the injection phase approximate solution (Table 3.1). Numerical simulations using STOMP were conducted for the injection phase data using $R = 1.0$ and $R = 1.4$ at port 1 and $R = 1.0$ and $R = 1.5$ at port 2. The simulation breakthrough curves provided a reasonable match to the injection phase approximate solution.

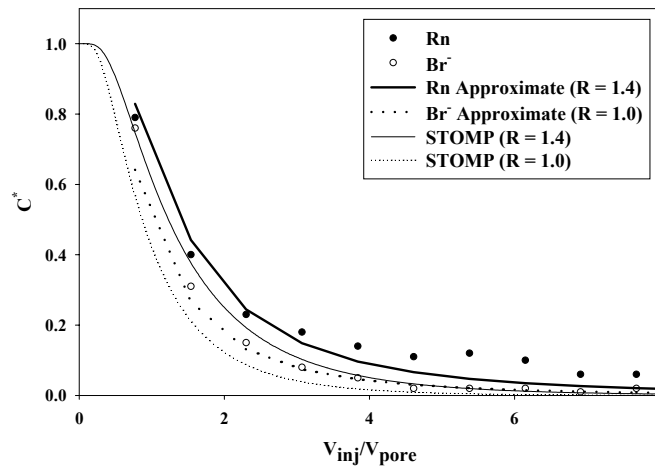


Figure 3.4a Injection phase breakthrough curves for lab Test 2, port 1 with 2 % TCE.

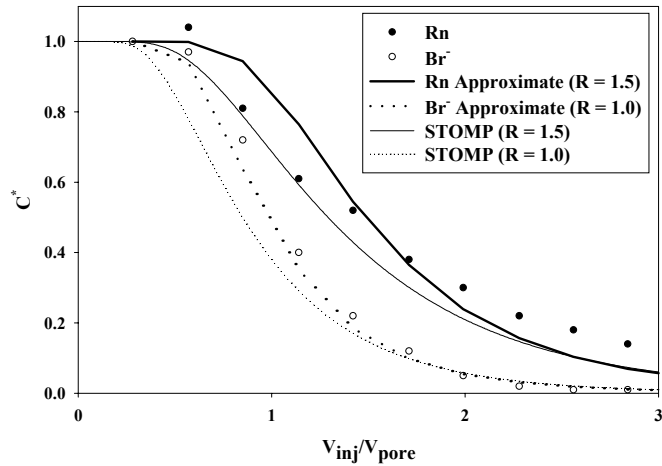


Figure 3.4b Injection phase breakthrough curves for lab Test 2, port 2 with 2 % TCE.

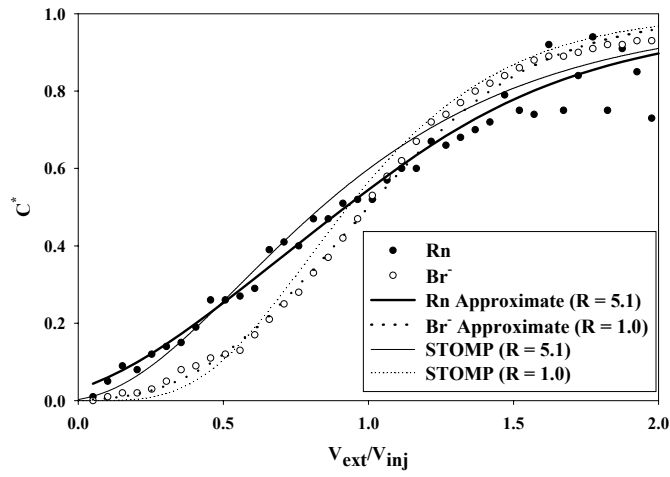


Figure 3.4c Extraction phase breakthrough curves for lab Test 2 with 2 % TCE.

Retarded radon transport was apparent in extraction phase breakthrough curves for Test 2 (Figure 3.4c). Normalized concentrations increased smoothly as the test solution was extracted from the sediment pack. The data were well fit by the extraction phase approximate solution, with a best-fit α_L of 4.0 cm (Table 3.1). An estimated value of $R = 5.1$ was obtained for radon using the extraction phase approximate solution (Table 3.1). Numerical simulations using STOMP were also conducted for the extraction phase data using $R = 1.0$ and $R = 5.1$. The simulation breakthrough curves provided a good match to the extraction phase approximate solution.

Field Tests

Radon retardation was investigated using extraction phase breakthrough curves from two wells at the field site. Radon transport was slightly retarded in Test 1 conducted in the absence of LNAPL (Figure 3.5a). Normalized concentrations increased smoothly as the test solution was extracted from the aquifer. However, the shapes of the extraction phase breakthrough curves differed from those in the laboratory tests. This is likely due to a greater apparent dispersion and/or heterogeneity in hydraulic conductivity in the natural sediment. The best-fit α_L was 38.6 cm (Table 3.1). The radon data were well fit by the extraction phase approximate solution; the estimated retardation factor for radon was 1.6 (Table 3.1).

Radon transport was retarded in Test 2 conducted in the presence of LNAPL (Figure 3.5b). Again, the shape of the extraction phase breakthrough curves differed from those from the laboratory tests. The best-fit α_L was 20.3 cm (Table 3.1). The bromide data were well fit by the extraction phase approximate solution, but the radon data were poorly fit by the extraction phase approximate solution; the estimated retardation factor for radon was 7.3 (Table 3.1).

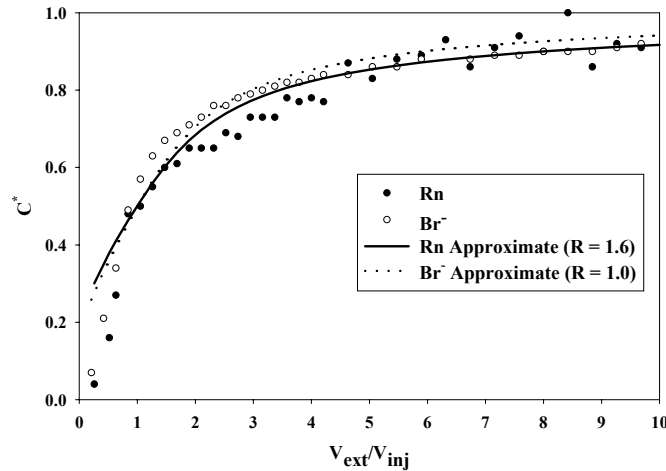


Figure 3.5a Extraction phase breakthrough curves for field Test 1 with no LNAPL.

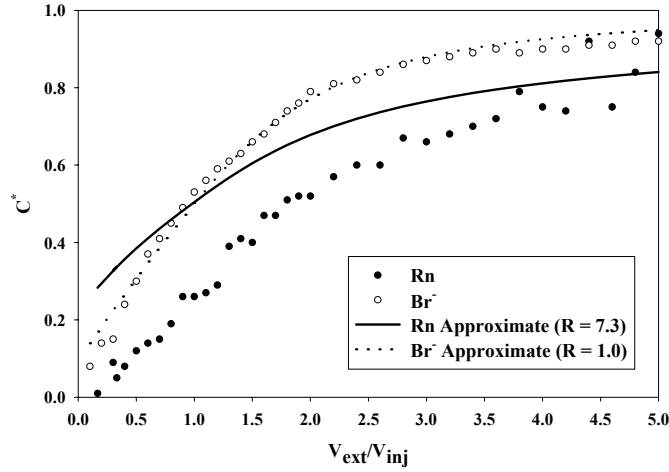


Figure 3.5b Extraction phase breakthrough curves for field Test 2 with LNAPL.

DISCUSSION

Laboratory Tests

The slight radon retardation observed during Test 1 may be attributed to the partitioning of radon between the pore water and trapped gas present in the sediment pack. Retarded transport of dissolved gases in the presence of trapped gas has been observed in previous column and PAM experiments in our laboratory (Fry et al., 1995; Fry et al., 1996). Assuming equilibrium partitioning between the trapped gas and aqueous phases, the retardation factor for a dissolved gas can be written as

$$R = 1 + H_{cc} \frac{S_g}{S_w} \quad (3.15)$$

where H_{cc} is the dimensionless Henry's coefficient and S_g is the trapped gas saturation. Fry et al. measured gas saturations of 11% in column experiments and between 7 and 22 % in PAM experiments conducted with the same sediment used in the laboratory push-pull tests. Using equation 3.15 and a value of $H_{cc} = 3.9$ for radon (Clever, 1979) the estimated gas saturation in our PAM sediment pack ranges from 0 to 9.3 % using radon retardation factors obtained from ports 1 and 2 during the injection phase. The higher gas saturation observed at port 2 is a function of the greater retardation factor estimated at that port ($R = 1.4$ for the injection phase approximate solution). The radon retardation factor of 1.1 obtained for the extraction phase approximate solution estimates a trapped gas saturation of 2.5 %.

During Test 2 radon was retarded due to 1) radon partitioning between TCE and the aqueous phase, and 2) radon partitioning between trapped gas and the aqueous phase. In order to estimate the portion of radon retardation due to TCE partitioning, retardation factors were adjusted to account for trapped gas partitioning using

$$R_{adj} = R_{test2} - (R_{test1} - 1.0) \quad (3.16)$$

where R_{adj} is the adjusted retardation factor, $R_{test\ 2}$ is the retardation factor from Test 2, and $R_{test\ 1}$ is the retardation factor from Test 1. For example, in Test 1 the method of moments retardation factor at Port 2 is 1.2, while in Test 2 the retardation factor is 1.7, yielding an adjusted retardation factor of 1.5. Adjusted retardation factors were used to calculate TCE saturations (Table 3.1).

Table 3.2. Aqueous TCE as a function of depth in the PAM sediment pack.

Depth Interval (cm)	TCE (mg/L)
0 – 5	3.9
5 – 10	9.8
10 – 15	77.2
15 – 20	273.2

Using equation 3.5, adjusted injection phase retardation factors, and $K = 58$, calculated TCE saturations ranged from 0.2 to 0.9 % (Table 3.1), which is less than the volume-averaged TCE saturation of 2 % in the sediment pack. This underestimation may be due to nonequilibrium radon partitioning and the heterogeneous distribution of TCE in the sediment pack. A heterogeneous TCE distribution with pooling toward the bottom of the sediment pack could result in underestimated radon retardation factors because of the reduced interfacial area between the TCE and the test solution. NAPL pools can create a mass transfer limitation to partitioning because of the long length scales of pooled NAPL relative to the scale of diffusion over the test time (Willson et al., 2000), thus violating the assumption of equilibrium partitioning. Aqueous TCE concentrations increased with depth upon the excavation of the PAM (Table 3.2), indicating that the TCE partially sank to the bottom of the sediment pack, which could account for the low retardation factors estimated during the injection phase. However, uncertainties in radon's K in TCE would also result in a miscalculation of S_n in the sediment pack, with a smaller value of K providing a larger calculated TCE saturation. The extraction phase adjusted radon retardation factor was 5.0 (Table 3.1). This corresponds to a TCE saturation of 6.5 %, which is larger than the TCE saturations obtained from the port data and is an overestimation of the volume-averaged TCE saturation of 2 % in the sediment pack. The reasons for the greater estimated retardation factor during the extraction phase are unclear. Because the extraction phase approximate solution closely matches the numerical solution (Figure 3.4c), the overestimation of the retardation factor and thus TCE saturation is not likely due to an error in the extraction phase approximate solution. A possible reason for the greater estimated retardation factor may be that the contact time between the test solution and the TCE is greater for samples taken during the extraction phase of the test. This may be explained as follows. For a sample taken during the injection phase, the test solution is subject to partitioning from the time the solution enters the PAM to when a sample is removed from a sampling port. In contrast, for a sample taken during the extraction phase the test solution is subject to partitioning from the time the solution enters the PAM, through the completion of the injection phase and flow reversal (the extraction phase) and, ultimately, until sampling of the solution at the injection/extraction ports. This could result in a more retarded radon breakthrough curve during the extraction phase relative to the injection phase.

Numerical simulations using STOMP were used to check the validity of the approximate solution by running simulations using the values of α_L that were best-fit by the extraction phase approximate solution for the R values estimated by the injection and extraction phase approximate solutions. The numerical simulation results show that α_L is adequately estimated by the extraction phase approximate solution; this is evident in the moderately good match between the extraction phase approximate solution and numerical simulation breakthrough curves (Figures 3.3c and 3.4c).

For Test 1, the best-fit values of α_L for the injection phase approximate solution were 3.8 cm at port 1 and 6.6 cm at port 2, while the best-fit value of α_L for the extraction phase approximate solution was 3.2 cm. (Table 3.1). The higher best-fit value of α_L at port 2 is a result of the more dispersed bromide breakthrough curve (Figure 3.3b). The reason for the more dispersed bromide breakthrough curve at port 2 is unclear. This resulted in the numerical simulations providing a poor match to the injection phase approximate solution at port 2. However, the numerical simulations provided a moderately good match to the injection phase approximate solution at port 1. For Test 2, the best-fit values of α_L for the injection phase approximate solution were 3.4 cm at port 1 and 2.1 cm at port 2. The difference between the port 2 best-fit values of α_L between Tests 1 and 2 is possibly due to the presence of TCE in Test 2. The injection of TCE into the sediment pack may have reduced the pore size distribution through which water could flow, thus reducing α_L . The best-fit value of α_L for the Test 2 extraction phase approximate solution was 4.0 cm. The numerical simulations provided a moderately good match to the injection phase approximate solution at ports 1 and 2.

Field Tests

The minimal radon retardation observed in Test 1 (Figure 3.5a) may be attributed to partitioning of radon between the pore water and trapped gas present in the aquifer. Radon was significantly retarded in Test 2 conducted in the LNAPL-contaminated portion of the site (Figure 3.5b), with an adjusted retardation factor of 6.7 (Table 3.1). Retardation in Test 2 is attributed to partitioning of radon between the injected test solution, LNAPL, and trapped gas in the aquifer. In Test 2 the extraction phase approximate solution provides a poor fit to the radon breakthrough curve, and thus the adjusted $R = 6.7$ has a high uncertainty. Note that for the radon breakthrough curve, $C^* = 0.5$ passes through $V_{\text{ext}}/V_{\text{inj}} = 2$. This may have resulted from a heterogeneous LNAPL distribution and/or nonideal transport (i.e., nonequilibrium partitioning) during the test. Schroth et al. (2000) found that simulated push-pull tests with linear nonequilibrium partitioning resulted in the partitioning tracer $C^* = 0.5$ passing through $V_{\text{ext}}/V_{\text{inj}}$ at values greater than 1. Nonequilibrium partitioning can occur in the presence of NAPL pools. Pools can create a mass transfer limitation to partitioning that may account for the tailing in the radon breakthrough curve and its poor fit to the extraction phase approximate solution. In this case LNAPL pools could inhibit the equilibrium partitioning of radon between the LNAPL and the test solution during the timescale of the push-pull test. In this test, nonideal radon breakthrough curve behavior limited the applicability of the method in accurately determining the LNAPL saturation.

CONCLUSIONS

Overall, the laboratory test results show that the methodology is capable of detecting and quantifying NAPL saturations. Using radon as a partitioning tracer requires only the injection of radon-free water containing a conservative tracer, while the single-well, push-pull test requires smaller water volumes compared to inter-well tracer tests. These factors can reduce the costs of determining NAPL saturations. However, future research is needed to investigate the reasons for the differences between injection and extraction phase retardation factors. The influence of nonequilibrium radon partitioning on breakthrough curve behavior and the role of heterogeneous NAPL distributions (i.e., layered systems) need to be determined. Numerical modeling should be employed to investigate the role of these phenomena in influencing injection and extraction phase retardation factors and calculated NAPL saturations. More detailed field investigations using the radon push-pull method described here are also needed where detailed information on residual NAPL saturations is available.

ACKNOWLEDGEMENTS

We thank Jennifer Field, Ralph Reed, Jason Lee, Mike Cantaloub, and Kyle Foster for help with laboratory methods and activities; Mark Lyverse and Jesse Jones for help with field activities; and Martin Schroth and Mark White for help with STOMP.

REFERENCES

- Annable, M.D., P.S.C. Rao, K. Hatfield, W.D. Graham, A.L. Wood, and C.G. Enfield, 1998. Partitioning tracers for measuring residual NAPL: field-scale test results. *Journal of Environmental Engineering*, 124:498-503.
- Cantaloub, M., 2001. Aqueous-organic partition coefficients for radon-222 and their application to radon analysis by liquid scintillation methods. Master's Thesis, Oregon State University.
- Clever, H.L., 1979. Solubility Data Series Volume 2. Pergamon Press, NY.
- Cohen, R.M. and J.W. Mercer, 1993. DNAPL Site Evaluation. CRC Press, Boca Raton, FL.
- Cunningham, J.C. and P.V. Roberts, 1998. Use of temporal moments to investigate the effects of nonuniform grain-size distribution on the transport of sorbing solutes. *Water Resources Research*, 34:1415-1425.
- Dwarakanath, V., N. Deeds, and G.A. Pope, 1999. Analysis of Partitioning Interwell Tracer Tests. *Environmental Science and Technology*, 33:3829-3836.
- Field, J.A. and T.E. Sawyer, 2000. High performance liquid chromatography-diode array detection of trichloroethene and aromatic and aliphatic anionic surfactants used for surfactant-enhanced aquifer remediation. *Journal of Chromatography A*, 893:253-260.
- Fry, V.A., J.D. Istok, L. Semprini, K.T. O'Reilly, and T.E. Buscheck, 1995. Retardation of dissolved oxygen due to a trapped gas in porous media. *Ground Water*, 33:391-398.

- Fry, V.A., J.D. Istok, and K.T. O'Reilly, 1996. Effect of trapped gas on dissolved oxygen transport – implications for in situ bioremediation. *Ground Water*, 34:200-201.
- Gelhar, L.W. and M.A. Collins, 1971. General analysis of longitudinal dispersion in nonuniform flow. *Water Resources Research*, 7:1511-1521.
- Gottipati, S., 1996. Radon-222 as a tracer for performance assessment of NAPL remediation technologies in the saturated zone: an experimental investigation. Master's Thesis, Oregon State University.
- Hopkins, O.S., 1995. Radon-222 as an indicator for nonaqueous phase liquids in the saturated zone: developing a detection technology. Master's Thesis, Oregon State University.
- Hunkeler, D., E. Hoehn, P. Höhener, and J. Zeyer, 1997. 222-Rn as a partitioning tracer to detect diesel fuel contamination in aquifers: laboratory study and field observations. *Environmental Science & Technology*, 31:3180-3187.
- Istok, J.D. and M.D. Humphrey, 1995. Laboratory investigation of buoyancy-induced flow (plume sinking) during two-well tracer tests. *Ground Water*, 33:597-604.
- Jin, M., M. Delshad, V. Dwarakanath, D.C. McKinney, G.A. Pope, K. Sepehrnoori, C.E. Tilburg, and R.E. Jackson, 1995. Partitioning tracer test for detection, estimation, and remediation performance assessment of subsurface nonaqueous phase liquids. *Water Resources Research*, 31:1201-1211.
- Lindsey, K.A. and G.K. Jaeger, 1993. Geologic setting of the 100-HR-3 operable unit, Hanford site, south-central Washington. WHC-SD-EN-TI-132, Rev. 0, Westinghouse Hanford Company, Richland, WA.
- Mercer, J.W. and R.M. Cohen, 1990. A review of immiscible fluids in the subsurface: properties, models, characterization and remediation. *Journal of Contaminant Hydrology*, 6:107-163.
- National Research Council, 1999. Risk Assessment of Radon in Drinking Water. National Academy Press, Washington, DC.
- Nelson, N.T. and M.L. Brusseau, 1996. Field study of the partitioning tracer method for detection of dense nonaqueous phase liquid in a trichloroethene-contaminated aquifer. *Environmental Science & Technology*, 30:2859-2863.
- Nelson, N.T., M. Oostrom, T.W. Wietsma, and M.L. Brusseau, 1999. Partitioning tracer method for the in situ measurement of DNAPL saturation: influence of heterogeneity and sampling method. *Environmental Science & Technology*, 33:4046-4053.
- Nichols, W.E., N.J. Aimo, M. Oostrom, and M.D. White, 1997. STOMP: Subsurface Transport Over Multiple Phases, Application Guide. PNNL-11216, Richland, WA.
- Schroth, M.H., J.D. Istok, and R. Haggerty, 2000. In situ evaluation of solute retardation using single-well push-pull tests. *Advances in Water Resources*, 24:105-117.
- Schwille, F., 1988. Dense Chlorinated Solvents in Porous and Fractured Media. Lewis Publishers, Chelsea, MI.
- Semprini, L., K. Broholm, and M. McDonald, 1993. Radon-222 deficit for locating and quantifying NAPL contamination in the subsurface. *EOS Transactions American Geophysical Union*, 76:F276.

- Semprini, L., M. Cantaloub, S. Gottipati, O. Hopkins, and J. Istok, 1998. Radon-222 as a Tracer for Quantifying and Monitoring NAPL Remediation. In: G.B. Wickramanayake and R.E. Hinchee (Editors), *Nonaqueous-Phase Liquids*. Battelle Press, Columbus, OH, pp. 137-142.
- Semprini, L., O.S. Hopkins, and B.R. Tasker, 2000. Laboratory, field and modeling studies of radon-222 as a natural tracer for monitoring NAPL contamination. *Transport in Porous Media*, 38:223-240.
- White, M.D. and M. Oostrom, 2000. STOMP: Subsurface Transport Over Multiple Phases, Version 2.0, User's Guide. PNNL-12034, Richland, WA.
- Willson, C.S., O. Pau, J.A. Pedit, and C.T. Miller, 2000. Mass transfer rate limitation effects on partitioning tracer tests. *Journal of Contaminant Hydrology*, 45:79-97.
- Wilson, R.D. and D.M. Mackay, 1995. Direct detection of residual nonaqueous phase liquid in the saturated zone using SF₆ as a partitioning tracer. *Environmental Science & Technology*, 29:1255-1258.
- Young, C.M., R.E. Jackson, M. Jin, J.T. Londergan, P.E. Mariner, G.A. Pope, F.J. Anderson, and T. Houk, 1999. Characterization of a TCE NAPL zone in alluvium by partitioning tracers. *Ground Water Monitoring and Remediation*, 19:84-94.

4. STATIC AND PUSH-PULL METHODS USING RADON-222 TO CHARACTERIZE DENSE NONAQUEOUS PHASE LIQUID SATURATIONS

INTRODUCTION

The release of nonaqueous phase liquids (NAPLs) to the subsurface environment can create long-term sources of ground water contamination as the NAPL slowly dissolves into ground water (Mercer and Cohen, 1990; Cohen and Mercer, 1993). Effective remediation of subsurface NAPL contamination requires that NAPL be accurately located and saturations quantified. This is particularly important for dense nonaqueous phase liquids (DNAPLs) since their high density causes them to migrate below the water table and move along pathways distinct from water flow (Schwille, 1988; Nelson and Brusseau, 1996).

Laboratory and field studies have shown that partitioning tracers can be used to locate and quantify NAPL contamination (Jin et al., 1995; Wilson and Mackay, 1995; Nelson and Brusseau, 1996; Annable et al., 1998; Nelson et al., 1999; Young et al., 1999). Partitioning tracers have the advantage of interrogating larger aquifer volumes compared to traditional coring techniques. These studies have typically involved the injection of a suite of conservative and partitioning tracers at one well, followed by the measurement of the tracers at one or more monitoring wells (i.e., an interwell tracer test). An alternative approach involves the use of single well “push-pull tests” in which the tracers are injected and extracted from the same well (Schroth et al., 2000; Davis et al., 2002). Retardation factors for injected partitioning tracers are determined from concentration breakthrough curves and, assuming linear equilibrium partitioning, NAPL saturations are calculated (see below).

Naturally occurring radon-222 (hereafter referred to as radon) can be used in lieu of injected partitioning tracers for locating and quantifying NAPL contamination. Radon is a naturally occurring, radioactive, inert isotope that occurs in ground water as a dissolved gas. A part of the uranium-238 decay series, radon has a half-life of 3.83 days and is continuously produced through the α -decay of radium-226 (half-life of 1600 years) that is contained within the structure of aquifer minerals and/or exists as secondary mineral coatings.

Radon has previously been used to investigate ground water recharge rates (Hamada and Komae, 1998), ground water residence times (Snow and Spalding, 1997), and ground water discharge to the ocean (Cable et al., 1996). Studies have shown that radon can be used as a partitioning tracer to locate and quantify NAPL contamination (Semprini et al., 1993; Hopkins, 1995; Gottipati, 1996; Hunkeler et al., 1997; Semprini et al., 1998; Semprini et al., 2000; Davis et al., 2002). In ground water, the equilibrium or ‘background’ radon concentration ($C_{w,bkg}$) is a function of the radium content (C_{Ra}) and radon emanation power (E_p) of the mineral phases and the bulk density (ρ_b) and porosity (n) of the aquifer (Semprini et al., 2000)

$$C_{w,bkg} = \frac{C_{Ra} E_p \rho_b}{n} \quad (4.1)$$

Values of $C_{w,bkg}$ are highly variable ranging to 270,000 pCi/L or more in public water supplies (Hess et al., 1985; National Research Council, 1999). Radon is moderately volatile, with a dimensionless Henry's coefficient (H_{cc}) of 3.9 at 20° C (Clever, 1979). Radon has an affinity for partitioning into NAPL; the linear partition coefficient (K) for radon is defined as

$$K = \frac{C_n}{C_{w,n}} \quad (4.2)$$

where C_n is the concentration of radon in the NAPL phase, and $C_{w,n}$ is the concentration of radon in the aqueous phase in the presence of NAPL.

Both static and push-pull methods using radon as a partitioning tracer can be used to locate and quantify NAPL contamination. The static method involves calculating NAPL saturations from a comparison of radon concentrations in ground water samples obtained from NAPL-contaminated and non-contaminated portions of the same aquifer. This method assumes secular equilibrium between radon emanation and decay, equilibrium radon partitioning between the water and NAPL phases, and a constant background radon concentration (Semprini et al., 2000). In the presence of NAPL, radon will be distributed between the water and NAPL phases as described by

$$C_n S_n + C_{w,n} S_w = \frac{C_{Ra} E_p \rho_b}{n} \quad (4.3)$$

where S_n and S_w are the NAPL and water saturations in the pore space ($S_n + S_w = 1$). Assuming linear equilibrium radon partitioning of radon between NAPL and water (equation 4.2), equation 4.3 can be rearranged as

$$C_{w,n} = \frac{C_{Ra} E_p \rho_b / n}{1 + S_n (K - 1)} \quad (4.4)$$

which can be further rearranged to solve for the NAPL saturation

$$S_n = \left(\frac{C_{w,bkg}}{C_{w,n}} - 1 \right) \left(\frac{1}{(K - 1)} \right) \quad (4.5)$$

where $C_{w,n}$ is the radon concentration in ground water in the NAPL contaminated zone and $C_{w,bkg}$ is the radon concentration in ground water in a 'background' zone outside of the NAPL contaminated zone or in the aquifer before NAPL contamination has occurred. The push-pull method consists of the injection (push) of a known volume of radon-free test solution containing a conservative tracer (i.e., bromide) into a single well, followed by the extraction (pull) of the test solution/ground water mixture from the same well (Schroth et al., 2000). Previous studies have shown that pull phase radon breakthrough curves show an increased dispersion relative to bromide due to retardation resulting from mass transfer of radon between NAPL and the test solution (Davis et al., 2002). NAPL saturations are determined by estimating the radon retardation factor (R) during the pull phase of the test, where $R > 1$ in the presence of NAPL. Assuming linear equilibrium partitioning the retardation factor for radon is (Dwarakanath et al., 1999)

$$R = 1 + \frac{K S_n}{S_w} \quad (4.6)$$

Once the retardation factor is known the NAPL saturation can then be calculated via (Dwarakanath et al., 1999)

$$S_n = \frac{R-1}{R+K-1} \quad (4.7)$$

In this study we evaluate the use of static and push-pull methods using radon as an in situ partitioning tracer to estimate TCE DNAPL (hereafter referred to as TCE) saturations in a laboratory physical aquifer model (PAM) after TCE contamination and remediation. Spatial and temporal changes in static radon concentrations are used to estimate changes in TCE saturations, and push-pull test radon retardation factors are used to estimate TCE saturations as a function of space and time and to estimate the efficacy of remediation.

METHODS

Experimental Methods

Static and push-pull tests were performed in selected portions of a large-scale rectangular PAM (Figures 4.1 and 4.2; experimental timeline shown in Table 4.1). The PAM consists of an aluminum box with interior dimensions of 4 m (length), 2 m (width), and 0.2 m (depth). Constant head reservoirs are located at each end of the PAM. Perforated aluminum plates covered with stainless steel screens separate the sediment pack from the reservoirs. The water height in the reservoirs is controlled by standpipe/overflow systems. An array of fully penetrating wells is fitted into the bottom of the PAM. The PAM is covered with an aluminum lid that is clamped to a flange around the perimeter. Sampling ports are located in the lid; these ports consist of a brass fitting through which a needle can be inserted into the sediment pack below. A more extensive description of the PAM can be found in Humphrey (1992).

The PAM was packed using the method of Istok and Humphrey (1995) with sediment from the Hanford Formation, an alluvial deposit of sands and gravels of mixed basaltic and granitic origin (Lindsey and Jaeger, 1993). The sediment was collected as a single batch from an outcrop at a quarry near Pasco, WA. The sediment was homogenized by manual mixing, air-dried to a water content between 2 and 3 wt %, and sieved to remove particles > 2 cm in diameter (which were < 0.01 % of the original outcrop material). The sieved sediment is a clean sand with approximately 30 % fine gravels and less than 5 % silt and clay. The sediment contains less than 0.001 wt % organic matter, and has a uniform bulk density (after packing) of 1.72 g/cm³ and calculated porosity of 0.39. After sediment packing the PAM was saturated with tap water from the constant head reservoirs, which was used as the synthetic ground water in all laboratory experiments.



Figure 4.1 Photograph of physical aquifer model (PAM) used in laboratory tests.

For some tests, a portion of the sediment pack contained a known initial quantity of liquid TCE. This was achieved by slowly injecting aliquots of neat TCE at depths between 2.5 and 17.5 cm through 18 ports in the PAM lid (these ports do not correspond to the sampling ports described above) using a 10 mL glass syringe (SGE, Ringwood, Australia) connected to a 12 gauge stainless steel needle (Aldrich Chemical, Milwaukee, WI). A total of 210.2 g (144 mL) of TCE was injected to create concentric zones of 6 % and 3 % TCE saturation (Figure 4.5). Following TCE injection, a push-pull test (described below) was conducted through the fully penetrating well to entrap TCE within the pore space (water samples were not obtained during this test).

Static and push-pull tests were performed under confined conditions. Each test was preceded by at least a three week rest period during which radon concentrations reached > 95 % of their equilibrium value as a result of concurrent radon emanation from sediment and decay (Adloff and Guillaumont, 1993). Static tests were performed under no-flow conditions by extracting 20 mL water samples through PAM sampling ports using a 20 mL plastic syringe (Becton-Dickinson, Franklin Lakes, NJ) attached to a 12 gauge stainless steel needle that was inserted into the sediment pack through a sampling port.

Push-pull tests were performed 1) in a fully penetrating well located in the center of the TCE-contaminated portion of the PAM (Figure 4.2), and 2) in sampling ports using a 12 gauge stainless steel needle inserted into the sediment pack. For the fully penetrating well tests, 10 L of test solution were injected and 20 L were extracted, while for the sampling port tests 1.2 L were injected and 2.4 L were extracted. Test solutions were injected and extracted using a piston pump (Fluid Metering, Oyster Bay, NY). The test solution consisted of tap water containing ~ 100 mg/L bromide, prepared from sodium bromide (Fisher Scientific, Fair Lawn, NJ) to serve as a conservative tracer. Dissolved radon was removed by bubbling compressed air through the test solution prior to injection. Injection and extraction pumping rates were constant at ~ 50 mL/min for the fully penetrating well tests and ~ 40 mL/min for the sampling port tests. Pull phase water samples were obtained using a 20 mL plastic syringe connected to a valve in a sampling line.

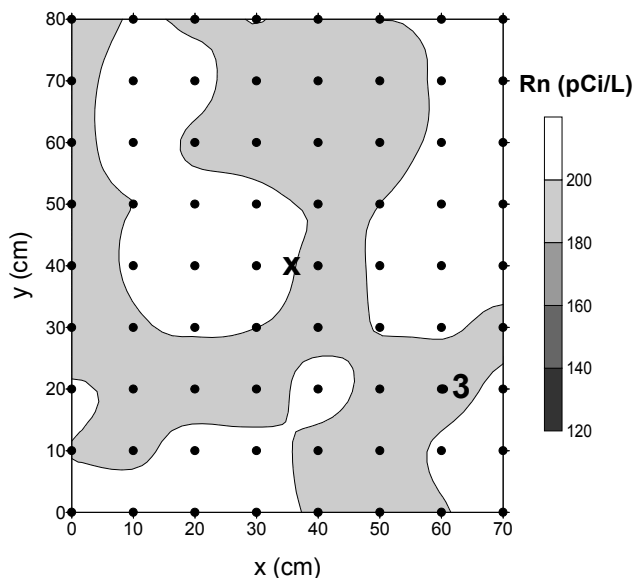


Figure 4.2 Plan view of portion of PAM used in laboratory tests, showing dimensions, fully penetrating well (x), sampling ports (•), and static radon concentrations prior to contamination of the PAM with TCE. Samples were obtained at a depth of 10 cm.

Time series concentration profiles of aqueous TCE and radon in the sediment pack after TCE contamination were obtained using a 15 L pull test (i.e., with no push phase preceding the pull phase) performed in the fully penetrating well. Water samples were obtained at depths of 7.5, 10 and 17.5 cm within the TCE-contaminated portion of the sediment pack using 20 mL plastic syringes and 12 gauge stainless steel needles. Also, the fully penetrating well was used to obtain depth-integrated samples over the entire sediment pack.

Following a series of static and push-pull tests, ethanol cosolvent and tap water flushes were used to solubilize and remove TCE from the sediment pack. A 75 % denatured ethanol (Fisher Scientific, Fair Lawn, NJ) solution was injected into the sediment pack (with four piston pumps) through four 12 gauge stainless steel needles set within the TCE-contaminated portion of the PAM. The injection rate was 5 mL/min for each of the pumps. Another piston pump was used to simultaneously extract the ethanol solution/PAM water mixture through the fully penetrating well located at the center of the TCE-contaminated portion of the PAM. This pump was calibrated at 20 mL/min to create a steady-state flow regime in the PAM. A total of 89 L of ethanol solution were injected into the TCE-contaminated zone of the PAM. Following the ethanol flushes, approximately 1150 L of tap water (~ 2 pore volumes) were flushed through the PAM from the constant head reservoirs through the fully penetrating well. Water samples were obtained during the ethanol and tap water flushes using a 5 mL glass syringe (SGE, Ringwood, Australia) connected to a valve located in a sampling line. Static and push-pull tests were performed after remediation of the sediment pack.

The sediment pack was then drained and four core samples were obtained adjacent to the fully penetrating well. Each core sample was divided into three sections of equal length

and each section placed in a 125 mL glass jar. Each jar was then filled with ~ 95 mL of methanol (Fisher Scientific, Fair Lawn, NJ), sealed, and placed on a mechanical shaker for 30 minutes. A 2 mL sample was collected by inserting a syringe needle through a septum in the jar lid and analyzed for methanol-extracted TCE.

Analytical Methods

Bromide concentrations were determined using a Dionex Model DX-120 ion chromatograph equipped with an electrical conductivity detector (Sunnyvale, CA). Aqueous radon samples were filtered through a 2.0 μm filter (Millipore, Bedford, MA) attached to a syringe and a 1.5 inch steel needle (Becton-Dickinson, Franklin Lakes, NJ). The filtered sample (~ 15 mL) was then dispensed into the bottom of a pre-weighed 20 mL borosilicate scintillation vial containing 5 mL of Ultima Gold F scintillation “cocktail” (Packard Instruments, Meriden, CT). Counting was performed with a Packard 2900 TR Liquid Scintillation Analyzer (LSA) as described by Cantaloub (2001). Aqueous TCE was quantified using a Waters HPLC using the method described by Field and Sawyer (2000), with a detection limit of 1 mg/L. The methodology of Cantaloub (2001) was used to determine the partition coefficient (K) for radon in the presence of TCE. This methodology incorporates a sequential liquid-liquid extraction technique using aqueous radium-226 and TCE. The radium-226 is used to generate radon-222. For each sequential extraction, an aliquot of TCE was added to a glass centrifuge tube containing aqueous radium-226, the solution was thoroughly mixed, and the TCE (now containing a proportion of the radon generated from the radium-226) removed. The TCE was then added to a liquid scintillation vial for counting. A value of $K = 50$ was determined, compared to a value of $K = 58$ for radon in the presence of trichloromethane (Clever, 1979).

Data Analysis

Static radon data were used to calculate TCE saturations (S_n , equation 4.5) after TCE contamination of the sediment pack, and after remediation. Radon and aqueous TCE concentrations and calculated values of S_n were plotted using the Surfer[®] software package (Golden Software, Golden, CO).

Push-pull test data analysis was performed using normalized bromide and radon concentrations. The normalized bromide concentration is defined as $C^* = 1 - C/C_o$, where C is the measured bromide concentration in a sample and C_o is the bromide concentration in the injected test solution (~ 100 mg/L). This calculation is performed to facilitate the comparison of bromide and radon breakthrough curves. The normalized radon concentration is defined as $C^* = C_w/C_b$, where C_w is the measured radon concentration and C_b is the background radon concentration in the sediment pack, which was measured prior to each push-pull test. Push-pull tests were performed within < 8 hours so that radon emanation could be neglected. For each push-pull test, pull phase normalized radon and bromide concentrations were plotted as a function of dimensionless time V_e/V_i , where V_e is the volume of solution extracted from the sediment pack at the time a water sample was obtained, and V_i is the total volume of solution injected into the sediment pack. Pull test radon and aqueous TCE concentrations were plotted as a

function of the volume of solution extracted from the sediment pack at the time a sample was obtained.

Numerical simulations were performed with the Subsurface Transport Over Multiple Phases (STOMP) code, a fully implicit volume-integrated finite difference simulator (White and Oostrom, 2000). Solute transport was simulated using PAM sediment pack properties for a range of retardation factors (R). The longitudinal dispersivity of the sediment pack was estimated for each push-pull test by fitting the experimental normalized bromide breakthrough curve to an approximate analytical solution for the pull phase of the test (Gelhar and Collins, 1971; Schroth et al., 2000) as described by Davis et al. (2002). This dispersivity value was then used in the simulation of each push-pull test for a range of retardation factors (R) using STOMP, thus producing a series of simulated breakthrough curves. A least-squares method was used to determine which simulated breakthrough curve (corresponding to a specific value of R) best fit the experimental normalized radon breakthrough curve for each push-pull test. The value of S_n for the best fit value of R was then calculated using equation 4.7.

RESULTS

Prior to TCE contamination, static radon concentrations from samples obtained at a depth of 10 cm ranged from 181 to 224 pCi/L (Figure 4.2), with this variability likely due to heterogeneity of porosity and radon emanation in the sediment pack. Results from the pull phase of a push-pull test conducted prior to TCE contamination at a depth of 10 cm in sampling port 3 (location shown in Figure 4.2) are shown in Figure 4.3. Breakthrough curves are displayed as normalized concentration (C^*) versus dimensionless time (V_e/V_i) for bromide and radon. Normalized concentrations increased smoothly as the test solution was extracted from the sediment pack, and radon transport was slightly retarded relative to bromide. The normalized bromide concentration data were well fit by a simulated $R = 1$ breakthrough curve, while the normalized radon concentration data were best fit by a simulated $R = 1.2$ breakthrough curve (Table 4.1). Additional push-pull tests performed under the same conditions at different sampling ports (data not shown) showed results similar to Figure 4.3. Following these tests TCE was injected into the PAM sediment pack as described above.

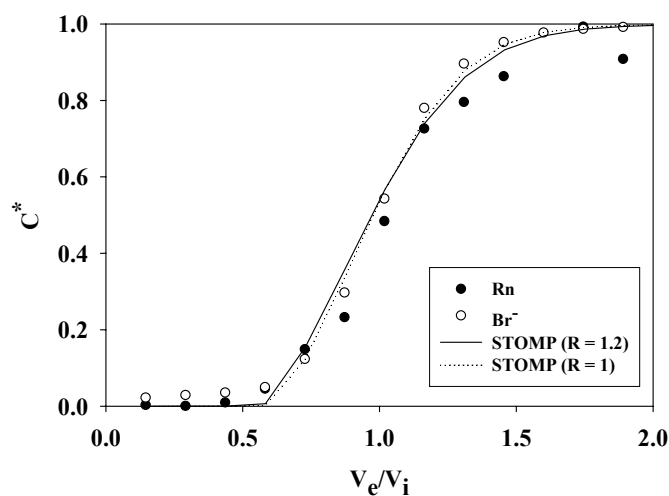


Figure 4.3 Pull phase breakthrough curves for a push-pull test conducted in sampling port 3 prior to contamination of the PAM with TCE. The test was conducted at a depth of 10 cm.

Two months after TCE contamination a push-pull test was conducted in the fully penetrating well. Normalized concentrations increased smoothly as the test solution was extracted from the sediment pack, and radon transport was retarded relative to bromide with the radon retardation manifested as greater dispersion relative to bromide (Figure 4.4). The normalized bromide concentration data were well fit by a simulated $R = 1$ breakthrough curve while the normalized radon concentration data were best fit by a simulated $R = 9.4$ breakthrough curve (Table 4.1). Another static test was then performed with radon samples again being obtained from a depth of 10 cm (Figure 4.5).

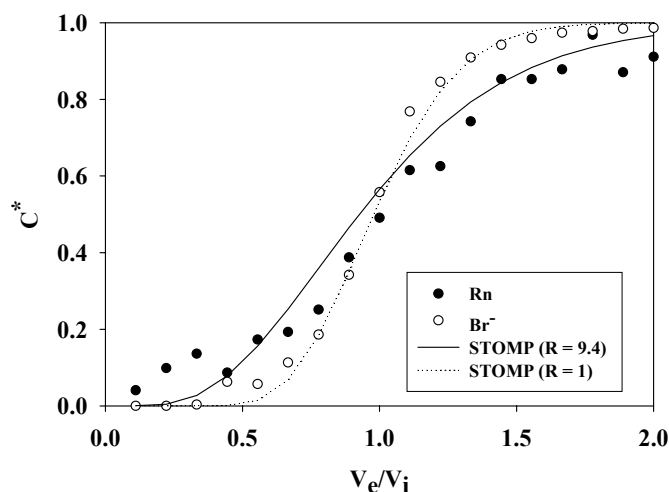


Figure 4.4 Pull phase breakthrough curves for the first push-pull test conducted in the fully penetrating well after contamination of the PAM with TCE.

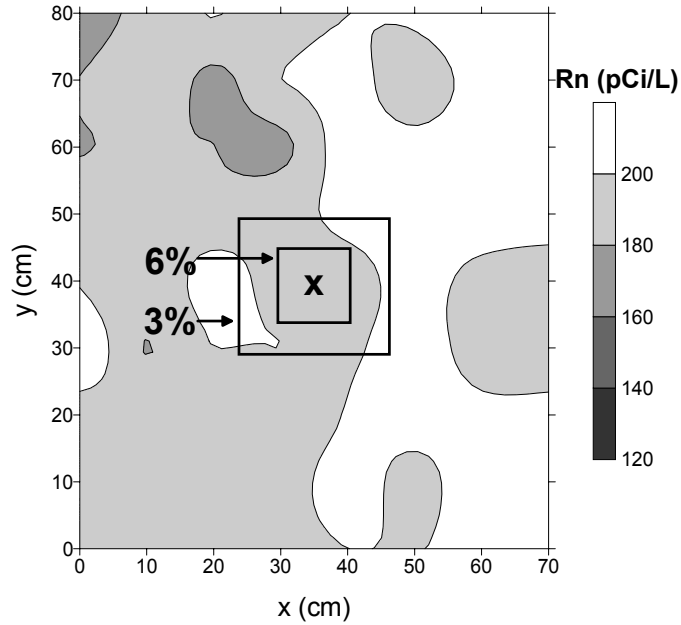


Figure 4.5 Plan view of static radon concentrations after contamination of the PAM with TCE. Samples were obtained at a depth of 10 cm.

Table 4.1 Experimental timeline and push-pull test results, showing best fit radon retardation factors (R), adjusted retardation factors, and TCE saturations (S_n).

Test Type	Months after TCE contamination	Figure	Test Location	Depth of Test (cm)	Volume injected (L)	R	Adjusted R	S_n (%)
static	-	4.2	sampling ports	10	-	-	-	-
push-pull	-	4.3	sampling port 3	10	1.2	1.2	1.0	0
push-pull	2	4.4	fully penetrating well	0-20	10	9.4	9.2	14.1
static	3	4.5	sampling ports	10	-	-	-	-
push-pull	8	4.6	fully penetrating well	0-20	10	3.8	3.6	4.9
pull	9	4.7(a,b)	sampling ports and fully penetrating well	0-20	-	-	-	-
static	20	4.8(a,b,c)	sampling ports	19.5	-	-	-	-
static	25	4.9(a,b,c)	sampling ports	19.5	-	-	-	-
push-pull	26	4.10	fully penetrating well	0-20	10	1.0	-	-
push-pull	27	4.11	sampling port 1	19.5	1.2	7.0	6.8	10.4
push-pull	27	4.12	sampling port 2	19.5	1.2	1.4	1.2	0.4

Radon concentrations ranged from 166 to 225 pCi/L. The radon retardation in the previous push-pull test, combined with the negligible change in static radon concentrations at the 10 cm depth relative to pre-contamination concentrations (Figure 4.2) supported a hypothesis that TCE had sunk to the bottom of the sediment pack. A second push-pull test was conducted in the fully penetrating well 8 months after TCE contamination. Normalized concentrations increased smoothly as the test solution was extracted from the sediment pack, although the radon data exhibited some unexplained tailing at the end of the test (Figure 4.6). Radon transport was retarded relative to bromide, but to a lesser extent than the earlier test (Figure 4.4). The normalized bromide concentration data were well fit by a simulated $R = 1$ breakthrough curve while the normalized radon concentration data were best fit by a simulated $R = 3.8$ breakthrough curve (Table 4.1), compared to the larger best fit $R = 9.4$ for the first push-pull test in the fully penetrating well. The decrease in R between the two tests indicated a change in TCE saturation and is consistent with the hypothesis that TCE had sunk.

A 15 L pull test was then conducted to further investigate the TCE distribution in the sediment pack. Time series concentration profiles show that radon concentrations decreased with depth with the exception of the 7.5 cm depth (Figure 4.7a), where partitioning to a gas phase at the top of the sediment pack probably resulted in reduced concentrations. The decrease in radon concentrations between 3 and 5 L at the 17.5 cm depth likely results from water originating from a zone of high TCE saturation toward the bottom of the sediment pack. Aqueous TCE concentrations increased with depth and approached the solubility limit (~ 1000 mg/L) at 17.5 cm (Figure 4.7b), which correlates well with decreasing radon concentrations with depth to indicate that TCE had sunk to the bottom of the sediment pack.

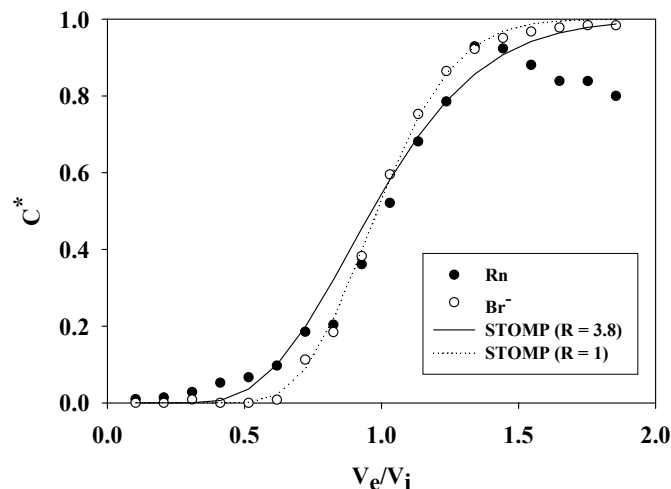


Figure 4.6 Pull phase breakthrough curves for the second push-pull test conducted in the fully penetrating well after contamination of the PAM with TCE.

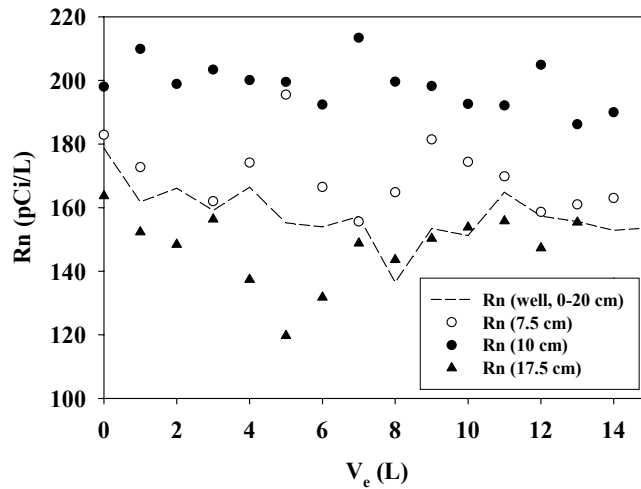


Figure 4.7a Time series concentration profile of radon concentrations (pCi/L) for a pull test conducted after contamination of the PAM with TCE. Samples were obtained from the fully penetrating well (average = 157.7, standard deviation = 9.1), and from needles located at depths of 7.5 cm (average = 170.1, standard deviation = 10.6); 10 cm (average = 197.0, standard deviation = 9.6); and 17.5 cm (average = 147.5, standard deviation = 11.3).

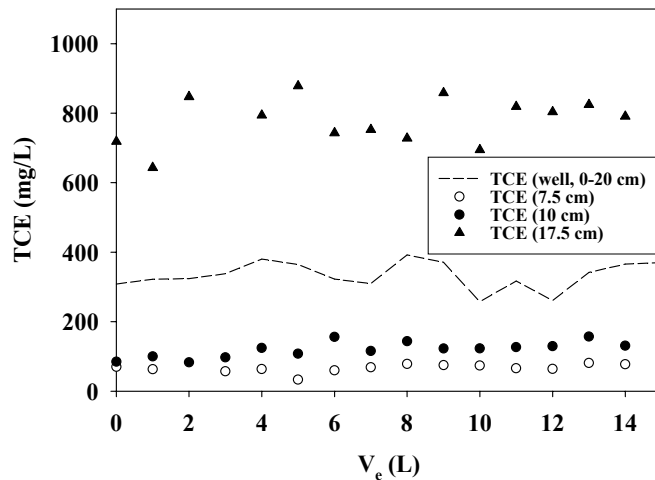


Figure 4.7b Time series concentration profile of aqueous TCE concentrations (mg/L) for a pull test conducted after contamination of the PAM with TCE. Samples were obtained from the fully penetrating well (average = 334.1, standard deviation = 39.4), and from needles located at depths of 7.5 cm (average = 66.7, standard deviation = 11.5); 10 cm (average = 120.8, standard deviation = 22.1); and 17.5 cm (average = 779.6, standard deviation = 65.3).

Following the 15 L pull test another static test was performed, with radon and aqueous TCE samples obtained at a depth of 19.5 cm. This depth was chosen to further investigate the hypothesis that TCE had sunk to the bottom of the sediment pack.

Unfortunately, radon samples were not collected from this depth prior to TCE contamination. Due to partitioning into TCE, radon concentrations were reduced in the sediment pack, ranging from 120 to 217 pCi/L (Figure 4.8a), compared to the previous static test conducted at a depth of 10 cm (Figure 4.5). The greatest radon concentration reductions occurred in the vicinity of the concentric zones of 6 % and 3 % TCE saturation. Aqueous TCE concentrations ranged from 251 mg/L to the solubility limit, with the highest concentrations located in the 6 % and 3 % TCE saturation zones (Figure 4.8b). Calculated TCE saturations (S_n) show a maximum value of 1.4 % (Figure 4.8c) in the vicinity of both the lowest radon concentrations and the highest aqueous TCE concentrations.

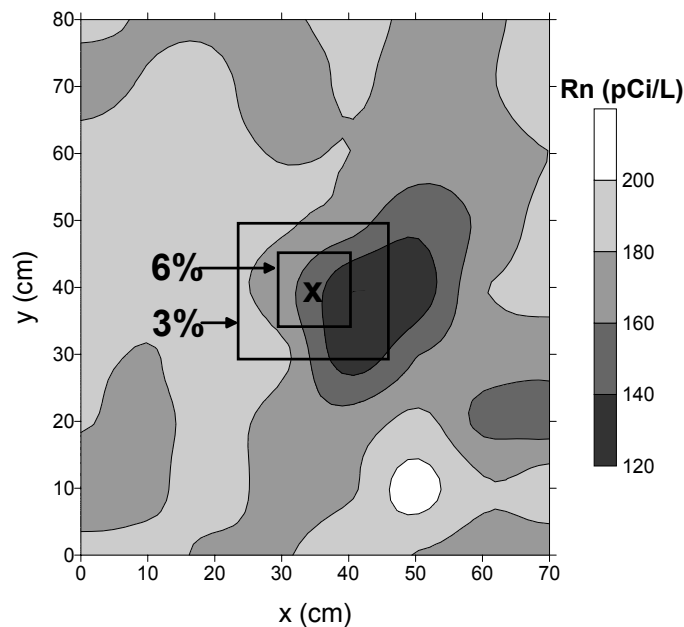


Figure 4.8a Plan view of static radon concentrations after contamination of the PAM with TCE. Samples were obtained from a depth of 19.5 cm.

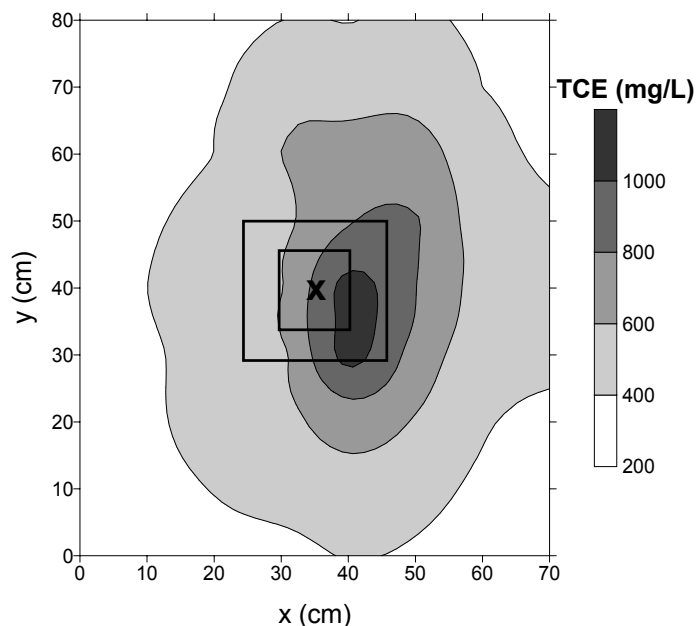


Figure 4.8b Plan view of static aqueous TCE concentrations after contamination of the PAM with TCE. Samples were obtained from a depth of 19.5 cm.

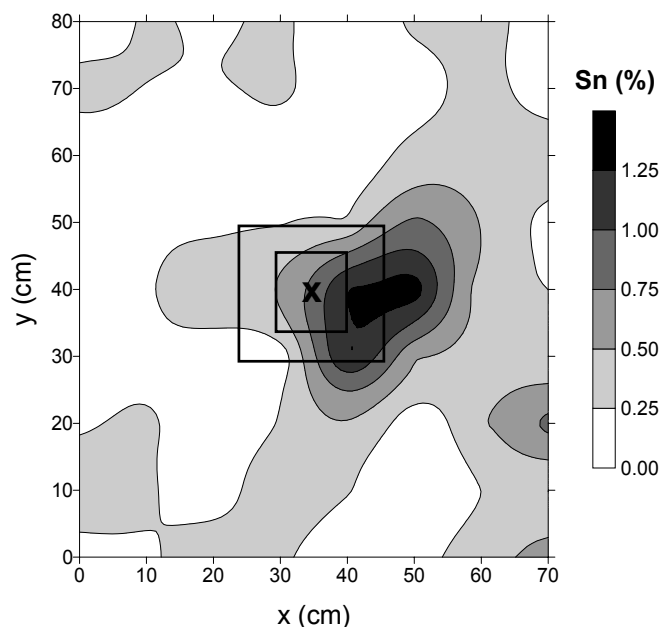


Figure 4.8c Plan view of calculated TCE saturations (S_n) after contamination of the PAM with TCE. Samples were obtained from a depth of 19.5 cm.

The TCE in the sediment pack was then remediated using a series of ethanol cosolvent and tap water flushes. Gross mass balance TCE calculations were performed using aqueous TCE data from the remediation activities and the 15 L pull and push-pull test immediately preceding remediation. These calculations showed that roughly 50 % of the injected TCE was removed over the course of these experiments. However, the actual amount of TCE removed is likely greater than 50 % since additional push-pull tests were performed where aqueous TCE was not sampled. The remediation was followed by a

three week rest period to allow for the equilibration of radon concentrations in the pore water. Another static test was then performed at a depth of 19.5 cm. Radon concentrations increased across portions of the PAM and decreased in other locations (ranging from 140 to 219 pCi/L, Figure 4.9a) and aqueous TCE concentrations were decreased (ranging from < 1 to 19 mg/L, Figure 4.9b). Calculated TCE saturations (S_n) show a maximum value of 1.3 % in the vicinity of the lowest radon concentrations (Figure 4.9c), although aqueous TCE concentrations were < 5 mg/L in this portion of the PAM.

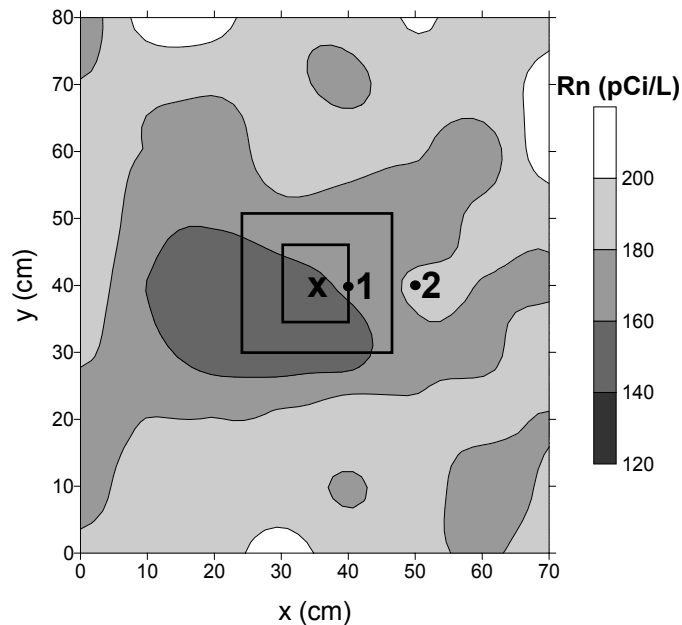


Figure 4.9a Plan view of static radon concentrations after PAM remediation. Samples were obtained from a depth of 19.5 cm.

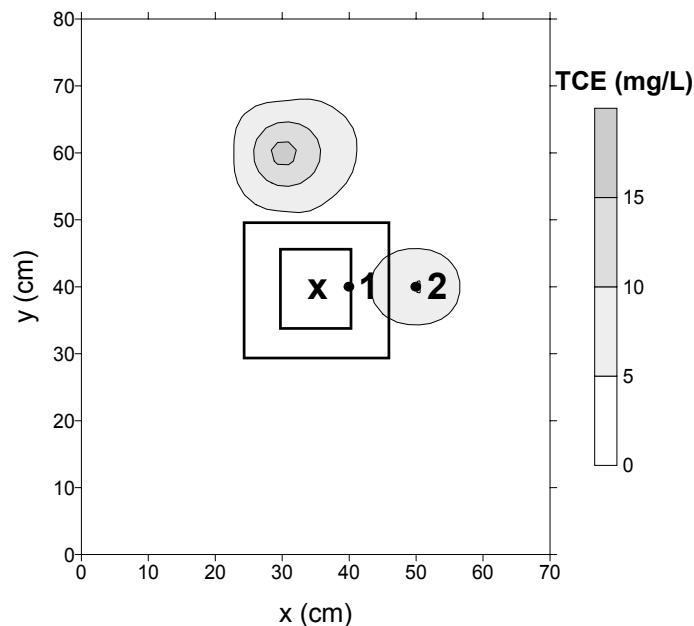


Figure 4.9b Plan view of static aqueous TCE concentrations after PAM remediation. Samples were obtained from a depth of 19.5 cm.

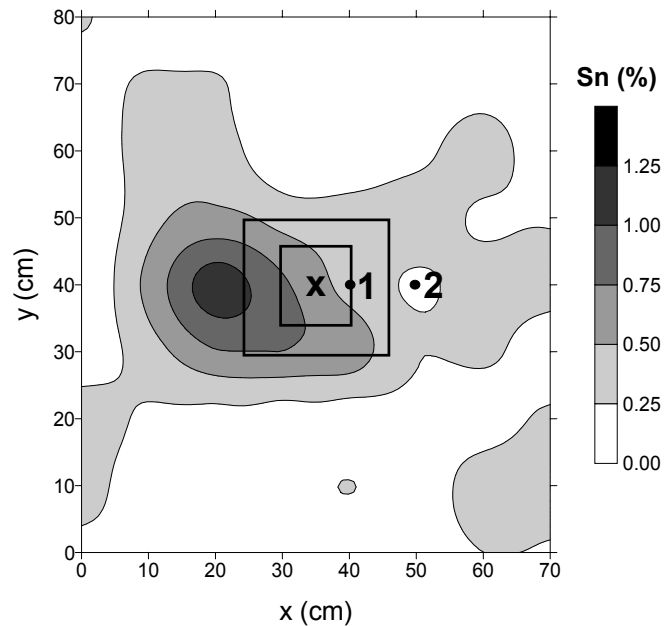


Figure 4.9c Plan view of calculated TCE saturations (S_n) after PAM remediation. Samples were obtained from a depth of 19.5 cm.

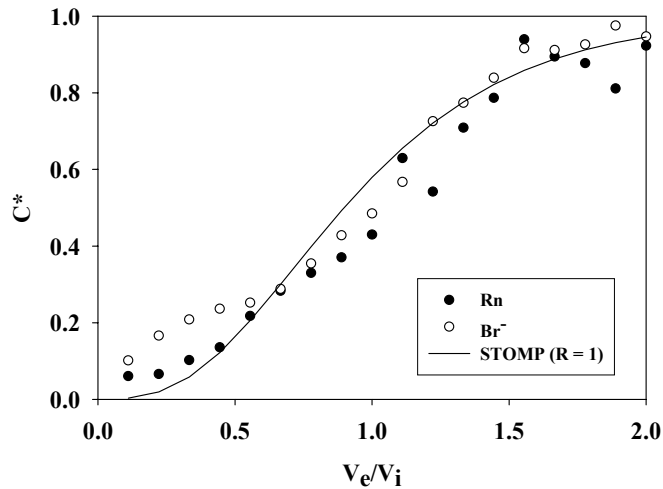


Figure 4.10 Pull phase breakthrough curves for the push-pull test conducted in the fully penetrating well after PAM remediation.

Another push-pull test was then performed in the fully penetrating well. Normalized concentrations increased smoothly as the test solution was extracted from the sediment pack, although there is no clear evidence for radon retardation relative to bromide (Figure 4.10). The normalized bromide concentration data were not well fit by a simulated $R = 1$ breakthrough curve. The normalized radon concentration data were best fit by a simulated $R = 1$ breakthrough curve, although the fit is poor (Table 4.1). The normalized bromide and radon concentration data show increased dispersion compared to identical

push-pull tests conducted before remediation (Figures 4.4 and 4.6), making breakthrough curve interpretation difficult.

Push-pull tests were then performed at a depth of 19.5 cm in sampling ports 1 (located in the TCE injection zone) and 2 (located outside the TCE injection zone, Figure 4.9a). These ports were chosen based on static sampling data (Figure 4.9c) which indicated that the sediment pack near sampling port 1 was contaminated with TCE, while there was a decreased likelihood of TCE contamination near sampling port 2. Unfortunately, push-pull tests were not performed in these sampling ports before remediation, which would have enabled a comparison of pre- and post-remediation radon retardation factors. For both push-pull tests normalized concentrations increased smoothly as the test solutions were extracted from the sediment pack (Figures 4.11 and 4.12). Radon transport was retarded relative to bromide in sampling port 1, and slightly retarded in sampling port 2. The normalized bromide concentration data were well fit by a simulated $R = 1$ breakthrough curve for both tests. The normalized radon concentration data were best fit by a simulated $R = 7$ breakthrough curve in sampling port 1 and simulated $R = 1.4$ breakthrough curve in sampling port 2 (Table 4.1). Following these push-pull tests the PAM was drained and four core samples were obtained adjacent to the fully penetrating well. All core samples showed methanol-extracted TCE concentrations below detection limits (1 mg/L).

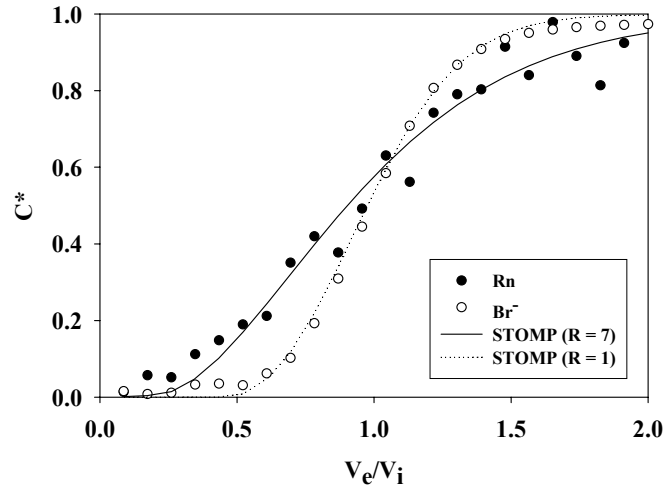


Figure 4.11 Pull phase breakthrough curves for a push-pull test conducted in sampling port 1 after PAM remediation. The test was conducted at a depth of 19.5 cm.

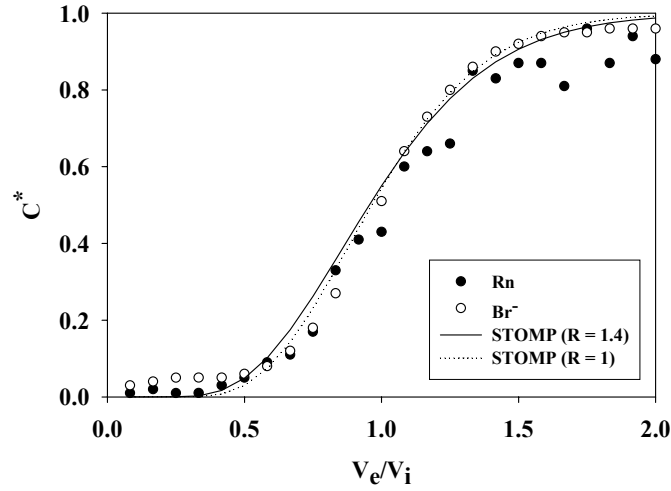


Figure 4.12 Pull phase breakthrough curves for a push-pull test conducted in sampling port 2 after PAM remediation. The test was conducted at a depth of 19.5 cm.

DISCUSSION

Partitioning of radon between the pore water and trapped gas present in the sediment pack is likely the cause of the slight radon retardation observed in the push-pull test conducted prior to TCE contamination (Figure 4.3). This phenomenon has been observed in previous laboratory push-pull tests using the same sediment (Davis et al., 2002). Assuming equilibrium partitioning between the trapped gas and aqueous phases, the retardation factor for a dissolved gas can be written as (Fry et al., 1995)

$$R = 1 + H_{cc} \frac{S_g}{S_w} \quad (4.8)$$

where H_{cc} is the dimensionless Henry's constant and S_g is the trapped gas saturation. Using equation 4.8, a value of $H_{cc} = 3.9$ for radon (Clever, 1979), and the best fit $R = 1.2$ for radon from the push-pull test, the estimated gas saturation in the sediment pack is 5 %.

Radon retardation during the push-pull tests conducted after TCE contamination was likely due to 1) radon partitioning between TCE and the aqueous phase, and 2) radon partitioning between trapped gas and the aqueous phase. In order to estimate the portion of radon retardation due to TCE partitioning, best fit R values were adjusted to account for partitioning of radon into the trapped gas using

$$R_{adj} = R_{post-TCE} - (R_{pre-TCE} - 1) \quad (4.9)$$

where R_{adj} is the adjusted retardation factor, $R_{post-TCE}$ is the retardation factor from a push-pull test conducted after TCE contamination, and $R_{pre-TCE}$ is the retardation factor from the push-pull test conducted prior to TCE contamination ($R = 1.2$, Figure 4.3). Adjusted retardation factors were used to calculate TCE saturations (S_n , Table 4.1). The best fit $R = 9.4$ for the push-pull test conducted after TCE contamination (Figure 4.4) is therefore adjusted to a value of $R = 9.2$. Using equation 4.7, the adjusted retardation factor, and $K = 50$, the calculated $S_n = 14.1$ %. This value overestimates the volume-averaged TCE

saturation of 1.2 % in the sediment pack, where the TCE saturation is averaged over the approximate 20 cm radius of influence of this push-pull test. The reasons for this overestimation are unclear, especially in light of the subsequent static and push-pull tests that indicated that TCE sank to the bottom of the sediment pack. A heterogeneous TCE distribution with pooling toward the bottom of the sediment pack would more likely result in smaller radon retardation factors because of the reduced interfacial area between the TCE and the injection solution. This reduced interfacial area due to the geometry of the pools would limit mass transfer and could violate the assumption of equilibrium partitioning (Chrysikopoulos and Kim, 2000; Willson et al., 2000). In addition, push-pull tests conducted in the fully penetrating well interrogated the entire 0 to 20 cm thickness of the PAM. Thus with a heterogeneous TCE distribution, the contribution of radon from layers of the sediment pack with either a lower TCE saturation or no TCE would serve to “dilute” the retarded radon response from layers contaminated with TCE, thus decreasing R .

Static radon samples obtained from a depth of 10 cm after TCE contamination (Figure 4.5) showed little change relative to pre-contamination radon concentrations (Figure 4.2), indicating that TCE had sunk below the 10 cm depth. The second push-pull test in the fully penetrating well (Figure 4.6) showed an adjusted $R = 3.6$, with a calculated $S_n = 4.9$ % (Table 4.1). The decrease in adjusted R values between these two push-pull tests indicates that additional TCE sank in the 6 months between the tests (Table 4.1). Although the push-pull tests may tend to overestimate S_n , the tests show that changes in retardation may indicate changes in TCE saturation distribution over time.

Results from the 15 L pull test following TCE contamination (Figures 4.7a and 4.7b) support the hypothesis that the TCE sank. The lowest radon and highest aqueous TCE concentrations were observed at a depth of 17.5 cm. The likely existence of a zone of greater S_n is shown by the decrease in radon concentrations between 3 and 5 L (Figure 4.7a). Assuming a cylindrical geometry, this zone is located approximately 11 to 14 cm from the well. Radon concentrations then increased as water from zones of lesser S_n was extracted. The decrease in radon concentrations at 7.5 cm (Figure 4.7a) is attributed to radon partitioning to a gas phase at the top of the sediment pack, which is consistent with a decrease in aqueous TCE concentrations at this depth. During the 15 L pull experiment it was determined that the upper 3 to 4 cm of the sediment pack was not water saturated; this was remedied by adjusting the PAM standpipe/overflow systems.

Static radon and aqueous TCE samples obtained after the 15 L pull test were obtained from a depth of 19.5 cm to account for the sinking of TCE. Radon concentrations were decreased after TCE contamination, with the greatest decreases occurring near the concentric zones of 6 % and 3 % TCE saturation (Figure 4.8a). Due to the sinking of injected TCE it is unlikely that these predicted TCE saturations were realized in the sediment pack. For example, a water sample obtained from the bottom of the sediment pack after TCE contamination contained neat TCE, supporting the hypothesis that TCE sank to the bottom of the sediment pack. The TCE injection scheme likely resulted in the highest TCE saturations in the 6 % zone, with lower saturations in the 3 % zone and the lowest saturations outside of the 3 % zone. The highest aqueous TCE concentrations

(Figure 4.8b) were observed in the vicinity of the lowest radon concentrations. Although aqueous TCE concentrations approaching the solubility limit were measured in these zones, calculated values of S_n (Figure 4.8c) were $\leq 1.4\%$, which were lower than expected. This is possibly due to the relationship between diffusion and the volume of water obtained from the sediment pack for each static sample (i.e., 20 mL). A radon sample obtained from directly adjacent to the TCE would have a decreased concentration (relative to the pre-TCE contamination concentration) due to partitioning of radon into TCE. However, as the sampling point moves away from the TCE, the emanation of radon from the sediment attenuates the effect of radon partitioning. A 20 mL sample interrogates a radius of approximately 2.3 cm, assuming a spherical shape. If TCE were not present within this sample radius, or if only a portion of the interrogated sediment was contaminated, the effect of partitioning on the observed radon concentration would be lessened. The non-linear relationship between radon concentration and S_n (equation 4.4) could also result in an underestimation of S_n . For example, a decrease in radon concentration in a sampling port from 200 to 100 pCi/L after TCE contamination would result in a calculated $S_n = 2.0\%$. However, if the sample containing radon at 100 pCi/L contained two equal volumes of water with 50 and 150 pCi/L, respectively, then calculating S_n individually for each of the volumes would result in calculated S_n values of 6.0 and 0.67 %, with an average $S_n = 3.3\%$. These phenomena could result in an underestimation of the TCE saturation in the sediment pack, as is evident in Figure 4.8c. The static method is therefore sensitive to sample size in a heterogeneous DNAPL distribution.

Figures 4.8a and 4.9a show that static radon concentrations at 19.5 cm increased in some locations after remediation, with the greatest increases occurring near the concentric zones of injected TCE. However, radon concentrations also decreased in some portions of the sediment pack. Aqueous TCE concentrations were decreased after remediation (Figure 4.9b), with concentrations < 5 mg/L across the majority of the PAM. A comparison of calculated S_n (Figures 4.8c and 4.9c) shows a decrease after remediation in the zones of highest S_n prior to remediation. Also noted is an increase in S_n in the vicinity of $x = 20$ cm, $y = 40$ cm. The decrease in radon concentrations and resulting increased values of S_n in this vicinity could be due to the movement of TCE (during remediation). However, the presence of relatively low (< 5 mg/L) concentrations of aqueous TCE in this vicinity may indicate a change in sediment pack physical properties during remediation causing localized decreases in radon concentrations. The creation of localized preferential flow paths during remediation could increase porosity and reduce the equilibrium radon concentration (equation 4.4).

A change in sediment pack physical properties is indicated by a comparison of the results from the push-pull tests conducted in the fully penetrating well before (Figures 4.4 and 4.6) and after remediation (Figure 4.10). The normalized bromide breakthrough curves from the post-remediation test have a greater dispersion than those from the pre-remediation tests, possibly due to the creation of preferential flow paths resulting from the pumping of over 1200 L of tap water and ethanol solution through the sediment pack during remediation. Preferential flow paths and a resulting increase in porosity could decrease the travel distance of the injection solution during the push-pull test, which

would result in increased dispersion in pull-phase breakthrough curves (Schroth et al., 2000). The simulation results provided poor fits to the post-remediation push-pull test normalized bromide and radon breakthrough curves, likely resulting from preferential flow paths. However, even with the increased dispersion of the normalized bromide and radon breakthrough curves, radon retardation was not evident in this push-pull test. This supports the contention that the majority of the TCE was removed by the end of the remediation activities.

The static test results after remediation, methanol-extracted TCE concentrations < 1 mg/L from core samples obtained adjacent to the fully penetrating well, and the gross mass balance on TCE provide additional evidence that the majority of the TCE was removed from the sediment pack by the end of remediation. However, two push-pull tests conducted at a depth of 19.5 cm in sampling ports 1 and 2 (Figures 4.11 and 4.12) highlight the influence of sample size and location on push-pull test results and the continued presence of TCE at the bottom of the sediment pack after remediation. These two push-pull tests had a radius of influence of approximately 9 cm. For sampling port 1 the adjusted $R = 6.8$ resulted in a calculated $S_n = 10.4$ % (Table 4.1), indicating the existence of a ‘pocket’ of higher S_n that was not detected by the push-pull test conducted in the fully penetrating well after remediation. Conversely, for sampling port 2 the adjusted $R = 1.2$ resulted in a calculated $S_n = 0.4$ %, indicating that little TCE remained in the vicinity of this sampling port.

These results show that push-pull test location in a heterogeneous TCE distribution can be critical in the calculation of S_n . Moreover, a comparison of the push-pull test conducted in the fully penetrating well after remediation with the push-pull test conducted in sampling port 1 highlights the sensitivity of the method to both sample size (i.e., volume of injection solution) and test design. In this case the two tests used different volumes of injection solution (10 L vs. 1.2 L). In addition, the test in the fully penetrating well interrogated the entire thickness of the PAM, while the test in sampling port 1 was focused at the bottom of the sediment pack. The two tests, although conducted within a horizontal distance of 5 cm of each other, interrogated different volumes of the sediment pack, with the 10 L push-pull test not showing clear evidence for any remaining ‘pockets’ of TCE. In contrast, the 1.2 L push-pull test, by nature of its location at the bottom of the sediment pack and smaller volume of injection solution, interrogated a smaller portion of the sediment pack with a greater S_n .

CONCLUSIONS

The results of the laboratory and modeling studies show that static and push-pull methods using naturally occurring radon as a partitioning tracer have the potential to characterize DNAPL saturations in the subsurface. These methods can be applied at contaminated field sites using existing monitoring wells. Radon has the potential benefit of being an in situ partitioning tracer and can be easily sampled using standard sampling techniques and liquid scintillation analysis. However, the application of these methods to characterizing field sites with heterogeneous DNAPL distributions is complicated by the methods’ sensitivity to test location, sample size, and test design. The static method is influenced by spatial changes in aquifer properties and DNAPL saturations. Sample size can also

critically influence results from static and push-pull tests. If DNAPL is heterogeneously distributed in the aquifer, static samples with different volumes may provide different estimates of DNAPL saturation. Similarly, a push-pull test conducted with a smaller volume of injection solution may yield a radon retardation factor different from a test conducted with a larger volume of injection solution at the same location. Test design can also influence push-pull test results through the selection of a specified thickness of an aquifer over which to conduct the test. When DNAPL is heterogeneously distributed (e.g., in a layered aquifer), push-pull tests can be performed using inflatable packers to isolate a suspected zone of DNAPL contamination. Tests conducted over the entire saturated thickness of the aquifer in the same well could yield a lesser retardation factor due to the contribution of higher radon concentrations from less contaminated portions of the aquifer. The sensitivity of the static and push-pull methods to these factors presents challenges to the application of these methods at field sites. The static and push-pull methods have the potential to provide quantitative information on changes in DNAPL saturations as a result of remediation. However, further study of the influence of these factors on the ability of the methods to quantify DNAPL saturations is warranted.

ACKNOWLEDGEMENTS

We thank Dr. Alan Fryar and two anonymous reviewers for their comments and suggestions. We also thank Mike Cantaloub, Jennifer Field, Ralph Reed, Adisorn Tovanabootr, Mark Humphrey, and Jesse Jones for assistance with laboratory and analytical activities, and Martin Schroth and Mark White for assistance with STOMP.

REFERENCES

- Adloff, J. and Guillaumont, 1993. *Fundamentals of Radiochemistry*. CRC Press, Boca Raton, FL.
- Annable, M.D., P.S.C. Rao, K. Hatfield, W.D. Graham, A.L. Wood, and C.G. Enfield, 1998. Partitioning tracers for measuring residual NAPL: field-scale test results. *Journal of Environmental Engineering*, 124:498-503.
- Cable, J.E., G.C. Bugna, W.C. Burnett, and J.P. Chanton, 1996. Application of ²²²Rn and CH₄ for assessment of groundwater discharge to the coastal ocean. *Limnology and Oceanography*, 41:1347-1353.
- Cantaloub, M., 2001. Aqueous-organic partition coefficients for radon-222 and their application to radon analysis by liquid scintillation methods. Master's Thesis, Oregon State University.
- Chrysikopoulos, C.V. and T. Kim, 2000. Local mass transfer correlations for nonaqueous phase liquid pool dissolution in saturated porous media. *Transport in Porous Media*, 38:167-187.
- Clever, H.L., 1979. *Solubility Data Series Volume 2*. Pergamon Press, NY.
- Cohen, R.M. and J.W. Mercer, 1993. *DNAPL Site Evaluation*. CRC Press, Boca Raton, FL.
- Davis, B.M., J.D. Istok, and L. Semprini, 2002. Push-pull partitioning tracer tests using radon-222 to quantify non-aqueous phase liquid contamination. *Journal of Contaminant Hydrology*, 58:129-146.
- Dwarakanath, V., N. Deeds, and G.A. Pope, 1999. Analysis of Partitioning Interwell Tracer Tests. *Environmental Science and Technology*, 33:3829-3836.

- Field, J.A. and T.E. Sawyer, 2000. High performance liquid chromatography-diode array detection of trichloroethene and aromatic and aliphatic anionic surfactants used for surfactant-enhanced aquifer remediation. *Journal of Chromatography A*, 893:253-260.
- Fry, V.A., J.D. Istok, L. Semprini, K.T. O'Reilly, and T.E. Buscheck, 1995. Retardation of dissolved oxygen due to a trapped gas in porous media. *Ground Water*, 33:391-398.
- Gelhar, L.W. and M.A. Collins, 1971. General analysis of longitudinal dispersion in nonuniform flow. *Water Resources Research*, 7:1511-1521.
- Gottipati, S., 1996. Radon-222 as a tracer for performance assessment of NAPL remediation technologies in the saturated zone: an experimental investigation. Master's Thesis, Oregon State University.
- Hamada, T. and T. Komae, 1998. Analysis of recharge by paddy field irrigation using ²²²Rn concentration in groundwater as an indicator. *Journal of Hydrology*, 205:92-100.
- Hopkins, O.S., 1995. Radon-222 as an indicator for nonaqueous phase liquids in the saturated zone: developing a detection technology. Master's Thesis, Oregon State University.
- Humphrey, M.D., 1992. Experimental design of physical aquifer models for evaluation of groundwater remediation strategies. Master's Thesis, Oregon State University.
- Hunkeler, D., E. Hoehn, P. Höhener, and J. Zeyer, 1997. 222-Rn as a partitioning tracer to detect diesel fuel contamination in aquifers: laboratory study and field observations. *Environmental Science & Technology*, 31:3180-3187.
- Istok, J.D. and M.D. Humphrey, 1995. Laboratory investigation of buoyancy-induced flow (plume sinking) during two-well tracer tests. *Ground Water*, 33:597-604.
- Jin, M., M. Delshad, V. Dwarakanath, D.C. McKinney, G.A. Pope, K. Sepehrnoori, C.E. Tilburg, and R.E. Jackson, 1995. Partitioning tracer test for detection, estimation, and remediation performance assessment of subsurface nonaqueous phase liquids. *Water Resources Research*, 31:1201-1211.
- Lindsey, K.A. and G.K. Jaeger, 1993. Geologic setting of the 100-HR-3 operable unit, Hanford site, south-central Washington. WHC-SD-EN-TI-132, Rev. 0, Westinghouse Hanford Company, Richland, WA.
- Mercer, J.W. and R.M. Cohen, 1990. A review of immiscible fluids in the subsurface: properties, models, characterization and remediation. *Journal of Contaminant Hydrology*, 6:107-163.
- National Research Council, 1999. Risk Assessment of Radon in Drinking Water. National Academy Press, Washington, DC.
- Nelson, N.T. and M.L. Brusseau, 1996. Field study of the partitioning tracer method for detection of dense nonaqueous phase liquid in a trichloroethene-contaminated aquifer. *Environmental Science & Technology*, 30:2859-2863.
- Nelson, N.T., M. Oostrom, T.W. Wietsma, and M.L. Brusseau, 1999. Partitioning tracer method for the in situ measurement of DNAPL saturation: influence of heterogeneity and sampling method. *Environmental Science & Technology*, 33:4046-4053.
- Schroth, M.H., J.D. Istok, and R. Haggerty, 2000. In situ evaluation of solute retardation using single-well push-pull tests. *Advances in Water Resources*, 24:105-117.

- Schwille, F., 1988. Dense Chlorinated Solvents in Porous and Fractured Media. Lewis Publishers, Chelsea, MI.
- Semprini, L., K. Broholm, and M. McDonald, 1993. Radon-222 deficit for locating and quantifying NAPL contamination in the subsurface. EOS Transactions American Geophysical Union, 76:F276.
- Semprini, L., M. Cantaloub, S. Gottipati, O. Hopkins, and J. Istok, 1998. Radon-222 as a Tracer for Quantifying and Monitoring NAPL Remediation. In: G.B. Wickramanayake and R.E. Hinchee (Editors), Nonaqueous-Phase Liquids. Battelle Press, Columbus, OH, pp. 137-142.
- Semprini, L., O.S. Hopkins, and B.R. Tasker, 2000. Laboratory, field and modeling studies of radon-222 as a natural tracer for monitoring NAPL contamination. *Transport in Porous Media*, 38:223-240.
- Snow, D.D. and R.F. Spalding, 1997. Short-term aquifer residence times estimated from ^{222}Rn disequilibrium in artificially recharged ground water. *Journal of Environmental Radioactivity*, 37:307-325.
- White, M.D. and M. Oostrom, 2000. STOMP: Subsurface Transport Over Multiple Phases, Version 2.0, User's Guide. PNNL-12034, Richland, WA.
- Willson, C.S., O. Pau, J.A. Pedit, and C.T. Miller, 2000. Mass transfer rate limitation effects on partitioning tracer tests. *Journal of Contaminant Hydrology*, 45:79-97.
- Wilson, R.D. and D.M. Mackay, 1995. Direct detection of residual nonaqueous phase liquid in the saturated zone using SF₆ as a partitioning tracer. *Environmental Science & Technology*, 29:1255-1258.
- Young, C.M., R.E. Jackson, M. Jin, J.T. Londergan, P.E. Mariner, G.A. Pope, F.J. Anderson, and T. Houk, 1999. Characterization of a TCE NAPL zone in alluvium by partitioning tracers. *Ground Water Monitoring and Remediation*, 19:84-94.

5. NUMERICAL SIMULATIONS OF RADON AS AN IN SITU PARTITIONING TRACER FOR QUANTIFYING NAPL CONTAMINATION USING PUSH-PULL TESTS

INTRODUCTION

Partitioning interwell tracer tests have been used to quantify nonaqueous phase liquid (NAPL) saturations in laboratory and field settings (Jin et al., 1995; Nelson and Brusseau, 1996; Annable et al., 1998; Nelson et al., 1999; Young et al. 1999). Recently, single-well ‘push-pull’ partitioning tracer tests have been used to quantify NAPL saturations (Davis et al., 2002; Istok et al., 2002). In a push-pull test, an injection solution containing partitioning and conservative tracers is injected (‘pushed’) into an aquifer through a well. The solution/groundwater mixture is then extracted (‘pulled’) from the same well. These tests have involved the use of both ‘ex situ’ (i.e., injected) and ‘in situ’ (i.e., naturally occurring radon) partitioning tracers. For the ex situ tracer method, partitioning and conservative (e.g., bromide) tracers are injected into the aquifer, while for the in situ tracer method, a radon-free injection solution (containing a conservative bromide tracer) is injected into the aquifer. In both cases the presence of NAPL is indicated by a greater dispersion of the extraction phase breakthrough curve (BTC) for the partitioning tracer relative to a conservative tracer (Schroth et al., 2000).

In situ radon has been used as a partitioning tracer for locating and quantifying NAPL in field and laboratory settings (Semprini et al., 1993; Hunkeler et al. 1997; Semprini et al., 1998; Semprini et al., 2000; Davis et al., 2002). The steady-state or ‘background’ radon concentration in groundwater ($C_{w,bkg}$) is a function of the radium content (C_{Ra}) and radon emanation power (E_p) of the mineral phase and the bulk density (ρ_b) and porosity (n) of the aquifer as described by (Semprini et al., 2000)

$$C_{w,bkg} = \frac{C_{Ra} E_p \rho_b}{n} \quad (5.1)$$

The partition coefficient (K) for radon is defined as

$$K = \frac{C_n}{C_{w,n}} \quad (5.2)$$

where C_n is the concentration of radon in the NAPL phase, and $C_{w,n}$ is the concentration of radon in the aqueous phase. Partition coefficients may be determined using the methodology of Cantaloub (2001) and range from 37 (o-xylene) to 50 (trichloroethene, or TCE) to 61 (cyclohexane). In the presence of NAPL, radon will partition between the water and NAPL phases as described by

$$C_n S_n + C_{w,n} S_w = C_{w,bkg} \quad (5.3)$$

where S_n and S_w are the NAPL and water saturations in the pore space ($S_n + S_w = 1$). Assuming linear radon partitioning between NAPL and water (equation 5.2), equation 5.3 can be rearranged as

$$C_{w,n} = \frac{C_{w,bkg}}{1 + S_n (K - 1)} \quad (5.4)$$

where $C_{w,n}$ is a non-linear function of S_n and K (shown in Figure 5.1 using $C_{w,bkg} = 200$ pCi/L and $K = 50$). Equation 5.4 can be further rearranged to solve for the NAPL saturation in an aquifer under natural gradient conditions

$$S_n = \left(\frac{C_{w,bkg}}{C_{w,n}} - 1 \right) \left(\frac{1}{(K-1)} \right) \quad (5.5)$$

Radon retardation during transport can be used to determine NAPL saturation. The retardation factor for a partitioning tracer is given by (Dwarakanath et al., 1999)

$$R = 1 + \frac{KS_n}{S_w} \quad (5.6)$$

which can be solved for S_n

$$S_n = \frac{R-1}{R+K-1} \quad (5.7)$$

Push-pull tests using radon as a partitioning tracer were performed in laboratory physical aquifer models (PAMs) containing TCE (Davis et al., 2002). Experimental conservative (bromide) tracer and radon extraction phase BTCs were fit to an approximate analytical solution of the governing transport equations in order to estimate a value for R , which was then used to calculate S_n . Numerically generated BTCs using the Subsurface Transport Over Multiple Phases (STOMP) code were used to investigate the validity of the approximate analytical solution, and provided good matches to the experimental and approximate analytical solution BTCs. However, this approach resulted in overestimations of S_n compared to injection phase BTC results and the estimated TCE saturation in the PAM. In this approach, radon transport during a push-pull test was modeled assuming to behave similarly to an injected tracer. These simulations used a step input of radon (during the injection phase) into radon-free, saturated PAM sediment. An initial concentration = 0 for all solutes in the model domain was used with an injection solution concentration (C_o) = 1 (i.e., normalized). The extraction phase concentration results (C) from the simulations were converted to ‘inverted’ concentrations (C^*) using $C^* = 1 - C/C_o$ to mimic the behavior of radon in a push-pull test, since 1) a radon-free solution is injected in laboratory and field push-pull tests, and 2) radon concentrations increase with time during the extraction phase of the test. Extraction phase BTCs were plotted as a function of dimensionless time V_e/V_i , where V_e is the volume of solution extracted from the aquifer at the time a sample was obtained at the well and V_i is the total volume of solution injected into the aquifer. In addition, these models incorporated NAPL throughout the domain (infinite distribution), while the laboratory push-pull tests interrogated sediment beyond the NAPL-contaminated zone in the PAM.

Although these simulations accounted for radon partitioning between the NAPL and aqueous phases during the push-pull test, they did not account for radon partitioning into NAPL prior to the test. Radon concentrations are decreased in the presence of NAPL, with the equilibrium radon concentration being a non-linear function of S_n (Equation 5.4; Figure 5.1). Furthermore, these simulations assumed that NAPL saturation was spatially homogeneous in the PAM. A heterogeneous NAPL distribution will affect initial radon

concentrations and partitioning behavior during the push-pull test and can affect estimations of R and S_n .

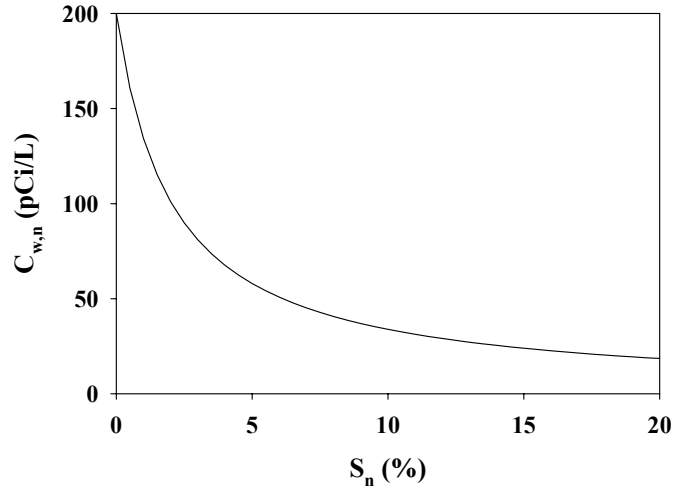


Figure 5.1 Aqueous phase radon concentrations ($C_{w,n}$) as a function of NAPL saturation, plotted using equation 4 with a background radon concentration ($C_{w,bkg}$) = 200 pCi/L and $K = 50$.

The goal of this study was to examine two factors that can influence interpretation of radon data from push-pull tests and resulting estimations of S_n : 1) the influence of NAPL on initial radon concentrations, and 2) heterogeneous NAPL saturation distributions. A revised method of interpreting radon BTCs is presented that reduces overestimation and results in an increase in sensitivity of the estimation method at small values of S_n . This method is then used to re-estimate values of S_n in previously conducted laboratory push-pull tests and to estimate S_n from field push-pull test data.

METHODS

Numerical Investigation Models

Simulations were performed with the STOMP code (White and Oostrom, 2000), a fully implicit volume-integrated finite difference simulator for modeling one-, two- and three-dimensional flow and transport, which has been extensively tested and validated against published analytical solutions as well as other numerical codes (Nichols et al., 1997). Simulations were based on a hypothetical push-pull test conducted in a 5 cm diameter well over a 91.4 cm long screened interval of an aquifer. The model aquifer is based on an aquifer composed of sediment from the Hanford Formation, an alluvial deposit of sands and gravels of mixed basaltic and granitic origin (Lindsey and Jaeger, 1993) previously used in laboratory push-pull tests. A solid density (ρ_s) of 2.9 g/cm³, porosity (n) = 0.35, calculated bulk density (ρ_b) = 1.89 g/cm³ and longitudinal dispersivity (α_L) = 4.0 cm were used in all simulations. Simulations incorporated an injection volume of 250 L and an extraction volume ranging from 500 to 2000 L. Injection and extraction pumping rates were constant at 1 L/min with no rest phase between the injection and

extraction phases. The computational domain consisted of a line of 500 nodes with a uniform radial node spacing of $\Delta r = 1.0$ cm. The model geometry and injection volumes resulted in the injection solution traveling 48 cm from the well, assuming plug flow of a conservative tracer. Simulations were performed using time-varying third-type flux boundary conditions to represent pumping at the well, with a constant hydraulic head. Constant head and zero solute flux boundary conditions were used to represent aquifer conditions at $r = 500$ cm.

Specified NAPL saturations were modeled using TCE and its $K = 50$ for radon. NAPL saturations (S_n) were incorporated into the model using solid:aqueous phase partition coefficients. First, equation 5.6 and $K = 50$ were used to solve for a retardation factor (R) for a given ratio of S_n to water saturation (S_w). Second, this calculated R value, the sediment porosity, and bulk density were used to solve for a solid:aqueous phase partition coefficient (K_d)

$$K_d = (R - 1) \left(\frac{n}{\rho_b} \right) \quad (5.8)$$

Simulations were performed with specified S_n values from 0 to 15.25 %, which corresponds to retardation factors (R) ranging from 1 to 10, respectively. The effects of initial radon concentrations and S_n heterogeneity on simulation results were investigated with three sets of simulations, with NAPL extending homogeneously from 1) $r \leq 500$ cm, 2) $r \leq 48$ cm (corresponding to the maximum travel radius of a conservatively transported tracer, as defined by plug flow), and 3) $r \leq 24$ cm (corresponding to half the maximum travel radius of a conservatively transported tracer), where r is the radial distance from the injection/extraction well. An initial radon concentration = 200 pCi/L (corresponding to $S_n = 0$ %) was emplaced at $r > 48$ cm for the second set of simulations and at $r > 24$ cm for the third set of simulations. Each simulation utilized 1) an injection radon concentration = 0 pCi/L, which corresponds to the true radon injection concentration in laboratory and field push-pull tests and negates the need for ‘inverting’ concentrations as described above, and 2) an initial radon concentration in the model that varied in space as a function of S_n . The simulations involving the PAM and field tests are described below.

RESULTS AND DISCUSSION

Injection Phase Results

The end of the injection phase of a simulated push-pull test (corresponding to $V_e/V_i = 0$) with $S_n = 0$ % for $r \leq 500$ cm results in conservative radon transport as shown in a radon concentration profile from $r = 0$ to 100 cm (Figure 5.2). The radon-free injection solution is transported to $r = 48$ cm, as measured by half the initial radon concentration at the injection well. In contrast, when $S_n \neq 0$ % over a specified portion of the model domain, radon transport is retarded. For the simulation where $S_n = 4$ % for $r \leq 500$ cm (i.e., a homogeneous NAPL distribution), the initial radon concentration in the model = 67.6 pCi/L (equation 5.4) and when $V_e/V_i = 0$, the radon-free injection solution is transported only to $r = 26$ cm as measured by half the initial radon concentration at the injection well (Figure 5.2).

The decrease in the transport distance of the radon-free injection solution is due to radon retardation resulting from partitioning between the injection solution and NAPL during transport. For the simulation where $S_n = 4\%$ for $r \leq 48$ cm and $S_n = 0\%$ for $r > 48$ cm (i.e., a heterogeneous NAPL distribution), when $V_e/V_i = 0$, the radon-free injection solution is again transported only to $r = 26$ cm (Figure 5.2). The mixing of radon-free injection solution, water with an initial radon concentration = 67.6 pCi/L for $r \leq 48$ cm, and water with an initial radon concentration = 200 pCi/L for $r > 48$ cm, combined with radon partitioning prior to the test and during transport, results in a complex, two-step radon concentration profile. For the simulation where $S_n = 4\%$ for $r \leq 24$ cm and $S_n = 0\%$ for $r > 24$ cm (i.e., a heterogeneous NAPL distribution), when $V_e/V_i = 0$, the radon-free injection solution is transported only to $r = 29$ cm (Figure 5.2). The change in the transport distance of the injection solution (vs. the previous simulation) is due to the mixing of radon-free injection solution, water with an initial radon concentration = 67.6 pCi/L for $r \leq 24$ cm, and water with an initial radon concentration = 200 pCi/L for $r > 24$ cm, combined with radon partitioning prior to the test and during transport. Thus when the portion of the model domain containing NAPL decreases, radon transport distance increases (i.e., radon retardation is lessened). These simulations show that both homogeneous and heterogeneous NAPL distributions result in radon retardation. Radon concentration profiles are influenced by both radon partitioning between the aqueous and NAPL phases prior to the push-pull test, and radon partitioning between the injection solution and NAPL during the test. Heterogeneity in NAPL distribution can affect injection phase radon concentration profiles due to the partitioning processes described above and mixing of water with different initial radon concentrations during the test.

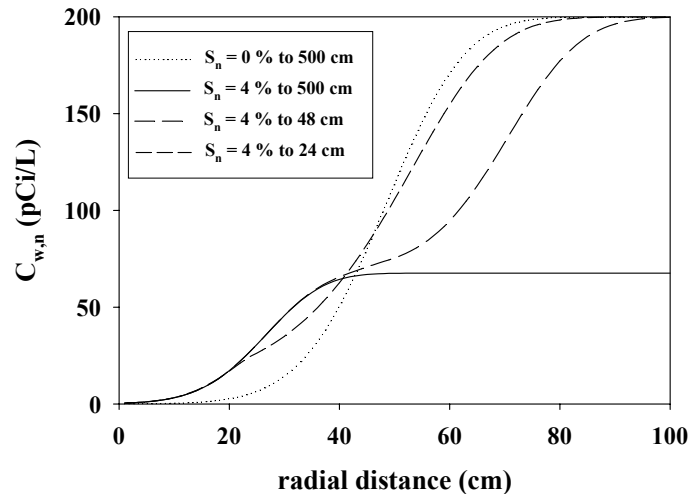


Figure 5.2 Simulated radon concentration profiles ($C_{w,n}$) at the end of the injection phase of push-pull tests with no NAPL ($S_n = 0\%$ to 500 cm); heterogeneous NAPL saturation ($S_n = 4\%$ to 48 cm) and ($S_n = 4\%$ to 24 cm); and homogeneous NAPL saturation ($S_n = 4\%$ to 500 cm).

Extraction Phase Results – Concentration Profiles

The extraction phase of a simulated push-pull test (beginning with $V_e/V_i = 0$ and continuing through $V_e/V_i = 4$) where $S_n = 4\%$ for $r \leq 500$ cm (i.e., a homogeneous NAPL

distribution) shows that radon concentrations increase with time as the injection solution/groundwater mixture is extracted from the well (Figure 5.3a). In this simulation the initial radon concentration is 67.6 pCi/L for $r \leq 500$ cm (equation 5.4). The radon concentration measured at the well ($r = 0$ cm) is 62.7 % of the initial radon concentration at $V_e/V_i = 1$, 88.6 % at 2, and 96.2 % at 3. Thus as the extraction phase of the test proceeds, radon concentrations at the well approach but do not exceed the initial radon concentration at the well. This holds true for any simulation with a homogeneous NAPL distribution.

The extraction phase of a simulated push-pull test (beginning with $V_e/V_i = 0$ and continuing through $V_e/V_i = 8$) where $S_n = 4$ % for $r \leq 48$ cm and $S_n = 0$ % for $r > 48$ cm (i.e., a heterogeneous NAPL distribution) shows that radon concentrations increase with time as the injection solution/groundwater mixture is extracted from the well (Figure 5.3b). In this simulation the initial radon concentration is 67.6 pCi/L for $r \leq 48$ cm and 200 pCi/L for $r > 48$ cm (equation 5.4). The radon concentration measured at the well ($r = 0$ cm) is 63.4 % of the initial radon concentration at $V_e/V_i = 1$, 102.5 % at 2, and 153.4 % at 3, and increases to 291.1 % at 8. As the extraction phase of the test proceeds, radon concentrations at the well exceed the initial radon concentration at the well at approximately $V_e/V_i = 2$. This is due to the influx of water with a radon concentration = 200 pCi/L from $r > 48$ cm, where $S_n = 0$ %. Such a response in push-pull tests might be utilized in identifying heterogeneous NAPL distributions.

The extraction phase of a simulated push-pull test (beginning with $V_e/V_i = 0$ and continuing through $V_e/V_i = 8$) where $S_n = 4$ % for $r \leq 24$ cm and $S_n = 0$ % for $r > 24$ cm (i.e., a heterogeneous NAPL distribution) shows that radon concentrations increase more quickly with time as the injection solution/groundwater mixture is extracted from the well (Figure 3c) compared to the previous simulation (Figure 5.3b). In this simulation the initial radon concentration is 67.6 pCi/L for $r \leq 24$ cm and 200 pCi/L for $r > 24$ cm (equation 5.4). The radon concentration measured at the well ($r = 0$ cm) is 91.6 % of the initial radon concentration at $V_e/V_i = 1$, 216.6 % at 2, and 273.4 % at 3, and increases to 295.9 % at 8. As the extraction phase of the test proceeds, radon concentrations at the well exceed the initial radon concentration at the well just after $V_e/V_i = 1$. This is due to the influx of water with a radon concentration = 200 pCi/L from $r > 24$ cm, where $S_n = 0$ %. Thus as NAPL is concentrated closer to the well, radon concentrations more rapidly exceed initial values at the well as the extraction phase proceeds. Conversely, if NAPL saturations were greater farther from the well, radon concentrations would possibly not approach initial values at the well.

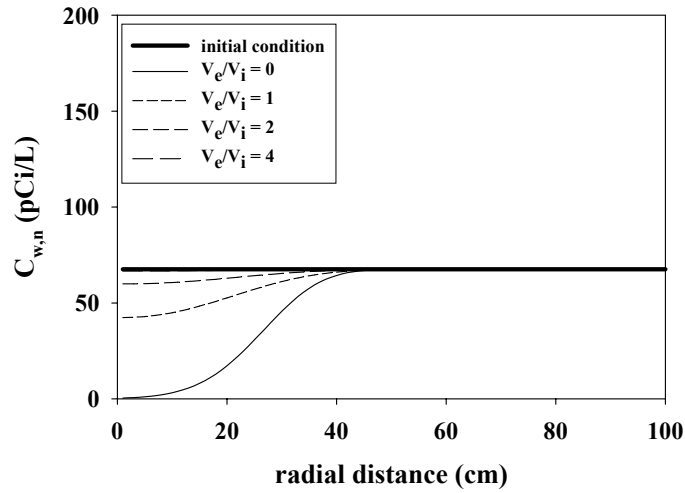


Figure 5.3a Simulated radon concentration profiles ($C_{w,n}$) during the extraction phase of a push-pull test, with a homogeneous NAPL saturation ($S_n = 4\%$ for $r \leq 50$ cm).

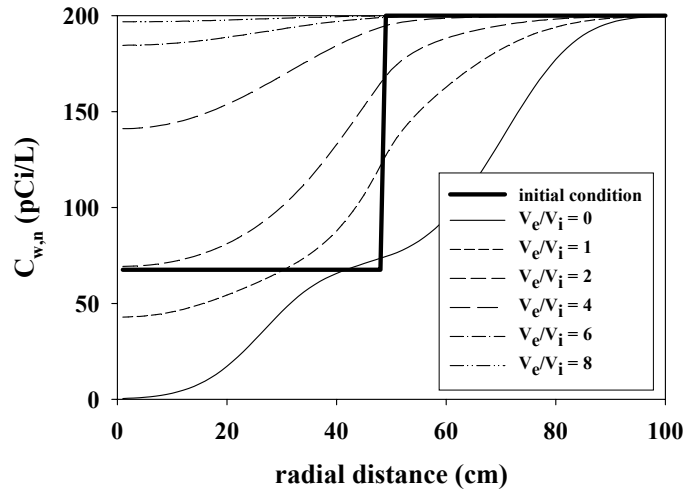


Figure 5.3b Simulated radon concentration profiles ($C_{w,n}$) during the extraction phase of a push-pull test, with a heterogeneous NAPL saturation ($S_n = 4\%$ for $r \leq 48$ cm; $S_n = 0\%$ for $r > 48$ cm).

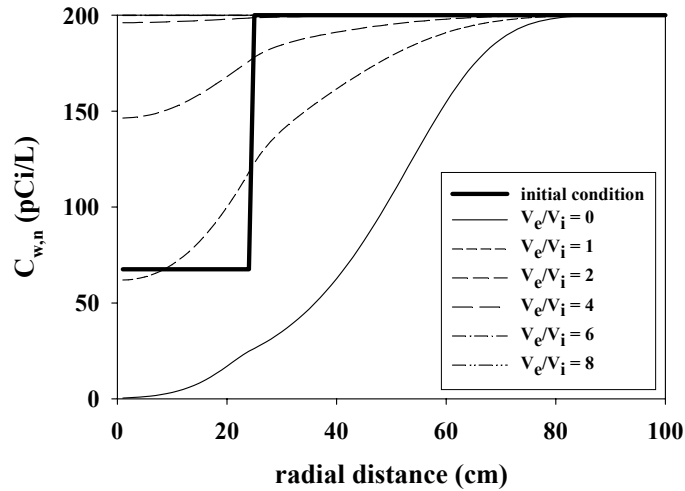


Figure 5.3c Simulated radon concentration profiles ($C_{w,n}$) during the extraction phase of a push-pull test, with a heterogeneous NAPL saturation ($S_n = 4\%$ for $r \leq 24$ cm; $S_n = 0\%$ for $r > 24$ cm).

Extraction Phase Results – Breakthrough Curves

Although radon concentration profiles provide useful information on radon transport behavior, usually the only radon concentration data available at field sites is obtained from the well in which the push-pull test is being conducted. To investigate radon BTC behavior, a set of six simulations was performed for a homogeneous NAPL distribution. Each simulation utilized a single value of S_n for $r \leq 500$ cm (Figure 5.4a), with each value of R corresponding to a value for S_n . The initial radon concentration was a function of S_n (equation 5.4), and ranged from 200 pCi/L for the first simulation ($S_n = 0\%$, $R = 1$) to 23.6 pCi/L for the sixth simulation ($S_n = 15.25\%$, $R = 10$). As the extraction phase approaches $V_e/V_i = 2$, for homogeneous NAPL distributions, radon concentrations approach but do not exceed their initial value at the well. For the simulation where $S_n = 0\%$, radon concentrations reach 92.1% of their initial value at the well. In contrast, for the simulation where $S_n = 15.25\%$, radon concentrations reach 86.3% of their initial value at the well. This decrease is due to the increase in dispersion of the radon BTC as S_n increases (Schroth et al., 2000). Radon BTCs show the greatest sensitivity at small values of S_n , which is due to the non-linear relationship between S_n and the initial radon concentration (Figure 5.1).

A second set of six simulations was performed for a heterogeneous NAPL distribution with a homogeneous value of S_n for $r \leq 48$ cm and $S_n = 0\%$ for $r > 48$ cm (Figure 5.4b). The initial radon concentration was a function of S_n (equation 4), and for $r \leq 48$ cm ranged from 200 pCi/L for the first simulation ($S_n = 0\%$, $R = 1$) to 23.6 pCi/L for the sixth simulation ($S_n = 15.25\%$, $R = 10$), while for $r > 48$ cm, the initial radon concentration = 200 pCi/L for each of the six simulations. As the extraction phase approaches $V_e/V_i = 2$, radon concentrations approach (and for $S_n = 1.96\%$ exceed) their initial value at the well. For the simulation where $S_n = 0\%$, radon concentrations reach 92.1% of their initial value at the well. These percentages vary as a function of S_n ,

reaching 112.3 % for $S_n = 1.96$ %, 95.1 % for $S_n = 5.66$ %, and 86.4 % for $S_n = 15.25$ %. The presence of $S_n = 0$ % for $r > 48$ cm produces greater radon concentrations for each simulation at $V_e/V_i = 2$ (Figure 5.4b) as compared to when S_n is constant for $r \leq 500$ cm (Figure 5.4a). Radon concentrations would increase beyond the initial radon concentration for $S_n > 0$ % if V_e/V_i progressed beyond 2, as shown in the radon concentration profiles for $S_n = 4$ % for $r \leq 48$ cm and $S_n = 0$ % for $r > 48$ cm (Figure 5.3b). However, the shapes of the radon BTCs are similar at early times for the two sets of simulations (Figures 5.4a and 5.4b), and again radon BTCs show the greatest sensitivity at small values of S_n .

A third set of six simulations was performed for a heterogeneous NAPL distribution with a homogeneous value of S_n for $r \leq 24$ cm and $S_n = 0$ % for $r > 24$ cm (Figure 5.4c). The initial radon concentration was a function of S_n (equation 5.4), and for $r \leq 24$ cm ranged from 200 pCi/L for the first simulation ($S_n = 0$ %, $R = 1$) to 23.6 pCi/L for the sixth simulation ($S_n = 15.25$ %, $R = 10$), while for $r > 24$ cm, the initial radon concentration = 200 pCi/L for each of the six simulations. As the extraction phase approaches $V_e/V_i = 2$, radon concentrations approach and exceed their initial value at the well to a greater degree than when NAPL extends to 48 cm. These percentages vary as a function of S_n , reaching 165.2 % of the initial value at the well for $S_n = 1.96$ %, 238.7 % for $S_n = 5.66$ %, and 188.9 % for $S_n = 15.25$ %. The presence of $S_n = 0$ % for $r > 24$ cm produces greater radon concentrations for each simulation at $V_e/V_i = 2$ (Figure 5.4c) as compared to when $S_n > 0$ % for $r \leq 48$ cm (Figure 5.4b) or when S_n is constant for $r \leq 500$ cm (Figure 5.4a). Radon concentrations would continue to increase beyond the initial radon concentration for $S_n > 0$ % if V_e/V_i progressed beyond 2, as shown in the radon concentration profiles for $S_n = 4$ % for $r \leq 24$ cm and $S_n = 0$ % for $r > 24$ cm (Figure 5.3c). The influence of $S_n = 0$ % at $r > 24$ cm results in greater slopes for radon BTCs compared to the previous simulations (Figures 5.4a and 5.4b). These results show that the shape of the radon BTCs and a comparison of initial radon concentrations at the well vs. late time concentrations could potentially be used to investigate heterogeneity in NAPL distribution.

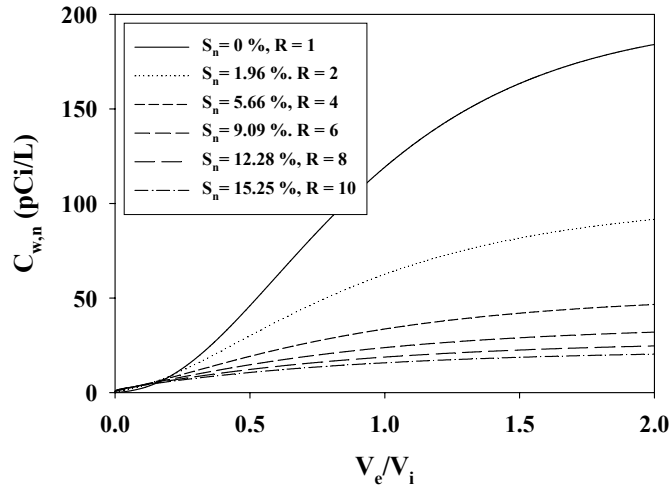


Figure 5.4a Simulated radon breakthrough curves during the extraction phases of six push-pull tests with homogeneous NAPL saturations ($S_n = 0$ to 15.25 % for $r \leq 500$ cm).

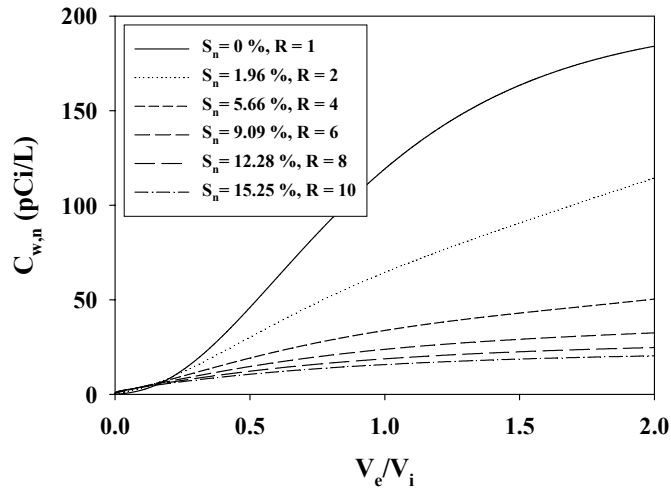


Figure 5.4b Simulated radon breakthrough curves during the extraction phases of six push-pull tests with heterogeneous NAPL saturations ($S_n = 0$ to 15.25 % for $r \leq 48$ cm; $S_n = 0$ % for $r > 48$ cm).

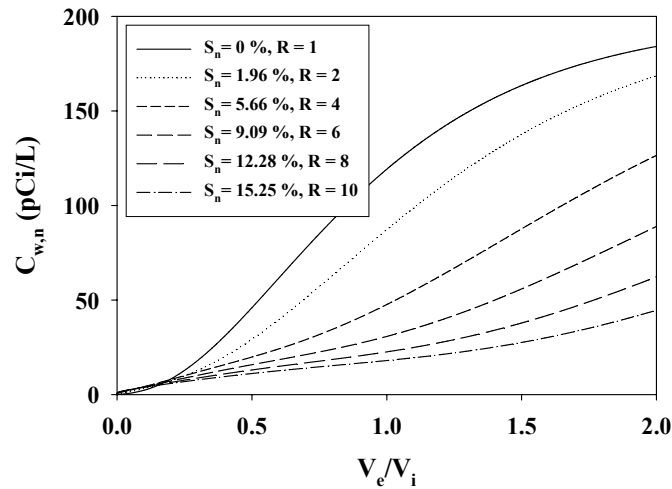


Figure 5.4c Simulated radon breakthrough curves during the extraction phases of six push-pull tests with heterogeneous NAPL saturations ($S_n = 0$ to 15.25 % for $r \leq 24$ cm; $S_n = 0$ % for $r > 24$ cm).

Extraction Phase Results – Normalized Breakthrough Curves

The normalization of each of the radon BTCs for the homogeneous NAPL distribution (Figure 4a) to the initial concentrations at the well results in radon BTCs that approach but do not exceed a normalized concentration = 1 at $V_e/V_i = 2$ (Figure 5.5a). The effect of increasing dispersion as S_n increases is apparent (Schroth et al., 2000). This figure applies to any idealized homogeneous NAPL distribution and by inverting the concentrations is analogous to the ex situ tracer test, since this set of simulations utilizes a step input during the injection phase into a model domain with a spatially constant initial condition. A drawback to normalizing to the initial radon concentration is the decrease in sensitivity of the radon BTCs to small values of S_n compared to the non-normalized method (Figure 5.4a). This drawback is a concern when fitting experimental radon BTCs to simulated BTCs in order to determine a best-fit value of R in order to estimate S_n .

Radon BTC normalization for the heterogeneous NAPL distribution where $S_n = 0$ % for $r > 48$ cm (Figure 5.4b) results in radon BTCs that approach a normalized concentration = 1 at $V_e/V_i = 2$ (Figure 5.5b). Normalized radon BTCs deviate from those in the homogeneous set of simulations (Figure 5.5a) as V_e/V_i approaches 2, and for $S_n = 1.96$ % the normalized concentration is > 1 .

Radon BTC normalization for the heterogeneous NAPL distribution where $S_n = 0$ % for $r > 24$ cm (Figure 5.4c) results in radon BTCs that exceed a normalized concentration = 1 at approximately $V_e/V_i = 1$ (Figure 5.5c). Comparing Figure 5c with Figures 5.5a and 5.5b shows that as the proportion of $S_n = 0$ % in the model domain increases, normalizing to the initial radon concentration results in greater deviations in radon BTCs, with normalized concentrations ≤ 2.5 at $V_e/V_i = 2$. Thus the interpretation of normalized radon BTCs becomes more difficult as heterogeneity in S_n increases. Moreover, the

shape of normalized BTCs is influenced by the radon concentration to which BTCs are normalized.

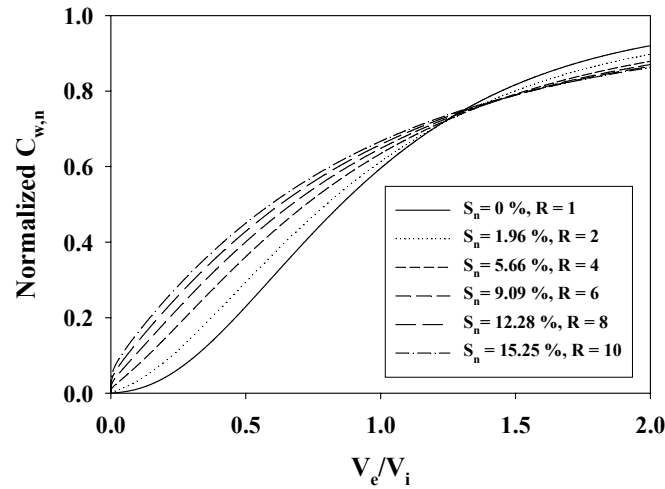


Figure 5.5a Simulated radon breakthrough curves during the extraction phases of six push-pull tests with homogeneous NAPL saturations ($S_n = 0$ to 15.25 % for $r \leq 500$ cm). Radon concentrations are normalized to the initial radon concentrations at the well for each value of S_n .

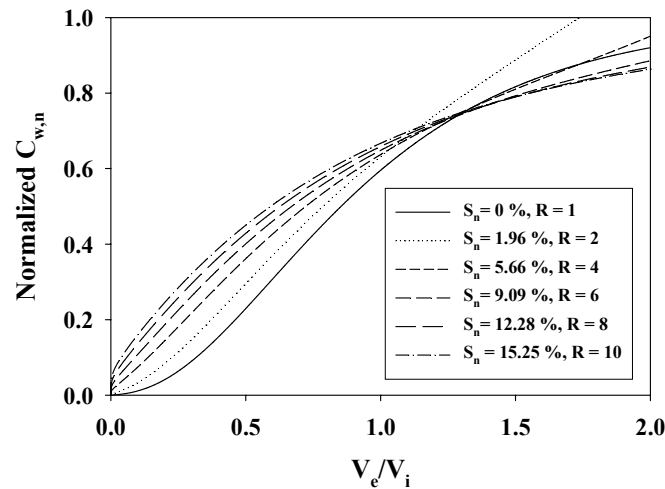


Figure 5.5b Simulated radon breakthrough curves during the extraction phases of six push-pull tests with heterogeneous NAPL saturations ($S_n = 0$ to 15.25 % for $r \leq 48$ cm; $S_n = 0$ % for $r > 48$ cm). Radon concentrations are normalized to the initial concentrations at the well for each value of S_n .

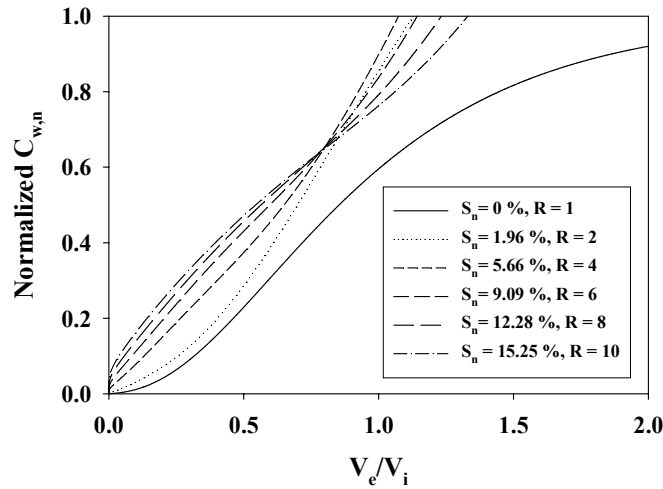


Figure 5.5c Simulated radon breakthrough curves during the extraction phases of six push-pull tests with heterogeneous NAPL saturations ($S_n = 0$ to 15.25 % for $r \leq 24$ cm; $S_n = 0$ % for $r > 24$ cm). Radon concentrations are normalized to the initial concentrations at the well for each value of S_n .

Revised Method for Radon BTC Interpretation

The simulation results show that non-normalized radon BTCs (Figures 5.4a, 5.4b, and 5.4c) have a greater sensitivity to small values of S_n than the corresponding normalized radon BTCs (Figures 5.5a, 5.5b, and 5.5c). Furthermore, these simulations also show that heterogeneity in S_n can result in extraction phase normalized radon concentrations > 1 . Conversely, a reversal of the simulated S_n distributions such that S_n increased with distance from the well would result in extraction phase normalized radon concentrations < 1 . Thus heterogeneity in S_n can introduce uncertainties in the applicability of the initial radon concentration at the well as a normalization value. The use of non-normalized radon BTCs to estimate S_n provides two advantages over normalized radon BTCs: 1) the sensitivity of non-normalized radon BTCs to small values of S_n can be utilized; and 2) the effect of heterogeneity in S_n on the shape of radon BTCs can be lessened.

The revised method for estimating S_n utilizing non-normalized radon BTCs requires obtaining a ‘background’ radon concentration ($C_{w,bkg}$; equation 1) from a non-contaminated portion of the contaminated aquifer. Using this sample as a ‘background’ concentration assumes homogeneity in porosity and radon emanation between the non-contaminated location chosen for the ‘background’ radon sample and the location with suspected NAPL contamination where the push-pull test is conducted. Extraction phase radon and bromide results are plotted in concentration units (pCi/L for Rn and mg/L for Br⁻) as a function of V_e/V_i . The y-axis of the plot shows radon concentrations ranging from 0 at the origin to a maximum value equal to the ‘background’ concentration. Bromide concentrations are plotted on a secondary y-axis with concentrations ranging from the injection solution concentration to 0 mg/L, with the injection solution concentration *at the origin* and 0 mg/L at the maximum or ‘background’ radon concentration. This inverts the bromide concentrations and causes the radon and bromide

BTCs to overlap. Numerical simulations are then performed to best-fit (using a least-squares procedure) the experimental bromide BTC to a non-retarded simulated BTC (i.e., with $R = 1$) by varying the sediment dispersivity (α_L). The best-fit α_L value is then used in subsequent simulations to best-fit (using a least-squares procedure) the experimental radon BTC to a simulated BTC corresponding to a particular value of R . For each simulated BTC, equation 5.4 is used to input the initial radon concentration in the model as a function of S_n and K . The initial radon concentration can be input into the model as a homogeneous or heterogeneous S_n distribution. Equation 5.7 is then used to calculate the value of S_n that corresponds to the best-fit R value.

PAM push-pull tests re-analysis

The revised method was applied to existing radon and bromide extraction phase data from push-pull tests performed in wedge shaped physical aquifer models (PAMs) by Davis et al. (2002). These push-pull tests were performed in clean sediment (Test 1) and TCE-contaminated sediment (Test 2), with the contaminated zone ($S_n \sim 2\%$) of Test 2 extending 74 cm from the narrow end of the PAM, beyond which $S_n = 0\%$. The tests were originally modeled using normalized BTCs without the incorporation of initial radon concentrations in the model domain, and resulted in overestimates of R and the likely S_n in the PAM (Table 5.1).

Test 1 was modeled using the revised method, with an average initial radon concentration = 197.6 pCi/L (measured in 4 sampling ports in this PAM before the test). The bromide data are well fit by a simulated $R = 1$ BTC, with a best-fit $\alpha_L = 1.9$ cm, and the radon data are best-fit by a simulated $R = 1.3$ BTC (Figure 5.6). The radon retardation in Test 1 is attributed to partitioning of radon between the trapped gas and aqueous phases, as described by Fry et al. (1995)

$$R = 1 + \frac{H_{cc} S_g}{S_w} \quad (5.9)$$

where H_{cc} is radon's dimensionless Henry's coefficient and S_g is the trapped gas saturation. Using equation 5.9, $H_{cc} = 3.9$ (Clever, 1979), and $R = 1.3$, the estimated $S_g = 7.1\%$. These values are similar to those from Davis et al. (2002) (Table 5.1), who reported a best-fit $\alpha_L = 3.2$ cm, $R = 1.1$, and estimated S_g ranging up to 9.3%. The best-fit $R = 1.3$ also compares favorably to the retardation factors measured in sampling ports 1 and 2 (located 15 and 30 cm from the narrow end of the PAM) during the *injection phase* of Test 1, which ranged from 1.0 to 1.4 (Davis et al., 2002).

Test 2 was also modeled using the revised method, with an average initial radon concentration = 262.1 pCi/L (measured in 4 sampling ports in this PAM prior to TCE contamination). A simulation was performed in which TCE contamination extended to 74 cm, with uncontaminated sediment at > 74 cm. The bromide data are well fit by a simulated $R = 1$ BTC, with a best-fit $\alpha_L = 3.7$ cm, and the radon data are best-fit by a simulated $R = 2.2$ BTC (Figure 5.7). The radon retardation in Test 2 is attributed to partitioning of radon between 1) the trapped gas and aqueous phase, and 2) the TCE and aqueous phase. The portion of radon retardation due to TCE partitioning was determined by adjusting R to account for trapped gas partitioning using (Davis et al., 2002)

$$R_{adj} = R_{test\ 2} - (R_{test\ 1} - 1.0) \quad (5.10)$$

where R_{adj} is the adjusted retardation factor, $R_{test\ 2}$ is the retardation factor from Test 2, and $R_{test\ 1}$ is the retardation factor from Test 1. Using equation 10, an adjusted R value of 1.9 is calculated, which results in an estimated $S_n = 1.8\%$ (Table 5.1). The best-fit $\alpha_L = 3.7\text{ cm}$ compares favorably with the best-fit $\alpha_L = 4.0\text{ cm}$ from Davis et al. (2002), while the estimated $S_n = 1.8\%$ is a more reasonable estimate of the TCE saturation in the sediment pack ($\sim 2\%$) than is the estimated $S_n = 7.4\%$ from Davis et al. (2002) (using $K = 50$). The adjusted $R = 1.9$ compares favorably with the adjusted retardation factors measured in sampling ports 1 and 2 during the *injection phase* of Test 2, which ranged from 1.1 to 1.5 (Davis et al., 2002). Thus the revised method results in better agreement of extraction and injection phase estimated R values and subsequent estimations of S_n . The new estimate of $S_n = 1.8\%$ is also in agreement with S_n values ranging from 0.7 to 1.6% from partitioning alcohol push-pull tests performed in this PAM at similar flowrates (Istok et al., 2002).

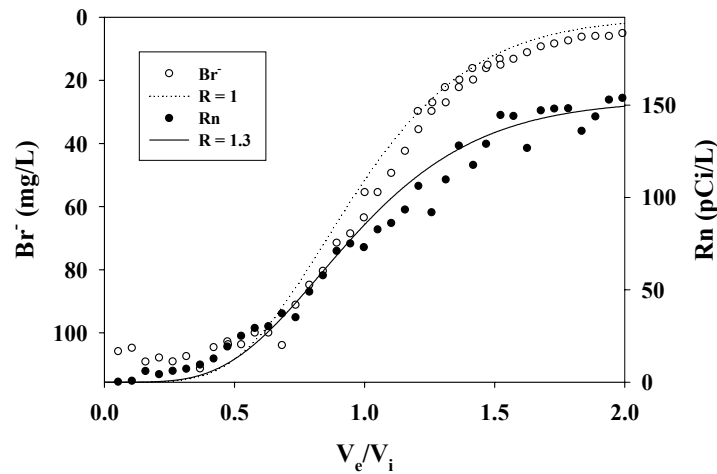


Figure 5.6 Radon (pCi/L) and bromide (mg/L) experimental and simulated ($R = 1$ and $R = 1.3$) breakthrough curves during the extraction phase of a push-pull test performed in a non-contaminated physical aquifer model (Test 1).

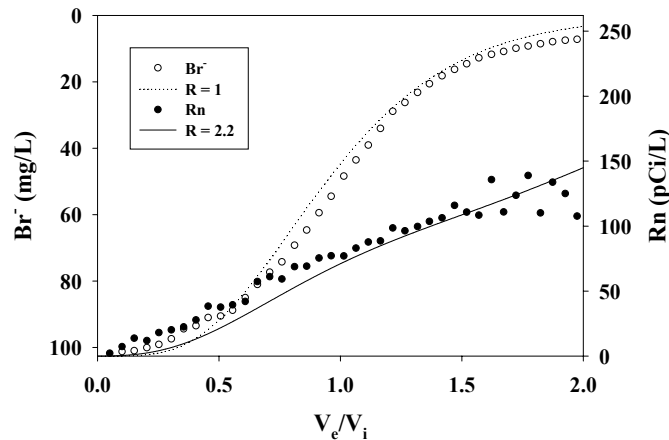


Figure 5.7 Radon (pCi/L) and bromide (mg/L) experimental and simulated ($R = 1$ and $R = 2.2$) breakthrough curves during the extraction phase of a push-pull test performed in a TCE-contaminated physical aquifer model (Test 2).

Table 5.1 Radon retardation factors (R), adjusted retardation factors for the effect of trapped gas (in *italics*), best-fit dispersivities (α_L), and calculated TCE saturations (S_n) from push-pull tests. Results from Davis et al. (2002) are shown on the left, while results using the revised method are shown on the right. A value of $K = 50$ was used to calculate S_n in the presence of TCE.

	From Davis et al. (2002)			Using revised method		
	R	α_L (cm)	S_n (%)	R	α_L (cm)	S_n (%)
Test 1, no TCE	1.1	3.2	-	1.3	1.9	-
Test 2, with TCE	5.1/ <i>5.0</i>	4.0	7.4	2.2/ <i>1.9</i>	3.7	1.8

Field push-pull test application

The revised method was applied to radon and bromide BTCs from a field test performed at a former petroleum refinery in the Ohio River valley. As further described in Davis et al. (2002) and Istok et al. (2002), the site consists of glacial outwash deposits that are contaminated with a mixture of petroleum light or LNAPLs including gasoline, heating oil, and jet and aviation fuel. Radon samples from a non-contaminated well showed a maximum concentration of 788.5 pCi/L. This value was used as the ‘background’ concentration for radon. A push-pull test was performed in a contaminated well in which LNAPL has been detected. Radon concentrations increased and bromide concentrations decreased smoothly as the test solution/groundwater mixture was extracted from the aquifer, with the radon BTC being retarded relative to the bromide BTC (Figure 5.8). Numerical simulations were performed for this test with LNAPL assuming to extend far beyond the radius of influence of the test. The simulation results fit the bromide BTC to a simulated $R = 1$ BTC using a best-fit $\alpha_L = 11$ cm. This value is less than the best-fit α_L

= 20.3 cm from the approximate analytical solution used to fit the normalized bromide BTC by Davis et al. (2002), where the BTC was adjusted to intersect a normalized concentration = 0.5 at $V_e/V_i = 1$. Using the revised method and $\alpha_L = 11$ cm, the radon BTC was best-fit by a simulated $R = 2.7$ BTC. Using the best-fit $R = 2.7$, a value of $S_n = 4.1\%$ was calculated using equation 5.7 and a value of $K = 40$ for radon in the presence of diesel fuel, as reported by Hunkeler et al. (1997). The relatively poor fits of the simulated BTCs to the experimental BTCs likely are a result of heterogeneities in hydraulic conductivity and porosity in the aquifer. In addition, the use of a K value for radon in the presence of diesel fuel adds uncertainty to the value of $S_n = 4.1\%$, since the actual LNAPL composition at the site is a mixture of LNAPLs. However, the method does provide an estimate for the LNAPL saturation in the vicinity of the well. Furthermore, a series of similar push-pull tests could be conducted in this well over time to track the efficacy of remediation and source zone removal.

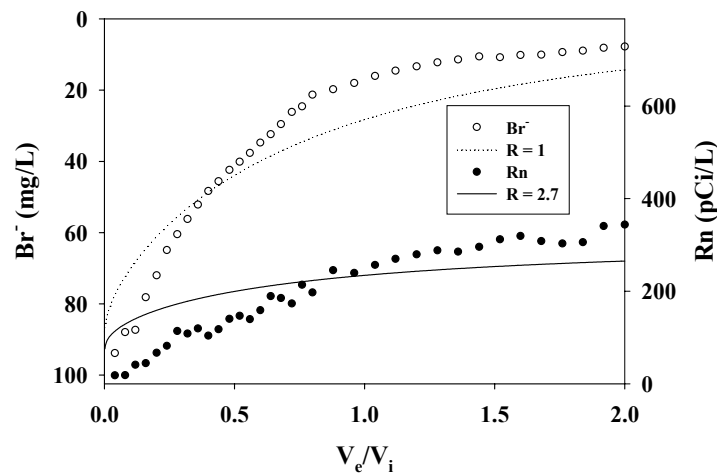


Figure 5.8 Radon (pCi/L) and bromide (mg/L) experimental and simulated ($R = 1$ and $R = 2.7$) breakthrough curves during the extraction phase of a push-pull test performed in a LNAPL-contaminated aquifer.

CONCLUSIONS

The revised method enhances the ability of the radon push-pull test to provide estimates for S_n at NAPL-contaminated sites. The effect of heterogeneity in S_n on radon BTCs is lessened, and a greater sensitivity to smaller values of S_n is realized. Also, the revised method more accurately represents the true condition of in situ radon partitioning both prior to and during the push-pull test. The method shows promise in providing estimates for S_n and showing changes in S_n over time as, for example, source zone remediation is effected. However, the revised method is potentially constrained by the need to obtain a ‘background’ radon sample from a non-contaminated well in the contaminated aquifer. Geologic properties with respect to radon emanation and porosity must be similar between the contaminated and non-contaminated wells. This may or may not be the case at a field site. The collection of radon samples from additional non-contaminated wells emplaced in the NAPL-contaminated aquifer could provide a range of ‘background’ values which could be used in conjunction with the revised method to provide a range of

estimated values of S_n . Also, it should be noted that estimated values of S_n represent a volume-averaged value, and may or may not be representative of the true value of S_n at a given location within the radius of influence of the push-pull test. These uncertainties highlight our view that push-pull test results provide an *estimate* of NAPL saturation in the immediate vicinity of the well in which the test was conducted.

ACKNOWLEDGEMENTS

We thank Jennifer Field, Ralph Reed, Jason Lee, and Mike Cantaloub for help with laboratory methods and activities; Mark Lyverse and Jesse Jones for help with field activities; and Martin Schroth and Mark White for help with STOMP.

REFERENCES

- Annable, M.D., P.S.C. Rao, K. Hatfield, W.D. Graham, A.L. Wood, and C.G. Enfield, 1998. Partitioning tracers for measuring residual NAPL: field-scale test results. *Journal of Environmental Engineering*, 124:498-503.
- Cantaloub, M., 2001. Aqueous-organic partition coefficients for radon-222 and their application to radon analysis by liquid scintillation methods. Master's Thesis, Oregon State University.
- Clever, H.L., 1979. Solubility Data Series Volume 2. Pergamon Press, NY
- Davis, B.M., J.D. Istok, and L. Semprini, 2002. Push-pull partitioning tracer tests using radon-222 to quantify non-aqueous phase liquid contamination. *Journal of Contaminant Hydrology*, 58:129-146.
- Dwarakanath, V., N. Deeds, and G.A. Pope, 1999. Analysis of Partitioning Interwell Tracer Tests. *Environmental Science & Technology*, 33:3829-3836.
- Fry, V.A., J.D. Istok, L. Semprini, K.T. O'Reilly, and T.E. Buscheck, 1995. Retardation of dissolved oxygen due to a trapped gas in porous media. *Ground Water*, 33:391-398.
- Hunkeler, D., E. Hoehn, P. Höhener, and J. Zeyer, 1997. 222-Rn as a partitioning tracer to detect diesel fuel contamination in aquifers: laboratory study and field observations. *Environmental Science & Technology*, 31:3180-3187.
- Istok, J.D., J.A. Field, M.H. Schroth, B.M. Davis, and V. Dwarakanath, 2002. Single-well "push-pull" tracer test for NAPL detection in the subsurface. *Environmental Science & Technology*, 36:2708-2716.
- Jin, M., M. Delshad, V. Dwarakanath, D.C. McKinney, G.A. Pope, K. Sepehrnoori, C.E. Tilburg, and R.E. Jackson, 1995. Partitioning tracer test for detection, estimation, and remediation performance assessment of subsurface nonaqueous phase liquids. *Water Resources Research*, 31:1201-1211.
- Lindsey, K.A. and G.K. Jaeger, 1993. Geologic setting of the 100-HR-3 operable unit, Hanford site, south-central Washington. WHC-SD-EN-TI-132, Rev. 0, Westinghouse Hanford Company, Richland, WA.
- Nelson, N.T. and M.L. Brusseau, 1996. Field study of the partitioning tracer method for detection of dense nonaqueous phase liquid in a trichloroethene-contaminated aquifer. *Environmental Science & Technology*, 30:2859-2863.
- Nelson, N.T., M. Oostrom, T.W. Wietsma, and M.L. Brusseau, 1999. Partitioning tracer method for the in situ measurement of DNAPL saturation: influence of

- heterogeneity and sampling method. *Environmental Science & Technology*, 33:4046-4053.
- Nichols, W.E., N.J. Aimo, M. Oostrom, and M.D. White, 1997. STOMP: Subsurface Transport Over Multiple Phases, Application Guide. PNNL-11216, Richland, WA.
- Schroth, M.H., J.D. Istok, and R. Haggerty, 2000. In situ evaluation of solute retardation using single-well push-pull tests. *Advances in Water Resources*, 24:105-117.
- Semprini, L., K. Broholm, and M. McDonald, 1993. Radon-222 deficit for locating and quantifying NAPL contamination in the subsurface. *EOS Transactions American Geophysical Union*, 76:F276.
- Semprini, L., M. Cantaloub, S. Gottipati, O. Hopkins, and J. Istok, 1998. Radon-222 as a Tracer for Quantifying and Monitoring NAPL Remediation. In: G.B. Wickramanayake and R.E. Hinchey (Editors), *Nonaqueous-Phase Liquids*. Battelle Press, Columbus, OH, pp. 137-142.
- Semprini, L., O.S. Hopkins, and B.R. Tasker, 2000. Laboratory, field and modeling studies of radon-222 as a natural tracer for monitoring NAPL contamination. *Transport in Porous Media*, 38:223-240.
- White, M.D. and M. Oostrom, 2000. STOMP: Subsurface Transport Over Multiple Phases, Version 2.0, User's Guide. PNNL-12034, Richland, WA.
- Young, C.M., R.E. Jackson, M. Jin, J.T. Londergan, P.E. Mariner, G.A. Pope, F.J. Anderson, and T. Houk, 1999. Characterization of a TCE NAPL zone in alluvium by partitioning tracers. *Ground Water Monitoring and Remediation*, 19:84-94.

6. A METHOD FOR DETERMINING AQUEOUS-ORGANIC PARTITION COEFFICIENTS FOR ^{222}Rn

INTRODUCTION

In their landmark article describing radon measurement by liquid scintillation methods (LSC), Prichard and Gesell (1977) refer to the ratio of the Ostwald coefficients for radon in toluene and radon in water as ranging from 50 to 52, and fairly constant. Parks (1979) also sites the ratio of Ostwald distribution coefficients for radon in various organic scintillators and radon in water as ranging between 30-50. In subsequent research, this ratio of Ostwald solubility coefficients has become identified as the radon partition coefficient while at the same time many radon Ostwald solubility coefficients are referred to as radon partition or distribution coefficients (McDowell and McDowell 1994; Bem et al. 1994).

The Ostwald solubility coefficient, L , can be shown to be a ratio of the concentration of a particular gas in the liquid phase, C_l to its concentration in the gas phase above the liquid, C_g (Clever 1979). Taking the ratio of Ostwald solubility coefficients for radon in a given solvent, L_s , to the solubility coefficient for radon in water, L_w yields a theoretical radon partition coefficient, K : a dimensionless ratio of the radon concentration in the solvent, C_s , to the radon concentration in water, C_w .

$$K = \frac{L_s}{L_w} = \left(\frac{C_s}{C_g} \right) \left(\frac{C_g}{C_w} \right) = \frac{C_s}{C_w} \quad (6.1)$$

A review of the literature indicates few experimentally determined values for the direct partitioning of dissolved radon gas between aqueous and organic phases. Hunkeler et al. (1997) determined a water-diesel fuel radon partition coefficient of 40 ± 2.3 at 12°C by measuring the radon concentration in tap water and then again in tap water equilibrated with 18 mL of diesel fuel. Wong et al. (1992) measured a radon partition coefficient value of 32.4 ± 1.5 for radon distributed between octanol and water. Neither method relied solely on analysis of radon in the organic phase, while both utilized different radon measurement techniques with associated detection efficiencies and calibration requirements.

A popular method for aqueous radon measurement is liquid scintillation counting which depends, in large part, on radon partitioning between the organic scintillation solution or “cocktail” and the aqueous sample. Several researchers have reported Ostwald solubility coefficients (L) related specifically to radon in liquid scintillation solutions. Horrocks and Studier (1964) determined a radon Ostwald solubility coefficient of 32 for a toluene based liquid scintillator at -15°C . As mentioned above, Prichard and Gesell (1977) cited, but did not measure, a radon Ostwald solubility value of 12.7 for radon in toluene and 0.255 for radon in water at 20°C . Parks and Tsuboi (1978) determined a radon distribution coefficient for radon partitioning between a p-xylene based emulsion scintillator and air of 10.88 at 8°C , and estimated a value of 18.87 for a toluene scintillator at 8°C based on Horrocks’s and Studier’s data. Lowery (1991) determined a radon partition coefficient value of 23 for radon distributed between a high-efficiency mineral oil based scintillation cocktail and well water of medium ionic strength. Finally,

Collé (1995), in a manner similar to Lowery, determined a value of 13 for the Ostwald solubility coefficient for radon partitioning between a 1,2,4 tri-methylbenzene based scintillation cocktail and air.

A simple, accurate method for directly measuring the partition coefficient for radon distribution between aqueous and organic phases has yet to appear in the literature. Our interest in the direct partitioning of dissolved radon gas between aqueous and organic phases stems from current investigations utilizing naturally occurring radon as an indicator of organic contamination in the saturated zone of the subsurface (Semprini et al. 2000; Semprini et al. 1998). Knowledge of aqueous-organic radon partitioning is desirable in order to estimate the extent of partitioning expected for various hydrocarbon contaminants. Additionally, as the research relies upon liquid scintillation analysis for analyzing radon in field and laboratory water samples, a better understanding of radon partitioning and its role in the liquid scintillation analysis method was warranted.

To this end, a simple method for measuring aqueous-organic radon partition coefficients was developed. The method is based on a multiple-equilibration procedure used for determining Henry's Law coefficients (Schwarzenbach et al. 1993; McAuliffe 1971) and uses sequential extractions of dissolved radon gas from an aqueous solution using equal volume aliquots of organic solvent. Each extraction removes a fixed fraction of radon from the solution. The radon-laden solvent is then added to a scintillation vial containing liquid scintillation cocktail. After sufficient time to allow radon and progeny to reach equilibrium, the set of extractions are counted on a liquid scintillation counter. The natural log of the net radon activity concentration in each extraction is plotted as a function of the extraction number. The slope of the resulting line is a function solely of the radon partition coefficient and the accurately measured volumes of the aqueous solution and organic extractions. Accurate knowledge of the instrument counting efficiency, quench, and standard solution activity are not required provided each sample in a set of extractions is counted under identical conditions.

THEORY

A distribution or partition coefficient is a dimensionless parameter expressing the ratio of a solute's concentration in one phase to its concentration in another phase (Leo et al. 1971; Cratin 1968). Provided there is no significant solute-solute interaction or strong specific solute-solvent interaction, once the system is in equilibrium the ratio of the solute concentration in the two phases remains constant regardless of the relative volumes of the two phases (Leo et al. 1971). Partitioning of dissolved radon, an inert monatomic gas, between water and an immiscible organic liquid describes a nearly ideal partitioning system. When an organic solvent is added to an aqueous solution containing dissolved radon gas, the radon distributes itself between the two liquid components. Upon reaching equilibrium, the radon concentration in each of the liquid phases is related by

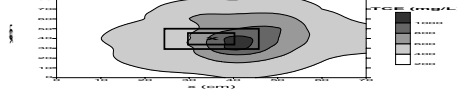
$$K = \frac{C_o}{C_w} \quad (6.2)$$

where K is the dimensionless radon partition coefficient and C_o and C_w are the radon concentrations (activity per unit volume, e.g. pCi/mL) in the organic and aqueous phases respectively. If a series of equilibrations are performed on a solution containing

dissolved radon, the radon concentration in the solvent after the first equilibration, $C_{o,1}$ can be expressed as

$$C_{o,1} = KC_{w,0} \quad (6.3)$$

where $C_{w,0}$ is the initial dissolved radon concentration in water (pCi/mL). In addition, the fraction of radon in the aqueous phase after equilibration, F_w , would be



$$F_w = \frac{C_{w,1}}{C_{w,0}} = \frac{C_{o,1}}{KC_{w,0}} = \frac{C_{o,1}}{C_{o,1}} = 1 \quad (6.4)$$

where V_w and V_o are the volumes (mL) of the aqueous and organic phases respectively and KC_w has been substituted for C_o . If the solvent were removed and a new volume of solvent added, the radon remaining in solution after the first extraction, $C_{w,1}$, would redistribute itself between the organic and aqueous phases. At equilibrium, the radon concentration in the second solvent aliquot, $C_{o,2}$ would be

$$C_{o,2} = KC_{w,1} = K[F_w]C_{w,0} \quad (6.5)$$

For a series of equilibrations, the concentration of radon in the organic solvent after the “ n th” extraction, $C_{o,n}$, can be expressed as

$$C_{o,n} = K[F_w]^n C_{w,0} = K \left[\frac{V_w}{KV_o + V_w} \right]^n C_{w,0} \quad (6.6)$$

Taking the natural log of eqn (6.6) yields a linear relationship between $C_{o,n}$ and the “ n th” extraction of the form

$$\ln[C_{o,n}] = n \cdot \ln \left[\frac{V_w}{KV_o + V_w} \right] + \ln[C_{w,0} \cdot K] \quad (6.7)$$

A plot of $\ln[C_{o,n}]$, the radon concentration in the organic extraction, versus the extraction number, n , yields a straight line with slope

$$\text{slope} = \ln \left[\frac{V_w}{KV_o + V_w} \right] \quad (6.8)$$

which is a function solely of the aqueous and organic volumes and the radon partition coefficient K . The slope is independent of the absolute radon activity or the dissolved radon activity concentration. Provided the set of “ n ” extractions are similar in composition and counted under identical conditions, there is no requirement for determining parameters such as measurement efficiency. The only requirement is accurate knowledge of the aqueous volume and insuring that each extraction is performed with the same volume of organic solvent.

Liquid Scintillation Analysis

Radioactive decay of ^{222}Rn produces four relatively short-lived daughter products. After approximately 3.5 hours ^{222}Rn achieves secular equilibrium with its next four progeny whereby all five of the radionuclides are at the same level of activity. Decay of the ^{222}Rn and daughters release alpha and beta radiation particles each of a known kinetic energy. The scintillators and solvent of a liquid scintillation cocktail convert this kinetic energy into light photons that are detected and amplified by a photomultiplier tube (PMT). The end result is production of a PMT pulse with an amplitude or pulse height proportional to the energy of the decay particle that induced the response. The number of pulses or “counts” induced at the PMT is proportional to the amount of radioactivity interacting in

the cocktail. An analog-to-digital converter transforms the analog PMT pulse to a digital value and assigns it to a channel in a multichannel analyzer (MCA). Most alpha particles are emitted with kinetic energies between 4 and 8 MeV. However, much of the energy is not directly converted to scintillation light. This low scintillation yield results, for example, in a 6.0 MeV alpha particle producing PMT pulses equivalent to those produced by a 600 keV beta particle. As a result, all alpha particles appear in an LSC energy range of approximately 200 to 800 keV, the same energy range over which many beta particles are detected (Packard 1992; Kessler 1989).

In what is frequently termed “traditional LSC” the alpha and beta induced PMT pulses are collected in a single MCA. Due to the lower alpha scintillation yield, the alpha and beta spectra overlap in the MCA and can not be effectively separated. Figure 6.1 shows a typical combined alpha-beta particle spectrum for a radon sample analyzed on a liquid scintillation analyzer. The two large peaks correspond to alpha particles. The right peak is from the 7.6 MeV alpha particle of ^{214}Po ; the left is due to both the 5.0 and 6.0 MeV alpha particles emitted from ^{222}Rn and ^{218}Po respectively. The broad, low height peak is the beta spectrum of ^{214}Pb and ^{214}Bi .

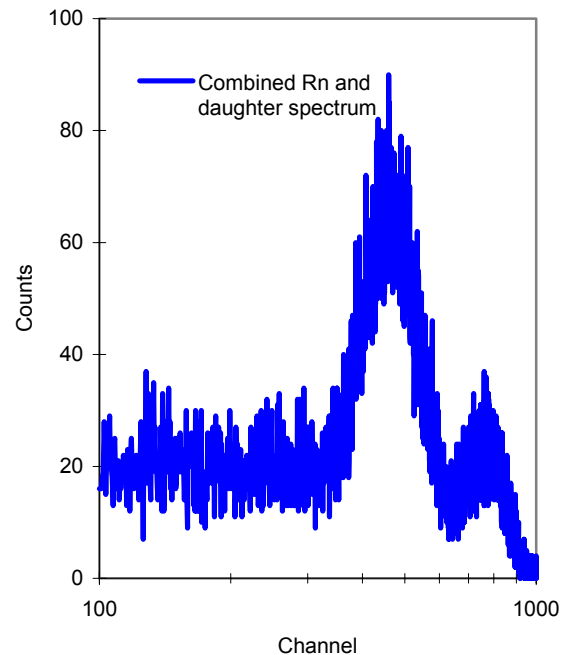


Figure 6.1. Typical LSC spectrum for ^{222}Rn and daughters. The right peak is the ^{214}Po alpha particle (7.6 MeV) while the larger peak is the combined ^{222}Rn (5.5 MeV) and ^{218}Po (6.0 MeV) alpha peak. The remaining signal is the beta particle spectrum from ^{214}Pb and ^{214}Bi .

Another characteristic property of alpha induced scintillation is their duration. PMT pulses induced by beta interaction in the scintillation cocktail are shorter in duration than pulses produced from alpha interaction. This results in an alpha pulse at the PMT having

a different shape than a beta pulse. In the early 1990's commercial liquid scintillation counters began providing an 'alpha-beta' separation option. Separation of alpha pulses from beta is achieved through measurement of the PMT pulse decay and the use of a selectable discriminator. Pulses decaying prior to the pulse discriminator setting (PDD) are classified beta while those decaying after the PDD setting are assumed to be the result of alpha scintillation events. Once classified as alpha or beta, the events are collected in separate MCAs. Figure 6.2 shows the previous radon sample spectrum separated into its alpha and beta components by pulse decay discrimination. The left spectra were obtained at a discriminator setting of 170. At right, is the same sample but analyzed at a PDD setting of 200. At the higher discriminator setting, fewer of the alpha PMT pulses can satisfy the discriminator setting and are thus classified as beta events. It is important to note that pulse discrimination does not affect counting efficiency per se, it only effects classification of a pulse as alpha or beta.

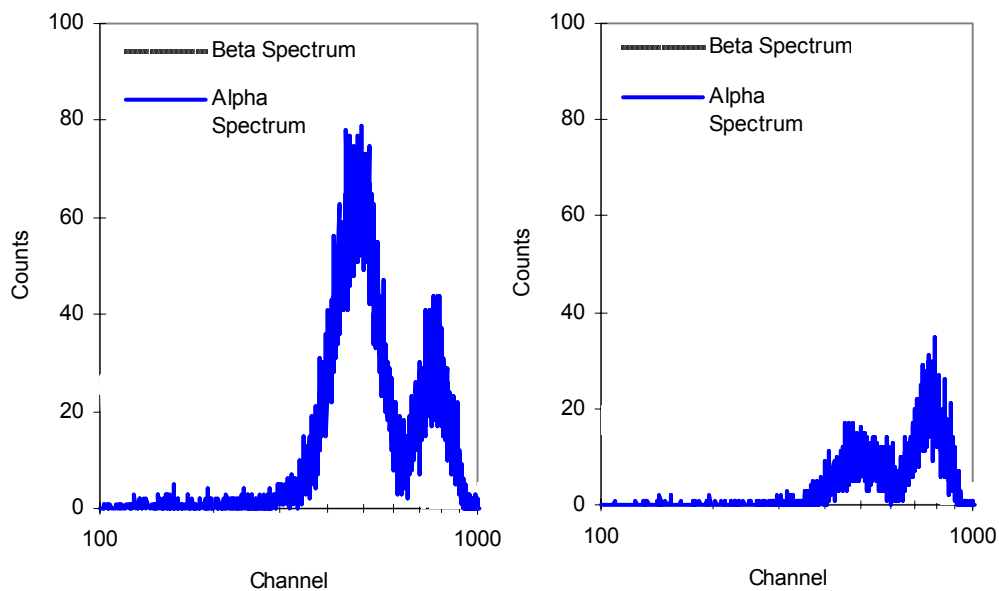


Figure 6.2. Radon alpha-beta spectra at two PDD settings. The spectra at left were obtained at a PDD setting of 170. The right spectra are the same sample analyzed at a PDD of 200. Notice the characteristic alpha peak of ^{222}Rn and ^{218}Po in the 'beta' spectra obtained at a PDD of 200.

Pulse shape discrimination allows quantifying either an alpha or beta emitter in a sample containing both alpha and beta emitting radionuclides (Kessler 1989). Alpha spectrum analysis provides two significant advantages. First, pulse decay discrimination results in separation of the background into alpha and beta components with the alpha background being up to an order of magnitude smaller depending on the discriminator setting.

A second advantage in analyzing just the alpha spectrum involves sample quench. Quench refers to either the reduction in the conversion of a particle's kinetic energy to photon light or the attenuation of scintillation photons once they are produced in the cocktail. Overall, both quenching processes reduce the efficiency with which the decay

particles can be detected. Alpha interaction in the scintillation cocktail is much more quench resistant than beta interaction. As such alpha particles are counted with high efficiency even when other chemicals are present in the scintillation cocktail (McDowell and McDowell 1994; Packard 1992; Yang et al. 1991).

Standards and Sampling

As mentioned previously, secular equilibrium between ^{222}Rn and its next 4 decay daughters is reached in approximately 3.5 hours. Radon-222 gas is itself a decay daughter produced by the alpha decay of ^{226}Ra . With a 3.83 day half-life, ^{222}Rn reaches secular equilibrium with its 1600 year half-life parent in approximately 28 days. Dissolved radon solutions were prepared by transferring a known volume of a 1000 pCi/mL ^{226}Ra solution into pre-weighed 100 mL glass volumetric flasks. The flasks were completely filled with deionized water, capped with a rubber septum, then set aside for at least 30 days to allow ^{222}Rn in-growth. Accurate knowledge of the ^{222}Rn concentration was not required, however; a total activity of 300 pCi per flask was targeted. Once aged, a portion of the solution was withdrawn from the flask using a 2 inch 18 gage needle attached to a 5 mL disposable syringe (Figure 6.3). The volumetric flask was quickly weighed, and then approximately 4 mL of organic solvent was immediately injected into the flask. The flask was inverted and shaken to disperse the solvent throughout the bulk fluid, then placed on a rotary mixer at 1 revolution per second. After 15 minutes mixing, the flask was removed, re-inverted, and set aside to allow phase separation. The organic solvent was removed from the neck of the volumetric flask using a 5 mL glass syringe and transferred to a pre-weighed liquid scintillation vial containing 10 mL of commercial scintillation cocktail. Another aliquot of organic solvent was quickly added to the flask and the process repeated.

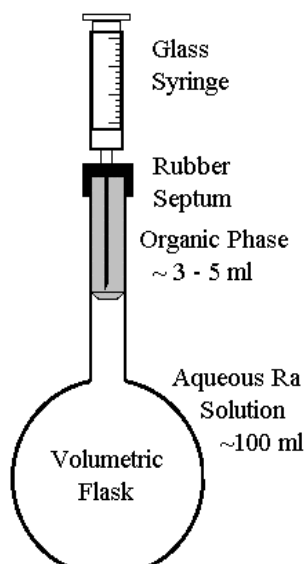


Figure 6.3. Schematic representation of radon extraction. From 3-5 mL of solvent is injected into the flask. After mixing and phase separation, the radon-laden solvent is removed by syringe and transferred to an LS vial. Another solvent aliquot is injected and the process repeated.

The solvent volume added for each extraction was determined by weighing the volumetric flask before and after each solvent addition. As a check, the solvent injection syringe was weighed while loaded with solvent and then again after injection into the flask. Similarly, the volume of solvent transferred to each liquid scintillation vial was determined by mass difference and the MSDS listed solvent density. Four sequential extractions were performed on a single ^{226}Ra - ^{222}Rn standard. Mixing, separation, and transfer times were kept as identical as possible for each of the four extractions. A single extraction required approximately 19 minutes, with 15 minutes for mixing, 3 minutes for separation, and roughly one minute for all solvent transfers. Background extractions were performed in an identical manner on ^{226}Ra solutions that had been purged of ^{222}Rn with laboratory air for a minimum of four hours prior to extraction. The ^{226}Ra and its metal ion daughters prefer the polar, aqueous environment and are not extracted by the non-polar solvent. The background extractions served as both the LSC background and accounted for potential ^{226}Ra carryover from water entrapment in the organic solvent. Multiple extraction experiments were performed using toluene, o-xylene, hexane, benzene, cyclohexane and three commercial liquid scintillation cocktails based on di-isopropyl-naphthalene, linear dodecylbenzene, and o-xylene solvents (Ultima Gold F, Opti-Fluor O and Insta-Fluor respectively).

Analysis

After at least a four-hour delay for in-growth of the radon daughters, the four vials in an extraction set were counted on a Packard TriCarb® 2500A/B liquid scintillation analyzer. The instrument allows for traditional LSC counting as well as alpha-beta counting through the use of pulse decay discrimination. Data reduction was performed on the combined alpha spectrum of ^{222}Rn and its two short lived alpha emitting progeny ^{218}Po and ^{214}Po . The alpha spectrum was used over the beta spectrum alone, and the combined

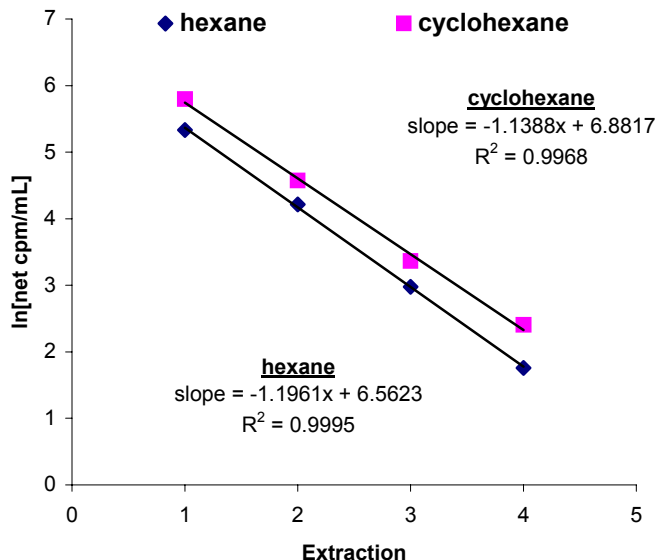


Figure 6. 4 Multiple extraction plot for hexane and cyclohexane. The slope of the regression line is proportional to K. The data fit is typical for all the experiments.

alpha-beta spectra (i.e. traditional) because of the high counting efficiency and quench resistance associated with alpha LSC. In determining K from eqn (6.8) counting efficiency and quench among the group of four sequential extractions is assumed constant. Small variations in cocktail volume, solvent volume, and entrained water could result in minor differences in chemical composition between the “identical extractions”. These variations were expected to affect the beta counting efficiency and beta spectra more than the alpha spectra. The alpha counting efficiency is expected to remain high and constant among samples regardless of water carryover or the solvent being evaluated.

Based on Bem et al. (1994), a PDD of 170 was used for all measurements. Measurement at this relatively high PDD setting insured discrimination of nearly all beta events and some alpha to produce a “beta-less” alpha spectrum that would be resistant to variations between the set of four extractions made from a single radon solution. Energy discrimination was also used in an effort to reduce background and increase measurement sensitivity. A counting interval of 350 to 850 channels was used to evaluate the sample and background spectra and determine the net alpha activity concentration. Samples were counted for four hours or until gross counts were acquired equivalent to a 2-sigma uncertainty of 5%. The sample vial gross count rate (cpm) was corrected for background then decay corrected back to a common time, usually 5 hours after extraction. The natural log of the normalized net count rate concentration for the sample was calculated and then plotted as a function of the extraction number.

RESULTS AND DISCUSSION

A plot of the sample count rate concentration versus extraction number for a set of four extractions performed with hexane and cyclohexane is shown in Figure 6.4. The data is well behaved and typical of the linearity observed for all the solvents and cocktails. The data was fit with a least squares linear regression and the resulting slope used for determining the value of K.

A rigorous sensitivity analysis was not performed on the experimental variables however several factors were evaluated for their potential affect on the measurements. Use of eqn (6.8) to determine K requires accurate knowledge of the equilibrating volumes. For the aqueous solution, the determination was straight forward and was accomplished by weighing the 100 mL flask and septum when empty and again right prior to injection of the first solvent aliquot. For the solvent, an average solvent volume obtained from the four solvent additions was required. Adding the same solvent volume for each extraction was essential and accurate reproducibility was acquired through sheer repetition. Similarly, solvent recovery from the aqueous solution was kept high by practice. Solvent recovery was calculated as the ratio of the radon-laden solvent removed from the volumetric flask to the volume of solvent that was injected into the flask. Table 1 shows the solvent recovery for a set of extractions performed with benzene. The relatively low recovery of the first solvent aliquot is typical for all the solvents and cocktails. The majority of the unrecovered solvent in the first extraction appeared to remain in the meniscus in the neck of the volumetric flask. Though immiscible in water, the solvents have a finite solubility which could contribute to low recovery in the first extraction as

the solution is saturated with the organic solvent. From the results the lower solvent recovery of the initial extraction is not critical to the method.

Table 6.1 Solvent recovery for benzene. Low solvent recovery in the first extraction is typical for all solvents tested.

Extraction	Solvent recovery in each extraction (%)		
	Sample 1	Sample 2	Sample 3
First	87.9	83.0	86.0
Second	93.0	93.6	95.3
Third	97.7	98.5	94.3
Fourth	96.0	95.1	96.0

A more significant variable in the procedure was thorough solvent dispersion and adequate mixing time. An implicit assumption of the method is that equilibrium conditions exist during each extraction. Mixing was enhanced by the presence of a small air bubble (~ 0.3 mL) within the two liquid phases. A bubble helped to initially disperse the solvent and greatly aided in keeping the solvent thoroughly dispersed during mixing. Though technically not a true single phase (liquid) two component (aqueous, organic) system, the effect of this small gas volume was considered minimal compared to the mixing benefit. Reproducibility of measurements was seriously affected without keeping a small air volume in solution (data not shown). One possible remedy is more vigorous shaking of the flask using a wrist shaker rather than a rotary mixer. The improved mixing and a single liquid phase system must be weighed against the potential for formation of an organic-water emulsion within the solution and its potential negative impact on efficient separation of the two phases.

In extracting ^{222}Rn from 0.5 L samples with 20 mL aliquots of toluene, Blackburn and Al-Masri (1993) determined five minutes for equilibrium extraction at laboratory temperature. Bem et al. (1994) used a similar mixing time for the same system. A study was performed to determine the equilibration time required for our experimental procedure. Figure 6.5, showing measured partition coefficients as a function of mixing time, suggests equilibrium was not achieved in 5 minutes and that greater contact time is required to attain equilibrium. Based upon the results, the aqueous-organic extractions were mixed for 15 minutes to insure near equilibrium conditions.

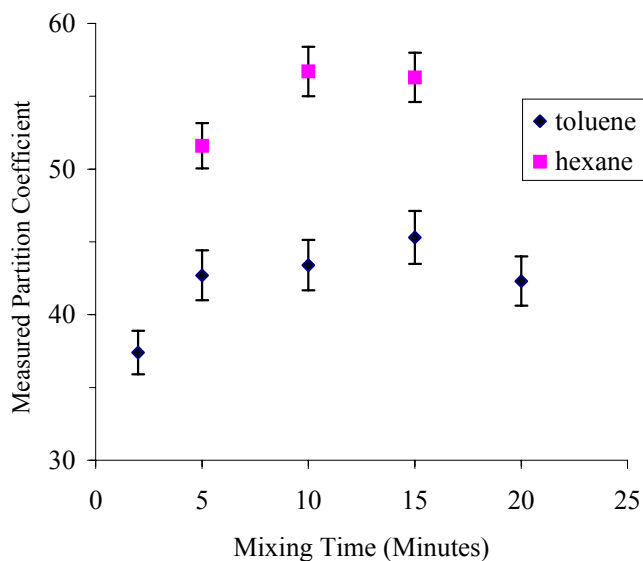


Figure 6.5 Measured radon partition coefficients as a function of mixing time. Equilibrium partitioning of radon between the aqueous and solvent phase was assumed after 15 minutes of mixing.

The literature contains few radon partition coefficients, thus the method was evaluated using solvents for which radon solubility data exists. Unfortunately, few radon Ostwald solubility coefficients exist in the literature for use in calculating a theoretical partition coefficient. A comprehensive data set was compiled by Clever (1979) and gives Ostwald coefficients for a number of organic compounds and water at various ionic strengths, along with an evaluation of the data's reliability. Table 2 lists the average measured radon partition coefficients for the pure solvents and scintillation cocktails, along with the Ostwald solubility coefficients at 20 °C, and their theoretical radon partition coefficient if applicable. The measured K values for the five solvents compare favorably with their estimated values, an exception being that for o-xylene with a 17% relative error. A plot of the K's measured for the five pure solvents as a function of their theoretically derived partition coefficients showed good agreement between measured and theoretical values and a correlation coefficient (R^2) value of 0.95. One possible explanation for the discrepancy in the o-xylene is chemical purity. The estimated theoretical value is for a mixture of ortho, meta and para xylene isomers and ethylbenzene. The value of 39 determined for the Insta-Fluor, which is 97-99% o-xylene, compares well with that for the o-xylene solvent. Though structurally similar, it is plausible the xylene isomers and ethyl benzene are physically different enough that a pure o-xylene solvent has a lower radon partition coefficient than a xylene isomers mixture. Overall the partition coefficients compare favorably with those estimated from solubility data.

Table 6.2 Measured and estimated theoretical radon partition coefficients for selected solvents. Measured partition coefficients are an average of two measurements for the Opti-Fluor O and Insta-Fluor and three for all others. The uncertainty is two times the standard deviation of the average K. The Ostwald solubility coefficient for water at 20 °C is 0.285. Densities are from the MSDS.

Solvent	Density 20°C (g/cm ³)	Ostwald solubility coefficient	Theoretical Partition Coefficient	Measured Partition Coefficient
n-hexane	0.66	16.56	58.1	56.5 ± 2.8
Cyclohexane	0.78	18.04	63.3	61.0 ± 4.0
Toluene	0.87	13.24	46.5	43.6 ± 1.5
Benzene	0.87	12.82	45.0	42.9 ± 2.9
o-xylene	0.87	12.75	44.7	37.0 ± 0.5
Insta-Fluor (o-xylene)	0.87	--	--	38.6 ± 2.6
Opti-Fluor O (dodecylbenzene)	0.89	--	--	35.3 ± 1.6
Ultima Gold F (di-isopropylnaphthalene)	0.98	--	--	32.4 ± 1.7

No Ostwald solubility data exists for the Opti-Fluor O and Ultima Gold F scintillation cocktails. As an informal check, liquid scintillation counting standards were prepared in 20 mL glass scintillation vials using ²²⁶Ra standard solution to Ultima Gold F volume ratios of 5:15, 10:10 and 15:5 (mL/mL). Assuming all the radon enters via the aqueous phase, the fraction of ²²²Rn in the cocktail phase once chemical and radiological equilibrium has been achieved can be expressed as

$$F_c = \frac{K}{[K + (V_s/V_c) + (V_g/V_c) \cdot (1/L_w)]} \quad (6.9)$$

where F_c is the fraction of radon in the cocktail phase, K is the aqueous-cocktail radon partition coefficient, L_w is the radon Ostwald solubility coefficient for water, and V_s , V_c , and V_g are the aqueous sample, cocktail, and gas phase volumes respectively. Values of L_w range from 0.250 to 0.285 for laboratory temperatures (Clever 1979).

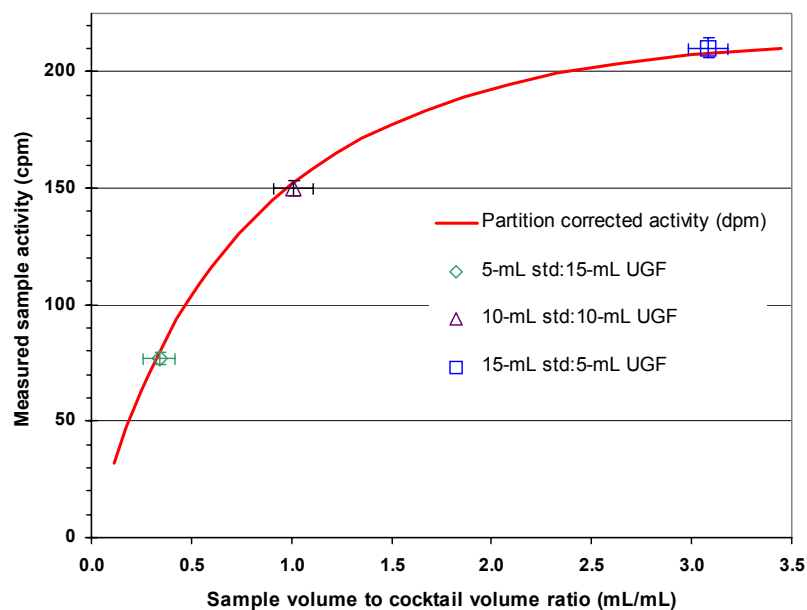


Figure 6.6 Measured activity as a function of the ratio of aqueous sample to cocktail volume. The solid curve is the theoretical activity expected in the organic phase due to radon partitioning between the water, cocktail (UGF) and gas headspace in an LS vial. Data points are the average of replicate 30 minute counts on duplicate samples. The combine alpha-beta spectrum was analyzed over 0-2000 channels.

Figure 6.6 shows the measured count rates and the theoretical fraction of ^{222}Rn expected in the cocktail phase as a result of partitioning, assuming values of 0.285 and 32.4 for L_w and K respectively. The agreement between the measured count rates and the theoretical activity expected in the cocktail as a result of radon partitioning suggests the value determined for K is accurate.

CONCLUSIONS

Few measured partition coefficients have been reported for the partitioning of dissolved radon gas between aqueous and organic liquids. A multiple extraction method was used to measure the aqueous-organic partition coefficients for dissolved radon gas and five solvents and three liquid scintillation cocktails. The method is fast, taking approximately one hour to complete a set of four extractions, and accurate. Excellent agreement was obtained between the measured radon partition coefficients and theoretical partition coefficients estimated from a ratio of Ostwald solubility coefficients for the solvents and water. Use of a commercial liquid scintillation analyzer with alpha-beta discrimination provided a stable automated counting configuration and minimized the possible effect of variations in solvent volume and entrained water among sequential extractions. The method is amendable to nearly any liquid hydrocarbon that is insoluble in water. Though the method focused on lighter-than-water solvents, it could be modified to accommodate solvents with a specific gravity exceeding one. In such case, extractions might take place

using a glass separatory funnel with the solvent removed from the bottom of the funnel. Many solvents are denser than water as a result of halogen functional groups which are notorious for significantly quenching the light output and hence counting efficiency of liquid scintillation cocktails. Alpha counting via pulse separation, however, can minimize this effect. This and a careful balance between the aqueous and organic volume used might still prove an erstwhile methodology.

REFERENCES

- Bem, H.; Bakir, Y. Y. Y.; Bou-Rabee, F. An improved method for low-level radon-222 determination in environmental waters by liquid scintillation counting with pulse shape analysis. *J. Radioanal. Nucl. Chem., Letters* 186(2):119-127; 1994.
- Blackburn, R.; Al-Masri, M. S. Determination of radon-222 and radium-226 in water samples by cerenkov counting. *Analyst* 118(3):873-876; 1993.
- Clever, H. L. ed. *Krypton, Xenon, and Radon -- Gas Solubilities, Solubility Data Series 2; Volume 18.* Oxford, UK; Pergamon Press; 1979.
- Collé, R. A precise determination of the ^{222}Rn half-life by 4π α - β liquid scintillation measurements. *Radioactivity and Radiochemistry*, 6(1):16-29; 1995.
- Cratin, P. Partitioning and the liquid-liquid interface. *Ind. Eng. Chem.* 60:14-19; 1968.
- Horrocks, D. L.; Studier, M. H. Determination of radioactive noble gases with a liquid scintillator. *Anal Chem.* 36:2077-2079; 1964.
- Hunkeler, D.; Hoehn, E.; Hohener, P.; Zeyer, J. ^{222}Rn as a partitioning tracer to detect diesel fuel contamination in aquifers: laboratory study and field observations. *Environ. Sci. Technol.* 31:3180-3187; 1997.
- Kessler, M. J. ed. *Liquid Scintillation Analysis Science and Technology.* Meriden, USA; Packard Instrument Company; 1989.
- Leo, A.; Hansch, C.; Elkins, D. Partition coefficients and their uses. *Chem. Rev.* 71(6):525-553; 1971.
- Lowery, J. D. Measuring low radon levels in drinking water supplies. *J. Amer. Water Works Assoc.* 83(4):149-153; 1991.
- McAuliffe, C. D. GC determination of solutes by multiple phase equilibrations. *Chem. Tech.* 1:46-49; 1971.
- McDowell, W. J.; McDowell, B. L. *Liquid scintillation alpha spectrometry.* Boca Raton, FL: CRC Press, Inc; 1994.
- Packard Instrument Company. The effect of quench on quantitating alpha radionuclides by liquid scintillation counting. Packard Application Note, ABA-003. Packard Instruments, Meriden, CN.; 1992.
- Parks, N. J. A more sensitive method for the assay of radon-222 concentrations in water samples with liquid scintillation counters. *Health Phys.* 36(2):207; 1979.
- Parks, N. J.; Tsuboi, K. K. Emulsion scintillation counting of radium, and radon. *Int. J. Appl. Radiat. Isotopes* 29:77-80; 1978.
- Pritchard, H. M.; Gesell, T. F. Rapid determination of radon-222 concentrations in water with a commercial liquid scintillation counter. *Health Phys.* 33(5):577-581; 1977.
- Schwarzenbach, R. P.; Gschwend, P. M.; Imboden, D. M. *Environmental Organic Chemistry.* John Wiley and Sons, New York; 1993.

- Semprini, L.; Hopkins, O. S.; Tasker, B. R. Laboratory, field and modeling studies of Radon-222 as a natural tracer for monitoring NAPL contamination, *Jour. Trans. Porous Media* 38(1/2):223-240; 2000.
- Semprini, L.; Cantaloub, M.; Gottipati, S.; Hopkins, O.; Istok, J. Radon-222 as a tracer for quantifying and monitoring NAPL remediation. In: *Proceedings on Remediation of Chlorinated and Recalcitrant Compounds: First International Conference*. Columbus, OH. Battelle Press; 1998.
- Wong, C.S.; Chin, Y.; Gschwend, P. M. Sorption of radon-222 to natural sediments. *Geochim. Cosmochim. Acta.* 56:3923-3932; 1992.
- Yang, D.; Zhu, Y.; Mobius, S. Rapid method for alpha counting with extractive scintillator and pulse shape analysis. *J. Radioanal Nucl. Chem., Articles* 147:177-189; 1991.

7. THE EFFECT OF SAMPLE, COCKTAIL AND HEAD SPACE VOLUME WHEN ANALYZING 222-RADON IN 5 mL SAMPLES BY LIQUID SCINTILLATION METHODS

INTRODUCTION

Aqueous radon measurement is frequently associated with the health concerns related to direct ingestion of radon or to waterborne radon's contribution to indoor radon levels (NRC, 1998). However, radon's unique chemical properties and its natural presence in subsurface fluids make it an excellent tracer of hydrologic processes. Radon has been effectively used as a tracer of water infiltration and recharge rates (Hamada and Komoe 1998; Snow and Spaulding 1997; Bertin and Bourg 1994), monitoring water body mixing (Cable et al. 1996), tracing stream flow paths (Corbett et al. 1997) and most recently for monitoring the remediation of subsurface nonaqueous phase liquid contamination (Semprini et al. 2000; Semprini et al. 1998; Hunkeler et al. 1997). In most of these field applications, logistics or transportation issues, not adequate sample availability, limits sample size. Sample analysis size can be a limiting factor. Because of its simple preparation methods, low detection limits and automated analysis, liquid scintillation counting (LSC) is frequently used for aqueous radon analysis. LSC analysis is limited to the standard 20 mL scintillation vial. The most commonly cited two-phase radon LSC method requires 10 mL of aqueous sample be injected beneath 10 mL of scintillation cocktail though 5 mL cocktail and 15 mL of sample is used in the standard method (APHA 1996). Either ratio reduces the aqueous sample size to between 10 and 15 mL. When very low concentrations are expected, such as in infiltration rate studies, radon extraction from samples of up to 1.0 L is used to concentrate the radon (Homada and Komoe 1998; Freyer et al. 1997; Bem et al. 1994).

There are instances, however, when aqueous sample volumes of even 10 mL are not feasible. This is often encountered in bench-scale work where the physical size of the experimental apparatus is limited, or where sample volumes greater than several mLs would disrupt representative flow paths or other analytical measurements. One facet of radon LSC research has been optimizing the volumes of sample and cocktail in the counting vial in order to achieve the highest counting efficiency while minimizing background (Mamoon et al. 1996; Lowery 1991). The underlining assumption has always been the availability of 20 mL or more of aqueous sample. Few researchers have focused on optimizing LSC counting conditions when the aqueous sample size is limited to only 5.0 mL. In such instances it is important that the LSC analysis protocol makes the most efficient use of the available radon. When small sample volumes are involved consideration must be given to the volume of cocktail used and the resulting vial headspace. If too little cocktail is utilized, the vial headspace has the potential to be a significant sink, reducing the amount of radon extracted into the cocktail and thus available for counting. Increasing the cocktail volume minimizes radon loss to the vial headspace; however, the benefit of the increased extraction efficiency may come at the expense of a larger background count rate. The situation is further complicated when counting radon and its alpha emitting daughters by employing pulse decay discrimination (PDD). With PDD, separation of the alpha induced events from the beta also results in separation of the background into alpha and beta components. The alpha background is typically 2 to 20 times lower than the total background. In alpha LSC, the reduced alpha

background may more than offset potential increases in background count rates as a result of an increased cocktail volume. In addition, the optimum pulse decay discriminator setting and the overall detection efficiency or conversion factor (cpm per pCi) may be dependent, in part, on the cocktail-sample volumes and the position of the cocktail-air meniscus relative to the instrument photomultiplier tubes.

Presented in this paper is an investigation into radon distribution within an LSC vial and the effects that the sample, cocktail and gas headspace volumes have on the radon LSC method. The counting efficiency, background count rates and figure of merit (FOM) for traditional and alpha-beta LSC are reported for five sets of 5 mL ²²²Rn standards having from 5.0 to 15.0 mL of scintillation cocktail.

BACKGROUND AND THEORY

With respect to two-phase LSC, radon is unique in that it distributes itself between the aqueous, organic (cocktail) and gas (headspace) phases within the LSC vial. When small sample sizes are involved (≤ 5 mL) in a standard 20 mL LSC vial, consideration must be given to the volume of cocktail used and the resulting vial headspace. The distribution of radon between the three phases within a LSC vial can be calculated using an activity balance and the known volumes of the three phases. Assuming all the radon enters via the aqueous phase, the fraction of radon in the cocktail phase once chemical equilibrium has been achieved can be expressed as:

$$F_c = \frac{K}{[K + (V_s/V_c) + (V_v/V_c)(H)]} \quad (7.1)$$

where F_c is the fraction of radon in the cocktail phase, K is the aqueous-organic radon partition coefficient (dimensionless), H the air:water partition coefficient (also the inverse of the Ostwald solubility coefficient, L) for radon, and V_s , V_c , and V_v are the sample, cocktail, and vial void (gas) phase volumes (mL) respectively. In a similar manner, the fraction of radon in the vial void or headspace, F_v , can be expressed as:

$$F_v = \frac{H}{[H + (V_s/V_v) + (V_c/V_v)K]} \quad (7.2)$$

Values of H typically range from 3.5 to 4.5 – Ostwald solubility coefficients of 0.225 to 0.285 - and are dependant on the ionic strength and temperature of the water (Lewis et al. 1987; Clever 1979). The magnitude of the aqueous-organic radon partition coefficient K is dependent on the base solvent used in the scintillation cocktail. Reported values range from 45 for toluene based scintillation cocktails (Prichard and Gesell 1977) to 23 for a high efficiency mineral oil (long chained aliphatic hydrocarbons and psuedocumene) cocktail (Lowery 1991). A value of 32 at approximately 20 °C was measured in our laboratory for an ‘environmentally friendly’ scintillation cocktail based on di-isoproplylnaphthalene (Cantaloub et al. 1997). Using values for K and H , the fraction of radon in the cocktail, headspace and aqueous phases can be determined for any sample:cocktail ratio. Figure 7.1 shows the radon fraction in the gas and cocktail phases as a function of the sample to cocktail volume ratio for 5.0 mL of sample and from 5 to 15 mL of scintillation cocktail. The curve was developed assuming a total vial volume of

23.5 mL and values of 34 and 4 for K and H respectively. As the curve demonstrates, with a low cocktail volume the gas headspace becomes a significant radon sink. With 5.0 mL of cocktail, nearly 25% of the radon can be expected to occupy the 13.5 mL void space above the cocktail. As cocktail volume increases more radon resides within the cocktail until at a cocktail volume of 15

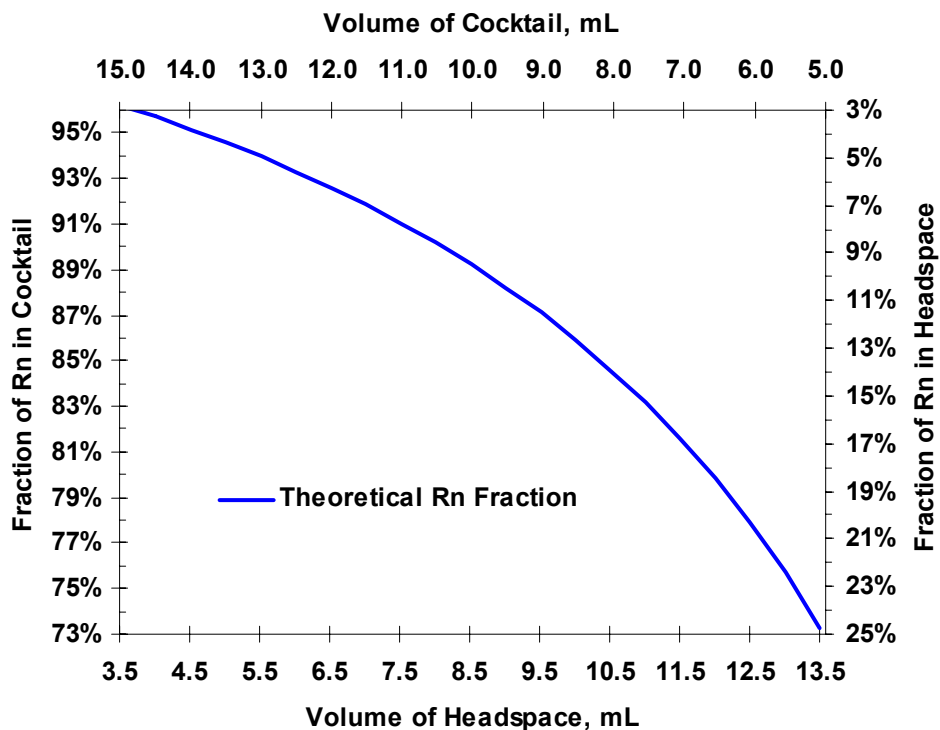


Figure 7.1 Theoretical distribution of radon between the cocktail and gas phases in a 20 mL LSC vial. The curve assumes 23.5 mL total vial volume and values of 32 and 4 for K and H respectively.

mL, more than 95% of the radon is expected in the cocktail phase. No more than 2% of the radon would be predicted to remain in the aqueous phase for any cocktail-headspace combination. This is anticipated with the low 5.0 mL sample volume and the highly polar aqueous environment being the least preferred phase for the non-polar radon atom. While Figure 7.1 suggests that minimizing the headspace radon sink is the most efficient sample to cocktail ratio, no conclusions as to the actual measurement efficiency or background count rates are possible. One expects the larger cocktail volume acting essentially as a larger detector, results in larger background count rates (Arcos and Barquero 1995). However until measurements are performed, it is not certain how large an effect an increased background will be to the overall method sensitivity.

MATERIALS AND METHODS

Standard and background vials were prepared with cocktail volumes of 5.0, 7.5, 10.0, 12.5 and 15.0 mL floating on top of 5.0 mL of aqueous sample. Radioactive standards were prepared by transferring 5.0 mL of a NIST traceable aqueous $^{226}\text{RaCl}_2$ solution into

pre-weighed 20 mL glass scintillation vials followed by the appropriate volume of a di-isopropylnaphthalene based liquid scintillation cocktail (Ultima Gold F, Packard Instrument Company). The ^{226}Ra solution activity was 100.2 ± 1.2 dpm/mL and contained 20 ppm BaNO_3 carrier and 0.5 M HCl. Background counting vials were prepared in an identical manner from a de-ionized water solution prepared to a similar ionic and acidic strength. Five standards and five matching background vials were prepared at each cocktail volume (Table 7.1). Auto-pipettes were used for all liquid transfers, however sample and cocktail volumes were determined by mass difference using a Mettler Type H6T analytical balance and the appropriate density. Once completed, the vials were capped with white urea, polycone lined caps and placed in a laboratory refrigerator to reach chemical and radiological equilibrium. None of the vials were shaken.

Table 7.1 Average liquid volume and sample activity for the five cocktail sets. Alpha sample alpha activity is the supported ^{222}Rn in equilibrium with ^{218}Po and ^{214}Po daughters; total sample activity includes ^{214}Pb and ^{214}Bi .

Sample to Cocktail Set	Aqueous Volume (ml $\pm 2\sigma$)	Cocktail Volume (ml $\pm 2\sigma$)	Total Activity (dpm $\pm 2\sigma$)	Sample Alpha Activity (dpm $\alpha \pm 2\sigma$)
5-5.0	5.07 ± 0.01	4.94 ± 0.11	2538 ± 3	1523 ± 2
5-5.0 bkgd	5.04 ± 0.03	4.99 ± 0.09		
5-7.5	5.06 ± 0.01	7.44 ± 0.04	2535 ± 2	1521 ± 1
5-7.5 bkgd	5.03 ± 0.02	7.43 ± 0.03		
5-10.0	5.06 ± 0.02	9.94 ± 0.03	2535 ± 5	1521 ± 3
5-10.0 bkgd	5.03 ± 0.01	9.94 ± 0.04		
5-12.5	5.06 ± 0.02	12.43 ± 0.04	2538 ± 7	1523 ± 4
5-12.5 bkgd	5.02 ± 0.01	12.44 ± 0.04		
5-15.0	5.06 ± 0.01	14.89 ± 0.06	2533 ± 2	1520 ± 1
5-15.0 bkgd	5.02 ± 0.02	14.88 ± 0.04		

After sufficient time for equilibration the vials were counted on a Packard Tri-Carb® 2500 TR/AB liquid scintillation analyzer having an attached chill unit operating at 15 °C. The liquid scintillation analyzer has the option for counting samples in the traditional mode or in the alpha-beta mode using pulse decay discrimination (PDD). In traditional mode, all scintillation events are combined into a single spectrum. Alpha-beta mode takes advantage of the fact that alpha induced scintillation's differ physically from beta induced events. In alpha-beta mode, scintillation events are classified as either alpha or beta based upon the lifetime of the negative pulse produced at the photo-multiplier tube (PMT). PMT pulses decaying prior to the selectable pulse decay discriminator setting, are classified beta while those present after the PDD are classified alpha. Each is collected into separate alpha and beta multi-channel analyzers (MCAs).

The five ^{226}Ra supported ^{222}Rn and five background vials in each set were counted in a single rack in alternating positions (odd-background; even-standards) to better estimate

the background over the sample counting interval. The samples were allowed a minimum of three days temperature equilibration on the detector deck following transfer from the refrigerator, and an additional 5 minutes for dark adaptation. Sample quench was monitored for 60 seconds using the instrument's external standard tSIE quench parameter. The cocktail sets were counted in the alpha-beta mode at 17 PDD settings over a range of 100 to 200. Background samples were counted for 60 minutes while the ^{222}Rn standards were counted for 60 minutes or until a 2σ relative uncertainty of 1% was reached in the alpha MCA. Alpha and beta MCA spectra from 0 - 2000 channels were saved for each sample and transferred to a personal computer for analysis. The spectra were converted to cpm per channel from which a five-vial average spectrum for the background vials and the ^{222}Rn samples was created.

RESULTS AND DISCUSSION

Radium-226 supported ^{222}Rn standards provide for a long-lived radon counting standard. Once in equilibrium, the cocktail phase contains ^{222}Rn and its next four progeny all in secular equilibrium with the ^{226}Ra parent which remains in solution. A total of five decay particles are available for counting; the three alphas of ^{222}Rn (6.0 MeV), ^{218}Po (6.5 MeV) and ^{214}Po (7.4 MeV), and two energetic beta with various endpoints (^{214}Pb and ^{214}Bi).

LSC is known for a nearly 100% counting efficiency of alpha particles and energetic beta particles. Assuming all the decay particles interacting in the cocktail are counted with 100% efficiency, the net count rate recorded in both the alpha and beta MCAs from 0-2000 channels should be an accurate reflection of the radon distribution between the cocktail, water, and gas phases. Figure 7.2 shows the average measured sample efficiency (cpm/dpm) for each cocktail set plotted with the theoretical radon partition curve from eqn (7.2). The data shows good agreement for the 15.0 and 12.5 cocktail volume samples, however, the measured counting efficiencies for the 10.0, 7.5, and 5.0 mL are greater than partitioning alone predicts. One possible explanation is the magnitude of the aqueous-organic radon partition coefficient. A value of 50 for K fits the 5.0, 7.5, and 10.0 data better, but results in the 15.0 and 12.5 mL measurements being below the predicted values. A partition coefficient of 50, however, for the diisopropylnaphthalene solvent is not consistent with previous research (Cantaloub et al. 1997). As the samples were counted at approximately 15 °C and the value of 32 was measured at 20 °C, a K of 36 or 40 may be warranted.

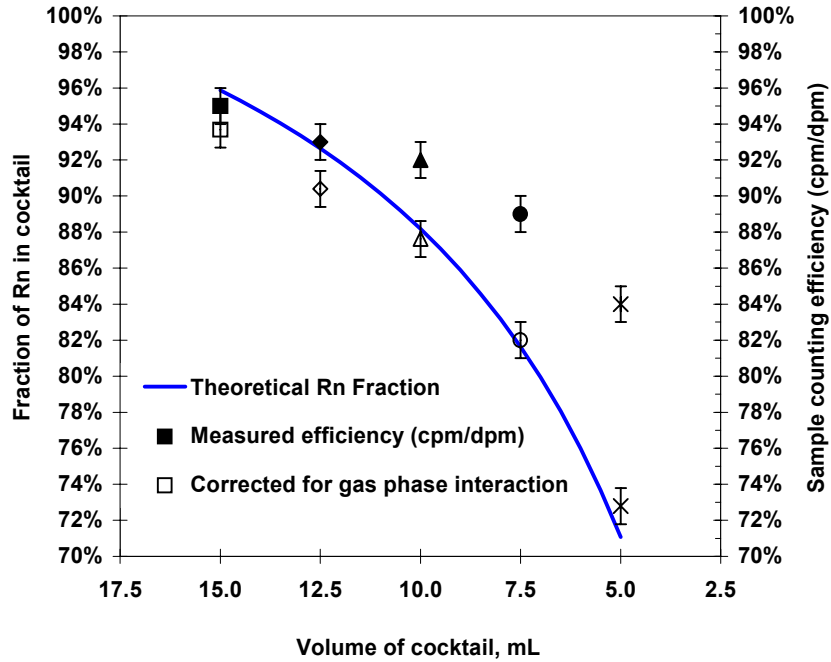


Figure 7.2 Measurement efficiency as a function of cocktail volume. Measured points are the average for five samples measured 18 times. Solid data points represent measured efficiencies while hollow data points the same values corrected for air luminescence. The theoretical Rn fraction assumes values of 32 and 0.225 for K and H respectively.

A second possibility is interaction of the gas phase ^{222}Rn and daughters with the liquid scintillation cocktail. Prichard and Gesell (1977) assumed 25% of the gas phase radionuclides contributed to the observed count rate by interacting at the cocktail-air meniscus. Murase et al. (1989) reported a counting efficiency of 42% for radon and its daughters in an empty LS vial as a result of air luminescence. Both imply that when a large headspace volume exists in the vial the measured count rates reflect both the radionuclides in the cocktail phase and some of the ^{222}Rn and daughters within the headspace. The fraction of radon in the gas phase for each sample:cocktail volume ratio can be calculated. If the ^{222}Rn and daughter decay particles are counted with 42% efficiency, then a ‘cocktail only’ corrected sample count rate and efficiency can be determined as:

$$\text{cpm}_{\text{corrected}} = \text{cpm}_{\text{measured}} - 0.42F_v \cdot \text{dpm}_{\text{std}} \quad (7.3)$$

$$\text{efficiency} = \frac{\text{cpm}_{\text{measured}} - 0.42F_v \cdot \text{dpm}_{\text{std}}}{\text{dpm}_{\text{std}}} = \frac{\text{cpm}_{\text{measured}}}{\text{dpm}_{\text{std}}} - 0.42F_v \quad (7.4)$$

where $\text{cpm}_{\text{measured}}$ is the measured net count rate, dpm_{std} is the calculated disintegration rate for radon and its daughters in the standard, and F_v is the fraction of radon expected in the vial headspace. The air luminescence adjusted values of are plotted as open data points in Fig 7.2 and agree well with the theoretical radon distribution expected in the vial as a result of partitioning. Even with air luminescence, the data clearly demonstrates the increase in sample counting efficiency as the vial void is filled with cocktail. The larger sample counting efficiency doesn’t necessarily make for the most sensitive

protocol. The signal to noise ratio or figure of merit (FOM) is frequently used in comparing radiation measurements system and is defined as:

$$\text{FOM} = \frac{[(\text{cpm}_{\text{measured}}/\text{dpm}_{\text{std}}) \cdot 100]^2}{\text{bkgd}} \quad (7.5)$$

where bkgd is the background count rate in cpm calculated over the same channel interval as the efficiency. Table 7.4 shows the 0-2000 channel full energy spectrum and the energy window optimized background count rate, sample counting efficiency and FOM for each sample:cocktail set for traditional LSC. The FOM is roughly the same for each cocktail set when analyzed in the full open window. While the increased cocktail volume raises the overall sample counting efficiency, the additional cocktail also increases the background counting rate though not as much as might be anticipated. A three-fold increase in cocktail volume from 5.0 to 15.0 mL resulted in a background count rate increase of roughly 5 cpm from 32.3 cpm to 38.4 cpm in the

Table 7.4 Average background, sample counting efficiency, and FOM for the five cocktail sets. Each value is the average of 17 measurements for the five vials analyzed in the traditional LSC mode.

Set	Full Window 0 – 2000 channel			Optimized Window 150-700 channels		
	Bkgd (cpm)	Efficiency (cpm/dpm)	FOM	Bkgd (cpm)	Efficiency (cpm/dpm)	FOM
5.0	32.26	0.84	219	2.84	0.61	1310
7.5	34.08	0.89	232	3.52	0.60	1023
10.0	35.63	0.92	238	4.10	0.60	880
12.5	36.36	0.93	238	4.74	0.60	843
15.0	38.38	0.95	235	5.27	0.66	817

full open window. When energy discrimination is applied, a more pronounced correlation between cocktail volume and background is evident. The 5.0 mL cocktail samples have a background count rate approximately two times lower than the 15.0 mL sample. The higher FOM for the lower volume cocktails is due almost solely to background. Though the low cocktail samples had a substantial increase in sample efficiency due to air luminescence, these counts occur in a low energy range of less than 18 keV and are excluded in the energy optimized window of 150 to 700 channels. Overall, the 5 mL cocktail and 5 mL of aqueous sample and the lower total sample counting efficiency that results from radon partitioning into the vial headspace is compensated for by lower background count rates and a higher figure of merit when energy discrimination is utilized.

As mentioned previously, in the alpha-beta count mode, pulses at the PMT are separated into separate MCAs depending upon the pulse duration and the selectable PDD setting. This not only separates true alpha and beta events, but also separates the background into alpha and beta components with the alpha background being up to a factor of 40 times lower than the beta background. Figure 7.3 shows the alpha backgrounds as a function of

cocktail volume over a range of PDD settings. Again, a strictly proportional relationship between cocktail volume and background is not evident, but a linear relationship between the two exists at all PDD settings. As PDD increases, not only does the magnitude of the alpha background count rate decrease, but the difference between background count rates for each sample set also becomes smaller. Overall, the magnitude of the alpha background is significantly lower than the background. This background reduction is one of the key benefits in performing radon LSC with pulse decay discrimination.

The optimum PDD setting for a given sample depends upon the cocktail solvent and overall sample chemistry. With a mixed alpha-beta sample such as ^{222}Rn , the optimum PDD setting can be determined by plotting the alpha MCA counting efficiency as a function of PDD setting. The mixed ^{222}Rn sample contains three alpha emitters and two beta emitters. At the optimum separation, 60% of the acquired signal

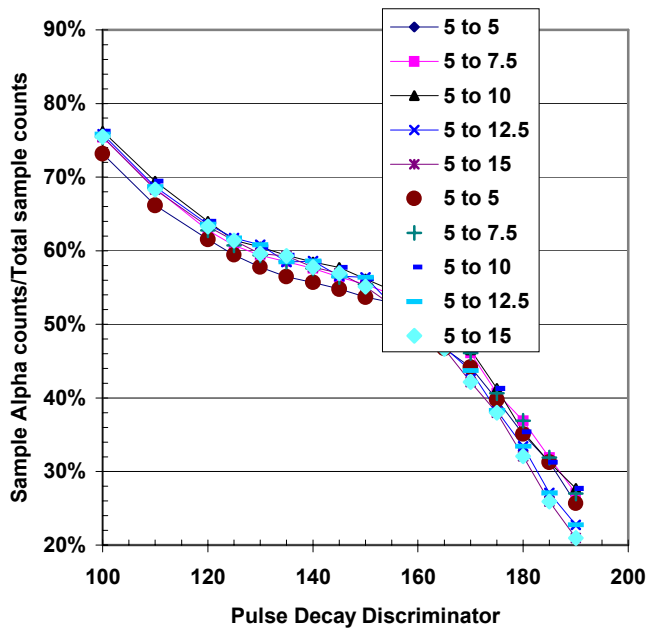


Figure 7.3 The alpha MCA background as a function of cocktail volume and PDD. Each datum is the average of 5 samples counted for 60 minutes and evaluated from 0-2000 channels.

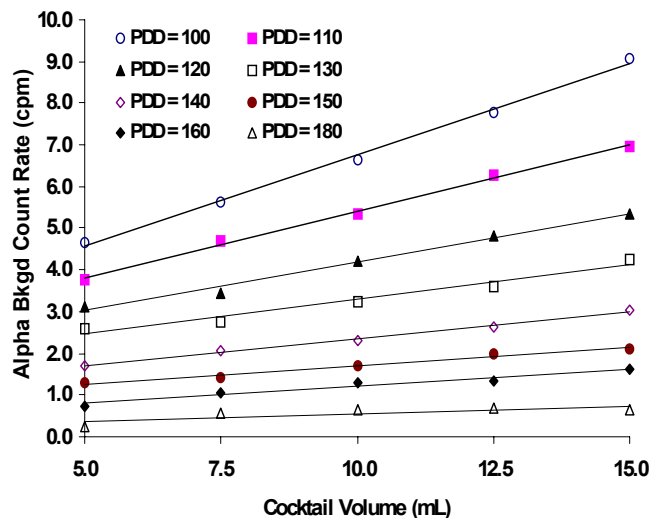


Figure 7.4 Alpha MCA efficiency as a function of PDD setting. Each datum is the average of five samples counted to a 2σ relative uncertainty of 1% or 60 minutes. Data evaluated from 0-2000 channels.

should reside in the alpha MCA and 40% in the beta MCA. Figure 7.4 shows the alpha counting efficiency as a function of PDD setting for each of the five sample:cocktail sets. The shape of the curves is primarily a function of the cocktail solvent and is consistent between the different volume sets and with previously published curves for this solvent (Spaulding and Noakes 1993). All the samples show a slight ‘plateau’ where changes in alpha separation efficiency are relatively small indicating a fairly stable system. The optimum separation PDD value is almost identical at a value of 130 for each set, the exception being the 5 mL sample which has a slightly lower optimum PDD setting of 125. Overall, cocktail volume had little affect on PDD. This is consistent with the fact that sample chemistry plays a more significant role in pulse separation. In the two-phase radon LSC method, many compounds which might effect cocktail chemistry remain in solution leaving the cocktail relatively pure and unaffected. Slight differences in optimum PDD are likely attributable to the position of the cocktail volume in relation to the PMT tube. In determining the optimum PDD setting for radon in the above manner, it must be remembered that the optimum PDD setting is only an approximation since even with a 60%:40% separation of pulses, it is not possible to determine how many of the alpha MCA events are actually due to misclassified beta events and vice a versa.

As was the case with the combined alpha and beta spectrum analysis, the lower cocktail volume samples provide a higher FOM. The difference in backgrounds and FOM between the traditional LSC and alpha LSC is clearly evident in the data of Table 7.5, which shows the full open and optimized energy window FOMs for the cocktail sets. The advantage of pulse decay discrimination is clearly evident with the

Table 7.5 Average figure of merit for each cocktail set at selected PDDs. Open window is 0 – 2000 channels. Optimum window varies for each sample but is generally between 150 and 700 channels.

Set	PDD – 140		PDD – 160		PDD – 180	
	Open	Optimum	Open	Optimum	Open	Optimum
5.0	2567	21080	6602	50412	10062	75572
7.5	3525	17444	5662	28150	5270	42624
10.0	3469	16025	4843	22757	4603	26306
12.5	3099	14270	4611	18604	3999	22304
15.0	2816	11756	3741	15189	3803	16723

full open window FOM at each PDD setting nearly a factor of 3 greater than the energy window optimized values from the combined alpha–beta spectrum. At a PDD of 140, the alpha separation efficiency is approximately 58% while at 160 the 50% alpha separation results in a nearly ‘pure’ alpha MCA spectrum. With the higher PDD setting an increasing number of true alpha events are misclassified as beta. The result are FOMs ranging from 15,000 to 50,000 with an energy window optimized counting efficiency of approximately 60%.

CONCLUSIONS

When analyzing for radon in small volume aqueous samples by LSC methods, the distribution of radon between the cocktail, aqueous sample and gas headspace phases must be considered. The interaction of headspace radon causes an increase in the measured counting efficiency over that predicted by partitioning theory when the vial headspace volume is large. Though overall sample counting efficiency increases with increasing cocktail volume, use of 5.0 mL of cocktail with 5.0 mL aqueous samples resulted in the most sensitive analysis protocol in both traditional LSC and radon alpha LSC with pulse decay discrimination. The decreased performance with increasing cocktail volume, as indicated by the FOM, is directly linked to background. In traditional LSC, energy optimized FOMs ranged from approximately 1300 for 5 mL of cocktail atop 5 mL of sample, to around 820 for 15 mL of cocktail. In alpha LSC at a PDD of 160, FOMs ranged from approximately 50000 to 15000 for 5 mL and 15 mL of cocktail respectively. In all cases, using a smaller cocktail volume resulted in a more sensitive counting protocol.

REFERENCES

- American Public Health Association. Standard Methods for the Examination of Water and Wasterwaster, 19th edition supplement, Washington, DC 1996.
- Arcos, J. M.; Barquero, L. R. LSC background prediction using three-dimensional modelling. *Appl. Radiat. Isot.* 46(9):929-931; 1995.
- Bem, H.; Bakir, Y. Y. Y.; Bou-Rabee, F. An improved method for low-level radon-222 determination in environmental waters by liquid scintillation counting with pulse shape analysis. *J. Radioanal. Nucl. Chem., Letters* 186(2):119-127; 1994.

- Bertin, C.; Bourg, A. C. Radon-222 and chloride as natural tracers of the infiltration of river water into an alluvial aquifer in which there is significant river/groundwater mixing. *Environ. Sci. Technol.* 28(5):794-798; 1994.
- Cable, J. E.; Bugna, G. C.; Burnett, W. C.; Chanton, J. P. Application of ^{222}Rn and CH_4 for assessment of groundwater discharge to the coastal ocean, *Limnol. Oceanogr.* 41(6):1347-1353; 1996.
- Cantaloub, M.G.; Higginbotham, J.; Semprini, L. The determination of Rn partition coefficients for several liquid scintillation cocktails. In *Proceedings of the 43rd annual conference on Bioassay, Analytical and Environmental Radiochemistry*, Charleston S.C., Nov. 9-13; 1997.
- Clever, H. L. ed. *Krypton, Xenon, and Radon --Gas Solubilities, Solubility Data Series 2; Volume 18.* Oxford, UK; Pergamon Press; 1979.
- Corbett, D. R.; Burnett, W. C.; Cable, P. H.; Clark, S. B. Radon tracing of groundwater input into Par Pond, Savannah River Site. *J. Hydrol.* 203:209-227; 1997.
- Freyer, K.; Treutler, H. C.; Dehnert, J.; Nestler, W. Sampling and measurement of radon-222 in water. *J. Environ. Radioactivity* 37(3):327-337; 1997.
- Hamada, H.; Komae, T. Analysis of recharge by paddy field irrigation using ^{222}Rn concentration in groundwater as an indicator. *J. Hydrol.* 205:92-100; 1998.
- Hunkeler, D.; Hoehn, E.; Hohener, P.; Zeyer, J. ^{222}Rn as a partitioning tracer to detect diesel fuel contamination in aquifers: laboratory study and field observations. *Environ. Sci. Technol.* 31:3180-3187; 1997.
- Lewis, C.; Hopke, P. K.; Stukel, J. J. Solubility of radon in selected perfluorocarbon compounds and water. *Ind. Eng. Chem. Res.* 26:356-359; 1987.
- Lowery, J. D. Measuring low radon levels in drinking water supplies. *J. Amer. Water Works Assoc.* 83(4):149-153; 1991.
- Mamoon, A.; Abulfaraj, W. H.; Sohsah, M.; Al-Haddad, K. H. Optimization of LS counting parameters for measurement of low levels of ^{222}Rn in water. *Radiat. Phys. Chem.* 47(5):715-717; 1996.
- Murase, Y.; Homma, Y.; Takiue, M. Effect of air luminescence counts on determination of ^{222}Rn by liquid scintillation counting. *Appl. Radiat. Isot.* 40(4):295-298; 1989.
- National Research Council, *Risk assessment of radon in drinking water*, Washington DC: National Academy Press; 1998
- Prichard, H. M.; Gesell, T.F. Rapid determination of radon-222 concentrations in water with a commercial liquid scintillation counter. *Health Phys.* 33:571-577; 1977.
- Semprini, L.; Hopkins, O.S.; Tasker, B.R. Laboratory, field and modeling studies of Radon-222 as a natural tracer for monitoring NAPL contamination, *Jour. Trans. Porous Media* 38(1/2):223-240; 2000.
- Semprini, L., M.G. Cantaloub, Gottitpati, S., Hopkins, O., and Istok, J. Radon-222 as a tracer for quantifying and monitoring NAPL remediation. In: *Proceedings of the Remediation of Chlorinated and Recalcitrant Compounds: First International Conference*, Monterey, CA May 18-21; 1998.
- Snow, D.D.; Spalding, R. F. Short-term aquifer residence times estimated from ^{222}Rn disequilibrium in artificially-recharged ground water. *J. Environ. Radioactivity* 37(2): 307-325; 1997.
- Spaulding, J.D.; Noakes, J.E. Determination of ^{222}Rn in drinking water, In: *Liquid Scintillation Spectrometry*, 1992, Tuscon, AZ; Radiocarbon; 1993.

8. DETERMINING RADON PARTITION COEFFICIENTS IN TCE AND PCE

The partition coefficient for aqueous phase radon in the presence of TCE or PCE (K) must be known in order to calculate DNAPL saturations (S_n). We performed experiments during 2002 to determine these values. Radon partitioning experiments were performed using an adaptation of the methodology described in Chapter 7. This method involves the sequential extraction of radon-enriched NAPL from a mixing vessel, and can be used for both light or LNAPLs and DNAPLs. A radium chloride solution of known activity was obtained from NIST and diluted to an activity of 40 pCi/mL. The radium chloride solution provided a means to generate radon-equilibrated water with a known activity equal to the radium chloride activity. Glass centrifuge tubes (50 mL) were filled with radium chloride solution, capped with a septum-equipped screw cap, and allowed to rest for 30 days to allow for secular equilibrium (i.e., the equilibration of radon concentrations). The exact mass of water and thus the exact radon activity in each centrifuge tube was determined by weighing using a 4-digit analytical balance.

For each centrifuge tube, a known volume and mass of water (3 mL) was removed using a syringe and vent line. A known volume and mass of TCE or PCE (3 mL) was then injected into the centrifuge tube, which was then vigorously mixed for 30 minutes. The 3 mL of TCE or PCE was then removed from the centrifuge tube using a syringe and vent line, and was immediately injected into a 20 mL LSC vial containing 17 mL of scintillation cocktail. A fresh 3 mL aliquot of TCE or PCE was then injected into the centrifuge tube, and the process repeated. This “sequential extraction” technique enabled the determination of the partition coefficient (K) for TCE or PCE as follows:

The fraction of radon remaining in the aqueous solution (in the centrifuge tube) after each extraction of 3 mL of TCE or PCE is described by

$$\frac{C_w V_w}{C_{NAPL} V_{NAPL} + C_w V_w} \quad (8.1)$$

where C_w is the concentration of radon in aqueous solution (pCi/L), V_w is the volume of aqueous solution in the centrifuge tube (L), C_{NAPL} is the concentration of radon in the NAPL (either TCE or PCE, pCi/L), and V_{NAPL} is the volume of NAPL (L).

Assuming a linear equilibrium partition coefficient ($K = C_{NAPL}/C_w$), equation 8.1 can be rewritten as

$$\frac{V_w}{KV_{NAPL} + V_w} \quad (8.2)$$

The concentration of radon in the NAPL after the n th extraction is equal to

$$C_{NAPL,n} = K \left(\frac{V_w}{KV_{NAPL} + V_w} \right)^n C_{w,0} \quad (8.3)$$

where the bracketed term is the fraction of radon remaining in aqueous solution after the n th extraction, and $C_{w,0}$ is the initial concentration of radon in aqueous solution in the centrifuge tube prior to the experiment. Equation 8.3 can be rewritten as

$$\ln(C_{NAPL,n}) = n \ln \left[\frac{V_w}{KV_{NAPL} + V_w} \right] + \ln(C_{w,0}K) \quad (8.4)$$

Thus a plot of extraction number (n) vs. the natural log of the radon concentration in each 3 mL NAPL sample can be obtained. The bracketed term in equation 8.4 is equal to the slope of the line. By knowing the precise values for V_{NAPL} and V_w , and determining the natural log of the radon concentration in each sequentially extracted 3 mL volume of TCE or PCE, the partition coefficient K can be determined. A plot of equation 6 for an experiment with PCE is shown in Figure 8.1. The results of the experiments (done in triplicate for TCE and PCE) are shown in Table 8.1. The values of K for TCE and PCE are similar, which is not surprising since both are chlorinated aliphatics.

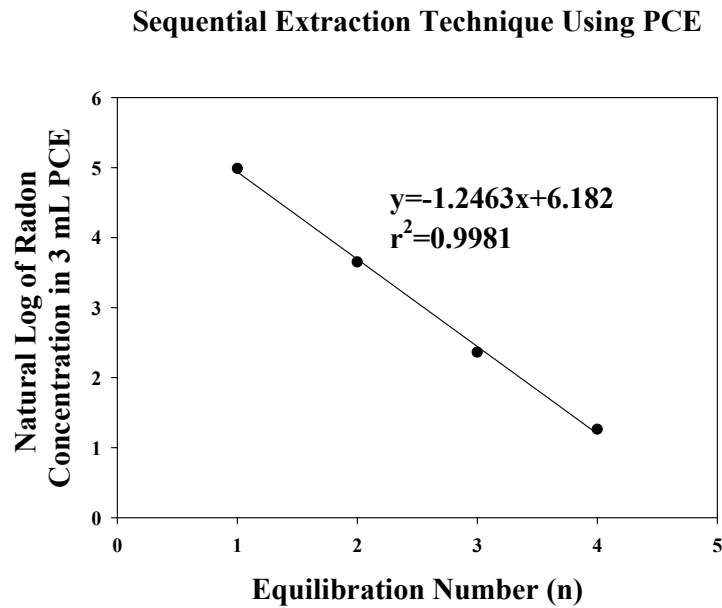


Figure 8.1 Plot of natural log of radon concentration in each 3 mL sequential extraction of PCE vs. equilibration number.

Table 8.1. Partition coefficients (K) for dissolved radon in aqueous solution in the presence of TCE or PCE.

	Mean K	95 % confidence	Mean r^2
TCE	50.02	1.78	0.9953
PCE	48.42	0.94	0.9954

9. MONITORING TCE DNAPL REMEDIATION USING NATURALLY-OCCURRING 222-RADON AS A PARTITIONING TRACER

INTRODUCTION

In this chapter, we investigate the ability of the 222-radon methods to monitor changes in NAPL saturation occurring during NAPL remediation of TCE contaminated sediment packs in laboratory physical aquifer models. Two remediation schemes were selected. The first involves flooding the NAPL-contaminated sediment pack with surfactant to solubilize and mobilize NAPL and the second involves flooding the NAPL-contaminated sediment pack with potassium permanganate to oxidize TCE to carbon dioxide gas. Mass balance calculations using measured aqueous TCE concentrations were used to estimate quantities of NAPL removed from the sediment pack by each remediation treatment. These results were compared with the results of static radon measurements and push-pull tests performed before and after NAPL emplacement and before and after surfactant and permanganate floods.

MATERIALS AND METHODS

Laboratory experiments were conducted using clean sediment collected from a surface exposure of a shallow, unconfined aquifer located at the Building 834 operable unit, Site 300 at Lawrence Livermore National Laboratory (LLNL) in Livermore, CA. The aquifer is formed in a Pliocene age nonmarine depositional sequence consisting of dense silty sand gradational to silty sandstone with minor gravel (Carpenter et al. 1984). The sediment was collected as a single batch, homogenized, sieved (< 5 mm), and air-dried prior to use. The sieved sediment is classified as a sandy loam with 76.9 % sand, 10.9 % silt, 12.1 % clay, a median grain diameter of 0.8 mm, a uniformity coefficient of 2.9, a particle density of 2.65 g/cm³, an organic carbon content of 0.0017, and a pH of 9; all determined using standard methods (Klute, 1986).

The sediment was packed into two physical aquifer models (PAMs) using the method of Istok and Humphrey (1995). The PAMs were constructed in a wedge-shape to simulate the radial flow field near a monitoring well during injection or extraction pumping (Figure 9.1). The PAMs were constructed of polypropylene with interior dimensions of 5 cm (width at narrow end), 50 cm (width at wide end), 125 cm (length), and 20 cm (height), and a total internal volume of 0.069 m³. Separate PAMs and sediment packs were used for the surfactant flood and permanganate flood experiments (see below). Test solutions were injected and extracted using injection/extraction ports located on a vertical plate at the model's narrow end. During the injection phase, flow was directed from the injection/extraction ports toward the model's wide end; during the extraction phase, flow was reversed. A constant head water reservoir was connected to the model's wide end to allow pore fluids to leave the sediment pack during the injection phase and to allow tap water to enter the sediment pack during the extraction phase. After the sediment pack was water saturated, the PAMs were sealed by installing a layer of closed cell foam and a lid containing 8 sampling ports (Figure 9.1). A known initial quantity of liquid TCE was then added to the sediment packs. This was achieved by first draining the sediment pack and then slowly injecting aliquots of neat TCE at depths from 7 to 10 cm into 53 injection ports located in the model lid between sampling ports 1 and 5 (Figure 9.1). A total of 920

g of TCE were injected, which represents a liquid TCE saturation equivalent to ~ 5 % of the total pore volume within the treated zone. After TCE injection, the sediment pack was re-saturated with tap water and then flushed for ~ 24 h with tap water to remove mobile TCE from the injection/extraction ports and to attempt to entrap liquid

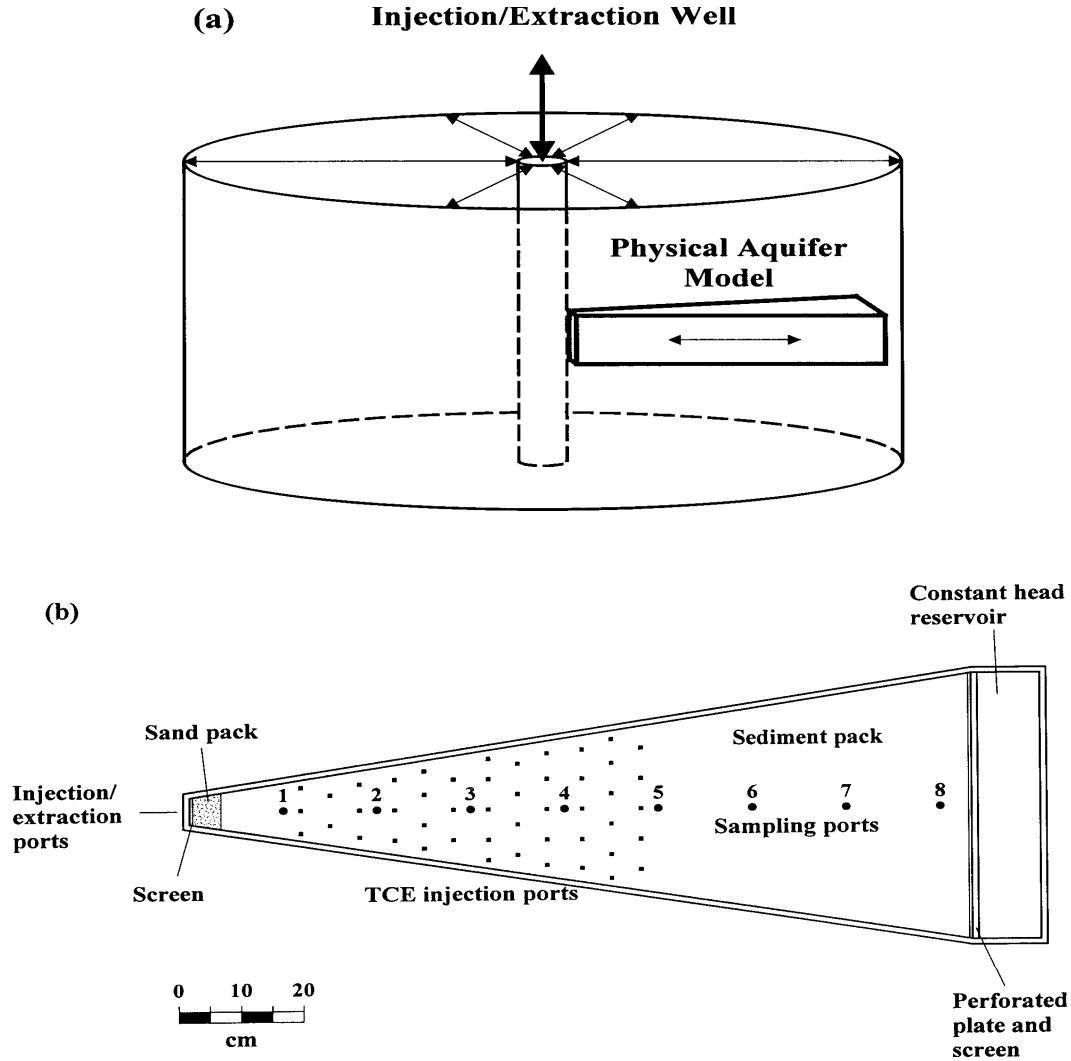


Figure 9.1 Schematic indicating (a) the portion of the flow field near an injection/extraction well represented by physical aquifer models used in laboratory push-pull tests and (b) plan view of a physical aquifer model.

TCE within the pore space. Less than 35 g of liquid TCE were removed from the sediment pack during the tap water flush as computed from measured aqueous TCE concentrations and flushing volumes.

All experiments were performed under confined conditions. Sampling ports were connected to brass ‘well’ screens that fully penetrated the saturated thickness of the sediment pack (Figure 9.1). Additional ‘wells’ were connected to manometers to measure hydraulic head.

The saturated hydraulic conductivity of the sediment pack was determined periodically from head and pumping rate measurements and was nearly constant ($1.0 \times 10^{-2} \pm 0.6 \times 10^{-3}$ cm/s) during all tests.

Surfactant floods were conducted using tap water containing 13,500 mg/L Dowfax 8390 (DOWFAX) (DOW Chemical Co., Midland, MI) consisting of 90% hexadecyl diphenyl oxide disulfonate and 10% dihexadecyl diphenyl oxide disulfonate components. Permanganate floods were conducted using tap water containing 5 wt % solutions of KMnO_4 . For each surfactant or permanganate flood ~ 9 L of test solution were injected. TCE concentrations were monitored in the sampling ports before-, during-, and after- each surfactant or permanganate flood and used to perform mass balance calculations for aqueous and NAPL TCE.

After each surfactant or permanganate flood, the PAM was allowed to sit under static (no-flow) conditions for ~ 21 days to allow radon concentrations to equilibrate. Then radon concentrations were measured at each sampling port under static (no-flow) conditions. These measurements were followed by one or more push-pull tests that were conducted by injecting ~ 9 L of radon-free tap water (prepared by bubbling overnight with compressed air) containing 100 mg/L Br^- (prepared from KBr) to serve as a conservative tracer. Extraction pumping began within 30 min after the end of the injection and continued until ~ 20 L had been extracted. Injection and extraction pumping rates were constant at ~ 15 mL/min. Water samples were collected from the sampling ports during the injection phase; additional water samples were collected from the injection/extraction ports during the extraction phase.

Bromide concentrations were determined using a Dionex Model DX-120 ion chromatograph equipped with electrical conductivity detector (Sunnyvale, CA). TCE concentrations were determined using a Waters Alliance Model 2690 High Performance Liquid Chromatograph (Milford, MA) with photodiode array detector. Water samples for radon analysis were filtered through a 0.45 μm filter (Millipore, Bedford, MA) attached to a syringe and a 2 inch steel needle (Becton-Dickinson, Franklin Lakes, NJ). The filtered sample (~ 15 mL) was then dispensed into the bottom of a pre-weighed 20 mL borosilicate scintillation vial containing 5 mL of Ultima Gold F scintillation “cocktail” (Packard Instruments, Meriden, CT). Counting was performed with a Packard 2500 TR/AB Liquid Scintillation Analyzer (LSA) as described by Cantaloub (2001).

RESULTS AND DISCUSSION

Monitoring Performance of Surfactant Floods

Samples obtained under static (no-flow) conditions before and after TCE NAPL emplacement in the PAM used for the surfactant flood experiments showed a substantial decrease after TCE emplacement in the NAPL-contaminated portion of the PAM (Figure 9.2). Before TCE emplacement radon concentrations ranged from 450-650 pCi/L throughout the PAM; after TCE emplacement radon concentrations decreased to 250-340 pCi/L in sampling ports 1-4 within the region of TCE NAPL contamination, while radon concentrations in uncontaminated portions of the PAM remained above 460 pCi/L

(Figure 9.2). The presence of NAPL was also detected in push-pull tests conducted before and after TCE emplacement. Extraction phase breakthrough curves for radon showed greater apparent dispersion due to retarded radon transport in the presence of TCE NAPL (Figure 9.3).

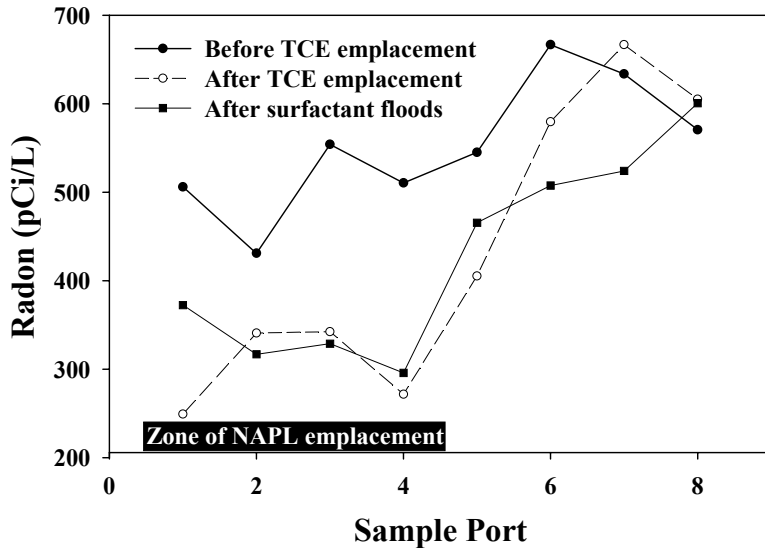


Figure 9.2 Static radon concentrations measured in sampling ports of physical aquifer model before- and after-TCE NAPL emplacement and after surfactant floods.

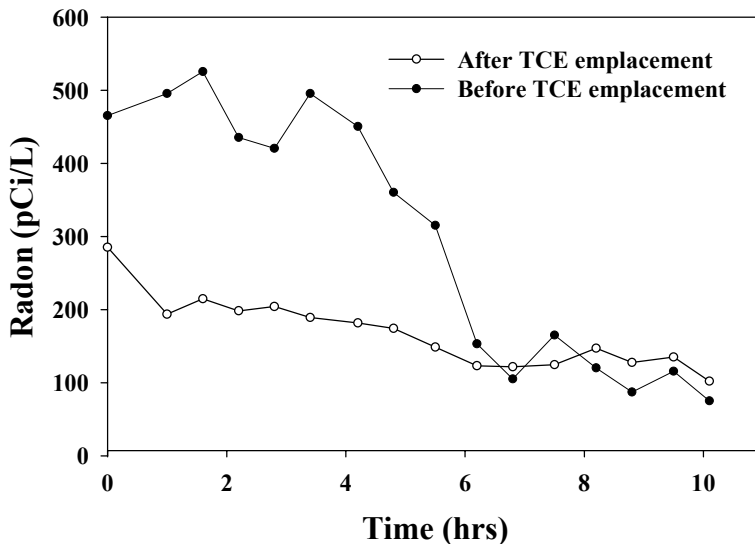


Figure 9.3 Radon concentrations at sampling port 2 during the injection phase of push-pull tests showing retarded transport and increased apparent dispersion of radon in the presence of NAPL.

Three identical surfactant floods were conducted as push-pull tests; the surfactant solution was injected and extracted from the narrow end of the physical aquifer models. Static radon measurements and push-pull testing performed before- and after- the series of surfactant floods indicated that negligible NAPL was removed during surfactant remediation. Static radon concentrations obtained from the sampling port show little change from those obtained prior to the surfactant floods (Figure 9.2). Push-pull tests confirmed no reduction in apparent dispersion of radon (data not shown).

Measurements of aqueous TCE concentrations confirmed that negligible TCE NAPL had been removed from the sediment pack by the surfactant floods. The maximum TCE concentration observed during the extraction phase of flood 1 was ~ 3.2 g/L with a corresponding TCE mass recovery of only ~ 35 g. During the extraction phase of floods 2 and 3 the maximum TCE concentration decreased to ~ 1.9 and ~ 0.6 g/L, respectively. TCE mass recovery also decreased to ~ 25 g in flood 2 and to ~ 8 g in flood 3. Thus, the total mass of TCE recovered was 35 g (initial water flush) + (35 + 25 + 8 g) from the surfactant floods for a total of 103 g, a reduction of ~ 0.11 % of the initial TCE mass. This corresponds to a reduction in TCE saturation of only 0.006 %, which is apparently not detectable in this system. Aqueous TCE measurements made as a function of depth in individual sampling ports indicated that density-driven flow had resulted in a plume of aqueous TCE sinking to the bottom of the sediment pack. After flood 1, TCE concentrations near the top of the sediment pack (3 cm depth) were generally uniform at ~ 0.5 g/L in ports 1 - 6 but increased to a maximum of 1.5 g/L at a depth of 18.3 cm at port 1. However, after floods 2 and 3, TCE concentrations increased at all depths > 3 cm in ports 1-5, to a maximum value of ~ 5 g/L in port 2 after flood 3. Although aqueous TCE concentrations increased with depth, data from sediment cores collected after flood 3 provided no evidence for the vertical redistribution of liquid TCE within the sediment pack; essentially all of the remaining TCE was located where it was emplaced (depths of 7-10 cm between ports 1 and 5). It should be noted that DOWFAX does not sorb appreciably to this sediment under the conditions of these tests and mass balance calculations based on measured surfactant concentrations showed that negligible DOWFAX remained in the sediment pack after each flood (Field et al. 199?).

Monitoring Performance of Permanganate Floods

Radon concentrations measured under static (no-flow) conditions before and after TCE emplacement in a second PAM also showed reduction in radon concentration in the presence of NAPL (Figure 9.4). Radon concentrations within the zone of NAPL emplacement increased progressively following each permanganate flood; while radon concentrations beyond port 6 remained essentially unchanged (Figure 9.4). Mass balances on the chloride ion extracted from the PAM indicated that permanganate had oxidized 7, 25, and 80 % of the emplaced NAPL following flood 1, 3, and 4, respectively. The qualitative agreement between the changing radon concentrations and independent mass balance calculations is encouraging and clearly demonstrates the potential of using static radon concentrations to monitor the progress of NAPL remediation.

Reduction in NAPL saturation was also detectable in the results of push-pull tests performed after permanganate floods 1, 3, and 4 as a progressive decrease in the apparent

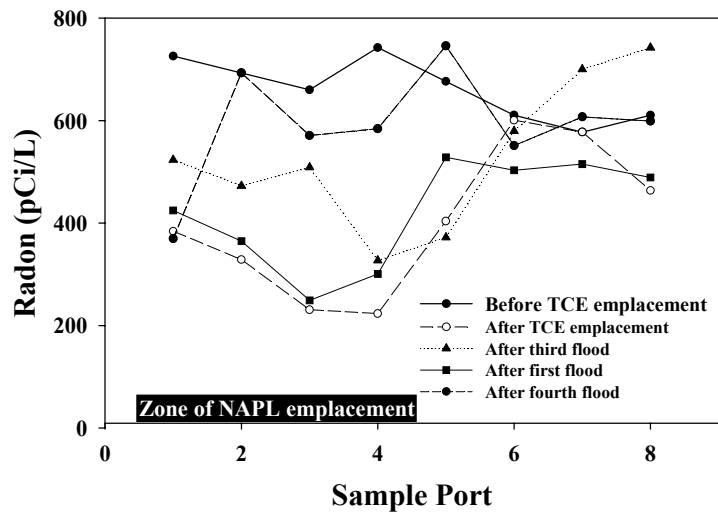


Figure 9.4 Static radon concentrations measured in sampling ports of physical aquifer model before- and after-TCE NAPL emplacement and after permanganate floods.

dispersion of radon following each flood (Figure 9.5). As NAPL was removed, radon concentration increased more quickly during the extraction phase of a test due to decreased radon partitioning and retardation. Thus, these results suggest it should be possible to monitor NAPL removal by performing a series of push-pull tests in a single well.

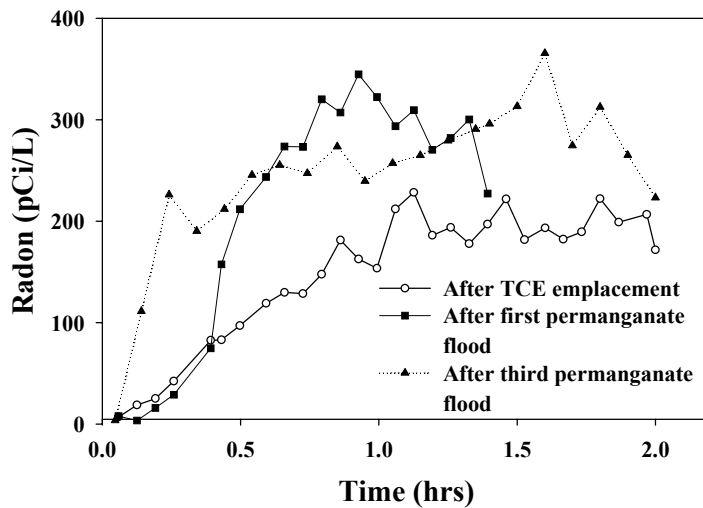


Figure 9.5 Radon concentrations at injection/extraction ports during the extraction phase of push-pull tests showing decreased retardation and apparent dispersion of radon following permanganate floods

CONCLUSIONS

Successful remediation of a NAPL contaminated site requires accurate knowledge of the NAPL presence and spatial distribution. Laboratory results presented here indicate that naturally occurring radon can be a sensitive indicator of subsurface NAPL. The preferential partitioning of radon from the pore water into residual NAPL results in a decrease in radon concentrations and a reduction in the apparent dispersion of radon that can be correlated to the degree of residual NAPL saturation. Monitoring subsurface NAPL using radon as an in situ indicator requires only passive sampling of groundwater from existing monitoring wells or short-duration tests performed in individual monitoring wells. Thus radon may prove useful as an inexpensive and accurate means of monitoring subsurface NAPL contamination.

REFERENCES

- Cantaloub, M., 2001. Aqueous-organic partition coefficients for radon-222 and their application to radon analysis by liquid scintillation methods. Master's Thesis, Oregon State University.
- Carpenter, D.W., J.J. Sweeney, P.W. Kasameyer, N.R. Burkhard, K.G. Knauss and R.J. Shlemon. 1984. *Geology of the Lawrence Livermore National Laboratory*. UCRL-53316. Lawrence Livermore National Laboratory, Livermore, CA.
- Cohen, R.M. and Mercer, J.W., DNAPL Site Evaluation, Boca Raton, FL: CRC Press. (1993).
- Davis, B.M., J.D. Istok, L. Semprini. 2002. Push-Pull Partitioning Tracer Tests Using Radon-222 to Quantify Non-Aqueous Phase Liquid Contamination. *Journal of Contaminant Hydrology* 58 (2002) 129-146
- Istok, J.D. and M.D. Humphrey, 1995. Laboratory investigation of buoyancy-induced flow (plume sinking) during two-well tracer tests. *Ground Water*, 33:597-604.
- Jin, M., Delshad, M., Dwarakanath, V., McKinney, D.C., Pope, G.A., Sepehrnoori, K., and Tilburg, C.E., "Partitioning tracer test for detection, estimation, and remediation performance assessment of subsurface nonaqueous phase liquids," *Water Resour. Res.* 31(4), 1201-11 (1995).
- Klute, A., Ed. 1986. *Methods of soil analysis: Part 1-physical and mineralogical methods*. Madison, WI: American Society of Agronomy.
- Schroth, M.H., J.D. Istok, R. Haggerty, 2001. In situ evaluation of solute retardation using single-well push-pull tests. *Advances in Water Resources*, 24:105-117.
- Semprini, L., Cantaloub, M., Gottipati, S., Hopkins, O., and Istok, J. "Radon-222 as a tracer for quantifying and monitoring NAPL remediation," in proceedings of The First International Conference on Remediation of Chlorinated and Recalcitrant Compounds, Columbus, OH Battelle Press (1998).
- Semprini, L., Hopkins, O., Gottipati, S., and Tasker, B., "Field laboratory and modeling studies of Radon-222 as a natural tracer for detecting NAPL contamination in the subsurface and monitoring the progress of remediation," *EOS, Trans. Amer. Geophys. Union*, 76(46), F276 (1995).